PNL-6853
UC-11

## DISCLAIMER

This report was prepared as an account of work sponsored by an agency of the United States Government. Neither the United States Government nor any agency thereof, nor any of their employees, makes any warranty, express or implied, or assumes any legal liability or responsibility for the accuracy, completeness, or usefulness of any information, apparatus, product, or process disclosed, or represents that its use would not infringe privately owned rights. Reference herein to any specific commercial product, process, or service by trade name, trademark, manufacturer, or otherwise does not necessarily constitute or imply its endorsement, recommendation, or favoring by the United States Government or any agency thereof. The views and opinions of authors expressed herein do not necessarily state or reflect those of the United States Government or any agency thereof.

# PRELIMINARY TESTING OF TURBULENCE AND RADIONUCLIDE TRANSPORT MODELING IN DEEP OCEAN ENVIRONMENT

PNL--6853

DE90 000921

Y. Onishi
D. C. Dummuller[a]
D. S. Trent

March 1989

Prepared for
the U.S. Environmental Protection Agency
under a Related Services Agreement
with the U.S. Department of Energy
Contract DE-AC06-76RLO 1830

Pacific Northwest Laboratory
Richland, Washington 99352

(a) Washington State University
Pullman, Washington

DISTRIBUTION OF THIS DOCUMENT IS UNLIMITED

MASTER

## DISCLAIMER

This report was prepared as an account of work sponsored by an agency of the United States Government. Neither the United States Government nor any agency thereof, nor any of their employees, makes any warranty, express or implied, or assumes any legal liability or responsibility for the accuracy, completeness, or usefulness of any information, apparatus, product, or process disclosed, or represents that its use would not infringe privately owned rights. Reference herein to any specific commercial product, process, or service by trade name, trademark, manufacturer, or otherwise does not necessarily constitute or imply its endorsement, recommendation, or favoring by the United States Government or any agency thereof. The views and opinions of authors expressed herein do not necessarily state or reflect those of the United States Government or any agency thereof.

---

## DISCLAIMER

Portions of this document may be illegible in electronic image products. Images are produced from the best available original document.

DO NOT MICROFILM
THIS PAGE

## DISCLAIMER

This program was prepared as an account of work sponsored by an agency of the United States Government. Neither the United States Government nor any agency thereof, nor Battelle Memorial Institute, nor any or their employees, makes **any warranty, expressed or implied, or assumes any legal liability or responsibility for the accuracy, completeness, or usefulness of any information, apparatus, product, or process disclosed, or represents that its use would not infringe privately owned rights.** Reference herein to any specific commercial product, process, or service by trade name, trademark, manufacturer, or otherwise, does not necessarily constitute or imply its endorsement, recommendation, or favoring by the United States Government of any agency thereof, or Battelle Memorial Institute. The views and opinions of authors expressed herein do not necessarily state or reflect those of the United States Government or any agency thereof.

PACIFIC NORTHWEST LABORATORY
*operated by*
BATTELLE MEMORIAL INSTITUTE
*for the*
UNITED STATES DEPARTMENT OF ENERGY
*under Contract DE-AC06-76RLO 1830*

Printed in the United States of America

Available to DOE and DOE contractors from the
Office of Scientific and Technical Information, P.O. Box 62, Oak Ridge, TN 37831;
prices available from (615) 576-8401. FTS 626-8401.

Available to the public from the National Technical Information Service,
U.S. Department of Commerce, 5285 Port Royal Rd., Springfield, VA 22161.

NTIS Price Codes, Microfiche A01

Printed Copy

| Pages | Price Codes |
|---|---|
| 001-025 | A02 |
| 026-050 | A03 |
| 051-075 | A04 |
| 076-100 | A05 |
| 101-125 | A06 |
| 126-150 | A07 |
| 151-175 | A08 |
| 176-200 | A09 |
| 201-225 | A10 |
| 226-250 | A11 |
| 251-275 | A12 |
| 276-300 | A13 |

Although the research described in this article has been funded wholly or in part by the United States Environmental Protection Agency (EPA), it has not been subjected to EPA review and therefore does not necessarily reflect the views of EPA and no official endorsement should be inferred.

## SUMMARY

Pacific Northwest Laboratory (PNL) performed a study for the U.S. Environmental Protection Agency's Office of Radiation Programs to 1) identify candidate models for regional modeling of low-level waste ocean disposal sites in the mid-Atlantic ocean; 2) evaluate mathematical representation of the models' eddy viscosity/dispersion coefficients; and 3) evaluate the adequacy of the k-$\epsilon$ turbulence model and the feasibility of one of the candidate models, TEMPEST©/FLESCOT©, to deep-ocean applications on a preliminary basis.

PNL identified the TEMPEST©/FLESCOT©, FLOWER, Blumberg's, and RMA 10 models as appropriate candidates for the regional radionuclide modeling. Among these models, TEMPEST/FLESCOT is currently the only model that solves distributions of flow, turbulence (with the k-$\epsilon$ model), salinity, water temperature, sediment, dissolved contaminants, and sediment-sorbed contaminants.

Solving the Navier-Stokes equations using higher order correlations is not practical for regional modeling because of the prohibitive computational requirements; therefore, the turbulence modeling is a more practical approach.

PNL applied the three-dimensional code, TEMPEST©/FLESCOT© with the k-$\epsilon$ model, to a very simple, hypothetical, two-dimensional, deep-ocean case, producing at least qualitatively appropriate results. However, more detailed testing should be performed for the further testing of the code.


© Copyright by Battelle Memorial Institute, Columbus, Ohio.

CONTENTS

SUMMARY . . . . . iii

1.0 INTRODUCTION . . . . . 1.1

2.0 REGIONAL MODELS FOR LOW-LEVEL RADIOACTIVE WASTE SITES IN THE MID-ATLANTIC . . . . . 2.1

3.0 REVIEW AND EVALUATION OF MATHEMATICAL REPRESENTATION FOR VISCOSITY AND DISPERSION COEFFICIENTS . . . . . 3.1

3.1 ZERO-EQUATION MODELS . . . . . 3.3

3.2 ONE-EQUATION MODELS . . . . . 3.8

3.3 TWO-EQUATION MODELS . . . . . 3.10

4.0 MODEL DESCRIPTION . . . . . 4.1

4.1 TEMPEST/FLESCOT MODEL . . . . . 4.1

4.2 HYDRODYNAMIC EQUATIONS . . . . . 4.2

4.3 HEAT TRANSFER . . . . . 4.6

4.4 MASS TRANSPORT . . . . . 4.7

4.5 TURBULENCE EQUATIONS . . . . . 4.7

4.6 SEDIMENT TRANSPORT EQUATION . . . . . 4.9

4.7 DISSOLVED CONTAMINANT TRANSPORT EQUATION . . . . . 4.11

4.8 SEDIMENT-SORBED CONTAMINANT TRANSPORT EQUATION . . . . . 4.12

5.0 MODEL APPLICATIONS . . . . . 5.1

5.1 EDDY VISCOSITY DISTRIBUTIONS . . . . . 5.1

5.1.1 Nonstratified Case . . . . . 5.1

5.1.2 Stratified Cases . . . . . 5.3

5.2 RADIONUCLIDE DISTRIBUTIONS . . . . . 5.5

5.2.1 Simulation Conditions . . . . . 5.5

5.2.2 Simulation Results of Stratified Case 4 . . . . . 5.8

5.2.3 Simulation Results of Stratified Case 5 . . . . . 5.8

5.2.4 Simulation Results of Nonstratified Case 6 . . . . . 5.9

6.0 SUMMARY AND CONCLUSIONS . . . . . 6.1

7.0 REFERENCES . . . . . 7.1

## FIGURES


5.1 Calculated Turbulent Kinetic Energy Over the Whole Flow Region for Nonstratified Case 1 . . . . . 5.11

5.2 Calculated Turbulent Energy Dissipation Over the Whole Flow Region for the Nonstratified Case 1 . . . . . 5.12

5.3 Calculated Eddy Viscosity Over the Whole Flow Region for the Nonstratified Case 1 . . . . . 5.13

5.4 Calculated Turbulent Kinetic Energy Near the Bottom for the Nonstratified Case 1 . . . . . 5.14

5.5 Calculated Turbulent Energy Dissipation Near the Bottom for the Nonstratified Case 1 . . . . . 5.15

5.6 Calculated Eddy Viscosity Near the Bottom for the Nonstratified Case 1 . . . . . 5.16

5.7 Vertical Distribution of Calculated Turbulent Kinetic Energy Near the Bottom for the Nonstratified Case 1 . . . . . 5.17

5.8 Vertical Distribution of Calculated Turbulent Energy Dissipation Near the Bottom for the Nonstratified Case 1 . . . . 5.18

5.9 Vertical Eddy Viscosity Near the Bottom for the Nonstratified Case 1 . . . . . 5.19

5.10 Calculated Velocity Distribution Near the Bottom for the Nonstratified Case 1 . . . . . 5.20

5.11 Calculated Turbulent Kinetic Energy Over the Whole Flow Region for Stratified Case 2 . . . . . 5.21

5.12 Calculated Turbulent Energy Dissipation Over the Whole Flow Region for the Stratified Case 2 . . . . . 5.22

5.13 Calculated Eddy Viscosity Over the Whole Flow Region for the Stratified Case 2 . . . . . 5.23

5.14 Calculated Turbulent Kinetic Energy Near the Bottom for the Stratified Case 2 . . . . . 5.24

5.15 Calculated Turbulent Energy Dissipation Near the Bottom for the Stratified Case 2 . . . . . 5.25

5.16 Calculated Eddy Viscosity Near the Bottom for the Stratified Case 2 . . . . . 5.26

5.17 Vertical Distribution of Calculated Turbulent Kinetic Energy Near the Bottom for the Stratified Case 2 . . . . . 5.27

5.18 Vertical Distribution of Calculated Turbulent Energy Dissipation Near the Bottom for the Stratified Case 2 . . . . . 5.28

5.19 Vertical Eddy Viscosity Near the Bottom for the Stratified Case 2 . . . . . 5.29

5.20 Calculated Velocity Distribution Near the Bottom for the Stratified Case 2 . . . . . 5.30

5.21 Calculated Turbulent Kinetic Energy Over the Whole Flow Region for Stratified Case 3 . . . . . 5.31

5.22 Calculated Turbulent Energy Dissipation Over the Whole Flow Region for the Stratified Case 3 . . . . . 5.32

5.23 Calculated Eddy Viscosity Over the Whole Flow Region for the Stratified Case 3 . . . . . 5.33

5.24 Calculated Turbulent Kinetic Energy Near the Bottom for the Stratified Case 3 . . . . . 5.34

5.25 Calculated Turbulent Energy Dissipation Near the Bottom for the Stratified Case 3 . . . . . 5.35

5.26 Calculated Eddy Viscosity Near the Bottom for the Stratified Case 3 . . . . . 5.36

5.27 Vertical Distribution of Calculated Turbulent Kinetic Energy Near the Bottom for the Stratified Case 3 . . . . . 5.37

5.28 Vertical Distribution of Calculated Turbulent Energy Dissipation Near the Bottom for the Stratified Case 3 . . . . . 5.38

5.29 Vertical Eddy Viscosity Near the Bottom for the Stratified Case 3 . . . . . 5.39

5.30 Calculated Velocity Distribution Near the Bottom for the Stratified Case 3 . . . . . 5.40

5.31 Calculated Dissolved Radionuclide Concentration (in p/Ci/L) Near the Bottom for the Stratified Case 4) . . . . . 5.41

5.32 Calculated Suspended-Silt-Sorbed Radionuclide Concentration (in pCi/g) Near the Bottom for the Stratified Case 4 . . . . . 5.42

5.33 Calculated Suspended-Clay-Sorbed Radionuclide Concentration (in pCi/g) Near the Bottom for the Stratified Case 4 . . . . . 5.43

5.34 Calculated Dissolved Radionuclide Concentration (in p/Ci/L) Near the Bottom for the Stratified Case 5 . . . . . 5.44

5.35 Calculated Suspended-Silt-Sorbed Radionuclide Concentration (in pCi/g) Near the Bottom for the Stratified Case 5 . . . . . 5.45

5.36 Calculated Suspended-Clay-Sorbed Radionuclide Concentration (in pCi/g) Near the Bottom for the Stratified Case 5 . . . . . 5.46

5.37 Calculated Dissolved Radionuclide Concentration (in p/Ci/L) Near the Bottom for the Stratified Case 6 . . . . . 5.47

5.38 Calculated Suspended-Silt-Sorbed Radionuclide Concentration (in pCi/g) Near the Bottom for the Stratified Case 6 . . . . . 5.48

5.39 Calculated Suspended-Clay-Sorbed Radionuclide Concentration (in pCi/g) Near the Bottom for the Stratified Case 6 . . . . . 5.49

## TABLES


2.1 Summary of Reviewed Hydrodynamic and Transport Models . . . . . 2.2

3.1 Variation in Eddy Diffusivity . . . . . 3.4

5.1 Initial Water Temperature and Salinity Distribution for Case 2 . . . . . 5.3

5.2 Initial Water Temperature and Salinity Distribution for Case 3 . . . . . 5.3

5.3 Simulation Conditions and Model Parameters for Cases 4 through 6 . . . . . 5.7

5.4 Calculated Radionuclide Concentration Sorbed by Bed Sediment in the Top 3-cm Bed Layer After 6 h Simulation . . . . . 5.9

# 1.0 INTRODUCTION

The U.S. Environmental Protection Agency (EPA) is investigating the potential environmental impacts and health risks from low-level radioactive waste (LLW) disposal on the deep-ocean bottom in the mid-Atlantic. Mathematical models can assist in predicting migration and fate of radionuclides from the LLW disposal site.

Pacific Northwest Laboratory (PNL) performed this study for EPA with the following objectives: 1) identify candidate models useful for regional modeling of the LLW ocean disposal sites, 2) review and evaluate mathematical representations of eddy viscosity and dispersion coefficients, and 3) apply the TEMPEST/FLESCOT model to a very simple hypothetical deep-ocean disposal case to evaluate the adequacy of the k-$\epsilon$ turbulent model on a preliminary basis and the feasibility of the TEMPEST/FLESCOT model to the deep-ocean applications.

Section 2.0 of this report summarizes PNL's review of representative mathematical models, Section 3.0 reviews and evaluates the mathematical equations for viscosity and dispersion coefficients, and a description of the TEMPEST/FLESCOT model and its governing equations is given in Section 4.0. Section 5.0 describes the applications of the TEMPEST/FLESCOT model in six cases, and conclusions are given in Section 6.0.

## 2.0 REGIONAL MODELS FOR THE MID-ATLANTIC LOW-LEVEL WASTE DEEP-OCEAN DISPOSAL

Low-level radioactive wastes (LLW) released from the 2800-m or 3800-m sites in the mid-Atlantic Ocean will not be distributed uniformly in either the vertical or horizontal direction on local (e.g., within several kilometers square) and regional scales (e.g., up to several hundred kilometers square), and the physical-oceanographic features exhibit complex three-dimensional behavior. Therefore, as discussed in Onishi et al. (1987), three-dimensional, coupled hydrodynamic-mass/energy transport models with proper representations of oceanic eddy viscosity and dispersion processes are required as regional radionuclide transport models.

The Pacific Northwest Laboratory (PNL) reviewed some representative mathematical models to evaluate their applicabilities and limitations for the LLW ocean disposal assessment (Onishi et al. 1987). Table 2.1 shows the review summary of these models. As shown in Table 2.1, with suitable model modifications or inclusions, such as turbulence closure, enhanced sediment transport, radionuclide, and/or curvilinear coordinate system setup, the FLESCOT model (Onishi and Trent 1982), the FLOWER model (Eraslan et al. 1983), and Blumberg's model (Blumberg and Herring 1986) would be appropriate candidates for regional radionuclide modeling to predict the transport and dispersion of LLW disposed in the 2800-m and 3800-m ocean sites (Onishi et al. 1987). Although the RMA 10 model (King 1982) does not incorporate a turbulence closure scheme, this model, with some modifications, is also an appropriate candidate for regional radionuclide modeling. These models are also applicable to a local scale covering a few square kilometers, such as the area within the 2800-m and 3800-m sites. To address the long-term, global-scale impact of LLW disposed in these sites, the output of these regional models is to be provided to global-scale models as boundary conditions or sink/source terms appears to be the only one which has comprehensive description of transport and fate of sediments, dissolved contaminants, and sediment-sorbed contaminants.

Among the regional-scale models shown in Table 2.1, FLESCOT© solves distributions of flow, turbulence, salinity, water temperature, sediments, dissolved contaminants (e.g., radionuclides, hazardous chemicals), and

TABLE 2.1. Summary of Reviewed Hydrodynamic and Transport Models (Onishi et al. 1987)

| Model | Simulated Substances: Flow | Turbulent Energy | Salinity | Water Temperature | Sediment | Dissolved Contaminant | Particulate Contaminant | Sediment-Contaminant Interactions | Time Dependency(a) | Solution Dimensions(b) | Scale(c) | Technique(d) |
|---|---|---|---|---|---|---|---|---|---|---|---|---|
| Simons (1973) | X | | | X | | | | | U | 3 | R | FD |
| Leenderste and Liu (1975) | X | | X | X | | | | | U | 3 | R | FD |
| Weatherly and Martin (1978) | X | X | | X | | | U | 3 | R | FD | | |
| RA10 (King 1982) | X | | X | X | X | X | X | | U | 3 | R | FE |
| FLESCOT© (Onishi and Trent 1982) | X | X | X | X | X | X | X | X | U | 3 | R | FD |
| | | | | | | | | | U | 3 | R | FD |
| TEMPEST© (Trent et al. 1989) | X | X | X | X | | | | | U | 3 | R | FD |
| FLOWER (Eraslan et al. 1983) | X | X | X | X | | | | | U | 3 | R | DE |
| REMIXCS (Freitas et al. 1985) | X | | | X | | | | | U | 3 | R | FD |
| Blumberg and Herring (1986) | X | X | X | X | | | | | U | 3 | R | FD |
| Sheng et al. (1978) | X | | | | | | | | U | 3 | R | FD |
| Davies (1980) | X | | | | | | | | U | 3 | R | FE |
| Tee (1981) | X | | | | | | | | U | 3 | R | FD/MC |

(a) "S" and "U" denote steady and unsteady states, respectively.
(b) "2", "3", and "C" denote two-, three-dimensional, and compartment models, respectively.
(c) "R" and "G" denote regional/local and global scales, respectively.
(d) "FD", "FE", "MC", "I", "A", and "DE" denote finite differences, finite element, method of characteristics, integration method, analytical, and discrete element models, respectively.

TABLE 2.1. (contd)

| Model | Simulated Substances: Flow | Turbulent Energy | Salinity | Water Temperature | Sediment | Dissolved Contaminant | Particulate Contaminant | Sediment-Contaminant Interactions | Time Dependency(a) | Solution Dimensions(b) | Scale(c) | Technique(d) |
|---|---|---|---|---|---|---|---|---|---|---|---|---|
| CAFE (Wang and Conner 1975) | X | | | | | | | | U | 2 | R | FE |
| RMA2 (Norton and King 1977) | X | | | | | | | | U | 2 | R | FE |
| FETRA (Onishi 1981) | | | | | X | X | X | X | U | 2 | R | FE |
| Spaulding and Pavish (1984) | | | | | | X | X | | U | 3 | R | AFD |
| Walker et al. (1985) | | | | | | X | | | U | 2 | R | A |
| EXAMS (Smith et al. 1977) | | | | | | X | X | X | S | C | R | I |
| WASP (Ditoro et al. 1981) | | | | | X | X | X | X | U | C | R | I |
| Bryan (1969) | X | | X | X | | | | | U | 3 | G | FD |
| Holland and Liu (1975) | X | | | | | | | | U | 2 | G | FD |
| Webb and Morley (1973) | | | | | | X | | | U | 3 | G | A |
| Shepard (1978) | | | | | | X | | | S | 3 | G | A |
| MARINRAD (Koplik et al. 1984) | | | | | | X | X | X | U | C | G | I |
| MARKA (Robinson and Marietta 1985) | | | | | | X | X | X | U | C | G | I |

sediment-sorbed contaminants. The sediment and contaminant transport is simulated in both ocean water column and bottom sediments. Thus, the FLESCOT© model can be a candidate model to be applied to the 2800 and 3800-m sites to predict the transport and accumulation of LLW on regional and local scales and to address the criteria (B)[1], (D)[2], and (J) as[3] listed in Section 424(i)(1) of Public Law 97-424.

The main strengths of the FLESCOT© model for the deep-ocean LLW disposal site assessment are listed here. The code

- is time-dependent, three-dimensional
- calculates hydrodynamic and energy transport
- calculates sediment transport for both cohesive and noncohesive sediment
- has the k-$\epsilon$ turbulence model, as a turbulent closure scheme, which needs to be tested in this study
- simulates both dissolved and sediment-sorbed radionuclide transport with interactions between radionuclides and sediments
- predicts sediment and radionuclide distributions at the ocean bottom with ocean bottom data
- has been applied to the coastal and estuarine environment to calculate flow and mass/energy transport, including sediment and contaminant transport
- is computationally efficient through the extensive use of vectorizing.

---

(1) An analysis of the environmental impact of the disposed action, at the site at which the applicant desires to dispose of material, upon human health and welfare and marine life.
(2) An analysis of the resulting environmental and economic conditions if the containers fail to contain the radioactive waste material when initially disposed at the specific site.
(3) A comprehensive monitoring plan to be carried out by the applicant to determine the full effect of the disposal on the marine environment, living resources or human health, etc.

The major limitation of the FLESCOT© code is the lack of model applications to the deep-ocean environment. The code must be tested to examine suitability of representations of turbulence/eddy viscosity and dispersion in the deep- ocean (such as the 2800- and 3800-m site) environment.

## 3.0 REVIEW AND EVALUATION OF MATHEMATICAL REPRESENTATION FOR VISCOSITY AND DISPERSION COEFFICIENTS

Determination of flow and constituent concentrations requires the solution of the governing equations for continuity, momentum, and scalar transport (temperature, salinity, sediments, and radionuclides) shown below. To solve these equations, the terms $\overline{u_i u_j}$ and $\overline{u_i \phi}$, known as the Reynolds stresses or turbulence correlations, must be determined.

Continuity
$$\frac{\partial U_i}{\partial x_i} = 0 \tag{3.1}$$

Momentum
$$\frac{\partial U_i}{\partial t} + U_J \frac{\partial U_i}{\partial x_j} + F_i = \frac{1}{\rho_r} \frac{\partial P}{\partial x_i} + \frac{\partial}{\partial x_j} \left(\nu \frac{\partial U_i}{\partial x_j} - \overline{u_i u_j}\right) + g_i \frac{\rho - \rho_r}{\rho_r} \tag{3.2}$$

Scalar Transport
(temperature, concentration)
$$\frac{\partial \phi}{\partial t} + U_i \frac{\partial \phi}{\partial x_i} = \frac{\partial}{\partial x_i} \left(\lambda \frac{\partial \phi}{\partial x_i} - \overline{u_i \phi}\right) + S_\phi \tag{3.3}$$

where $U$ = mean flow velocity
$F_i$ = Coriolis parameter
$\rho$ = density
$\rho_r$ = reference density
$P$ = instantaneous static pressure
$\nu$ = molecular viscosity
$u$ = turbulent fluctuating velocity
$g_i$ = gravity in the $x_i$ direction
$\phi$ = scalar quantity
$\lambda$ = molecular diffusivity
$S_\phi$ = volumetric source term.

Two methods are available to determine $\overline{u_i u_j}$ and $\overline{u_i \phi}$. One method for determining turbulence correlations uses exact equations. In this method, the exact equations create higher order correlations that must then be solved or modeled. Mellor (1973) developed a method for modeling the second-order turbulence correlations using the exact equations and modeling higher order terms. Mellor and Yamada (1974, 1982) developed a series of models using the same method. However, these higher order methods require extensive computational time and are not very practical for modeling with a large number of computational cells.

The second method, which probably is simpler, is to use the concept of eddy viscosity/diffusivity to define the turbulence correlations. The concept of eddy viscosity was developed by assuming that the eddy viscosity is similar to molecular viscosity, but eddy viscosity is based on the state of the turbulence and not the properties of the fluid. Rodi (1984) developed the concept of eddy viscosity and diffusivity more fully. The simplest method is to use values specified directly for the viscosity and assume the diffusivity is a function of the eddy viscosity and the turbulent Prandtl number for heat transport or the turbulent Schmidt number for mass transport (Rodi 1984)

$$k_v = \frac{E_v}{\sigma_t} \tag{3.4}$$

where $k_v$ = eddy diffusivity
$E_v$ = eddy viscosity
$\sigma_t$ = turbulent Prandtl or Schmidt number.

However, it is not reasonable to have a constant eddy viscosity in a deep ocean. Thus, we will discuss how to obtain nonhomogeneous, anisotropic eddy viscosity/diffusivity. Three types of models use the eddy viscosity/diffusivity concept to attempt to predict the values of the turbulence correlations. One way to specify the eddy viscosity is to use a functional relationship based on depths and shear velocities similar to that developed by Munk and Anderson (1948). Because this method does not use a partial

difference equation to express turbulence process, it is called a zero-equation model. This relationship can be modified to take into account the stabilizing effects of stratification.

One-equation models are the second way of determining eddy viscosity. One-equation models work well where the length scale can be clearly defined, such as in the benthic boundary layer. If the length scale is not as clearly defined, problems arise, and thus the third method, two-equation models, was developed. The k-$\epsilon$ model is a two-equation model developed to solve production, dissipation, advection, and diffusion of turbulent kinetic energy, which are then related to the turbulence correlations.

## 3.1 ZERO-EQUATION MODELS

Equations describing the mean velocity field can be developed from the Navier-Stokes equation. To solve these equations requires that values be obtained for the turbulence correlations, $\overline{u_i u_j}$, $\overline{u_i \phi}$. If the eddy viscosity concept is used to model these turbulence correlations, then (Rodi 1984)

$$\overline{u_i u_j} = E_v \left(\frac{\partial U_i}{\partial x} + \frac{\partial U_j}{\partial x}\right) - 2/3\ k\ \delta_{ij} \tag{3.5}$$

where k = turbulence kinetic energy

All terms are known except the eddy viscosity. The first method proposed here is zero-equation models, which means they do not require the solution of any additional partial differential equations to resolve the flow field. The use of zero-equation models is limited by the fact that the transport of turbulence is not taken into account.

Specifying the eddy viscosity is one method used to obtain a closure for the turbulence equations. This can be done by specifying a constant eddy viscosity throughout the flow field or specifying the values for specific regions in the flow field. Specifying a constant-eddy viscosity is common, but it is not a true turbulence model, and the results are quite crude. In applications in the deep ocean, this method does not give an accurate representation of what is actually occurring.

As seen in Table 3.1, the eddy diffusivity varies by several orders of magnitude over the depth of the ocean, and because eddy diffusivity is directly related to the eddy viscosity, one can expect the eddy viscosity to vary also. The Prandtl or Schmidt number is assumed to be constant in most cases. The specification of regional values is an improvement, but the result is still rather crude.

An alternative to specifying values of eddy viscosity/diffusivity directly is the development of a functional relationship for the variance of the eddy viscosity/diffusivity throughout the depth. This concept has been used in estuaries and shallow ocean regions, but no study has been done for the deep oceans. In shallow regions where studies have been done, the flow never develops beyond the boundary layer, whether it is on the surface or the bottom. This results in the conclusion that it should be possible to use the current functional relationships for the boundary layers; however, these relationships will not apply in the interior. A new relationship should be developed; alternatively, it might be possible to use a constant value of eddy viscosity/diffusivity, because not much variation is expected in the interior regions.

Many methods have been developed to determine the value for the vertical eddy diffusivity for an unstratified boundary layer. Because stratification can play a major role in the stabilization of turbulent flows, methods have also been developed for modifying the eddy diffusivity as a function of the

TABLE 3.1. Variation in Eddy Diffusivity (U.S. Atomic Energy Commission 1975)

| Layer | Depth, m | Vertical Eddy Diffusivity, $K_V$, $cm^2/s$ |
|---|---|---|
| Surface | 75 | 50.0 |
| Intermediate | 500 | 0.1 |
| Deep | 2000 | 1.0 |

Richardson number (Ri). One of the first such methods was developed by Munk and Anderson (1948). The eddy viscosity for shear layers in a stratified flow is defined by

$$E_{vo} = \kappa\, z\, U_*(1 - \frac{z}{h}) \tag{3.6}$$

where $\kappa$ = von Karman's constant ($\approx$0.4)
$z$ = distance above the bottom
$U_*$ = shear velocity
$h$ = depth of flow.

To account for stratification

$$\frac{E_v}{E_{vo}} = (1 + 10\ Ri)^{-1/2} \tag{3.7}$$

and

$$\frac{K_v}{K_{vo}} = (1 + 3.33\ Ri)^{-3/2} \tag{3.8}$$

where $E_{vo}$ and $K_{vo}$ are the values of eddy viscosity and diffusivity for the neutral case. This model was found to work reasonably well for most flows, but problems occurred in situations in which mixing through and below the thermocline occurred. A site-specific method takes the form

$$\frac{E_v}{E_{vo}} = (1 + b\ Ri)^{-n} \text{ for } Ri \leq 1 \tag{3.9}$$

and

$$\frac{E_v}{E_{vo}} = (1 + b)^{-n} \text{ for } Ri > 1 \tag{3.10}$$

where b and n are empirical coefficients.

Wang (1982) used a form of the Munk and Anderson formula for modeling flows around a circular island with a shelf along the shore. Two models were run. In the first run, the shelf sloped from 40 to 200 m at the shelf break, and in the second model the depth was held constant at 100 m. The eddy viscosity and diffusivity were modeled by

$$E_v = 5 + 50\ (1 + 10\ Ri)^{-1/2} \tag{3.11}$$

$$K_v = 50\ (1 + 3.33\ Ri)^{-3/2} \tag{3.12}$$

respectively. If one compares the results for a case in which $Ri \rightarrow 0$, the values obtained compare with the values for the surface layer in Table 3.1. This is to be expected in the shallow depths being modeled.

Blumberg (1977), in a paper on estuarine circulation, used another formulation for the definition of the eddy diffusivity:

$$k_{vo} = k_1^2\ z^2\ (1 - \frac{z}{h})\ \ |(\frac{\partial u}{\partial z})| \tag{3.13}$$

where $k_1$ = empirical constant ($\approx$0.10 for tidally averaged flow)
$z$ = distance above the bottom
$h$ = depth of flow.

For diffusion adjusted for stratification:

$$K_v = k_1^2 z^2 \left(1 - \frac{z}{h}\right)^2 \left|\frac{\partial u}{\partial z}\right| \left(1 - \frac{Ri}{Ri_c}\right)^{1/2} \tag{3.14}$$

and

$$E_v = K_v (1 + Ri) \tag{3.15}$$

$Ri_c$ is the critical Richardson number beyond which turbulence is suppressed by stratification. There is some disagreement as to what this value should be. Blumberg (1977) recommends a $Ri_c$ value of 10, which seems high when compared with other recommendations. Geyer (1973) did extensive studies in the Fraser estuary and found that a $Ri_c$ of 0.25 was the point beyond which mixing is suppressed. It is possible that internal waves cause mixing to occur at higher Richardson numbers, but the maximum observed value was approximately 1. A value of 0.25 agrees with other experimental values of $Ri_c$ and is the preferred choice for a critical Richardson number.

$K_v$ will approach zero as one nears the surface (Blumberg 1977). This does not agree with the values of Table 3.1, which show the value of $K_v$ approaching 50 $cm^2/s$. This large eddy diffusivity is probably caused by wind stress on the surface and will vary with the magnitude of the stress. It is possible to avoid the eddy diffusivity approaching zero at the surface by measuring z from the surface in the upper regions.

A high eddy diffusivity is found in the upper region, where surface stresses cause active mixing. The diffusivity decreases as one reaches the middle region and remains relatively constant. Near the bottom the diffusivity again increases because of the bottom stress, although it is not as great as near the surface.

Zero-equation models are simple and have been used extensively in engineering, but the method is rather crude. Although history and transport

are not taken into account, quite good results have been obtained in some cases. If a reasonable relationship can be found for the interior region, this method is the simplest to use.

## 3.2 ONE-EQUATION MODELS

One-equation models require that one additional partial differential equation be solved to obtain a closure for the turbulence equations. The eddy viscosity is set proportional to a velocity scale and a length scale, and a partial differential equation is developed for the velocity scale. The length scale is determined by empirical means. The use of the differential equation allows the model to include the history and transport effects of the turbulence. The most common velocity scale is turbulence kinetic energy (k). The exact turbulent kinetic energy (TKE) equation can be obtained through manipulation of the Navier-Stokes equations (Rodi 1984)

$$\frac{\partial k}{\partial t} + U_i \frac{\partial k}{\partial x} = - \frac{\partial}{\partial x} \overline{\left[u_i \left(\frac{u_i u_j}{2} + \frac{P}{\rho}\right)\right]} \tag{3.16}$$

$$- \overline{u_i u_j} \frac{\partial U_i}{\partial x_j} - \beta g_i \overline{u_i \phi} - \overline{\frac{\partial u_i}{\partial x_j} \frac{\partial u_i}{\partial x_j}}$$

where $P$ = pressure

$\rho$ = density

$\beta$ = volumetric expansion coefficient

$g_i$ = gravity.

The exact equation involves the turbulence correlations and requires that several model assumptions be made to solve the equation. The diffusion flux is set proportional to the gradient of k

$$\overline{-u_i \left(\frac{u_j u_j}{2} + \frac{P}{\rho}\right)} = \frac{E_v}{\sigma_k} \frac{\partial k}{\partial x_i}$$

The dissipation is modeled by

$$\epsilon = C_D \frac{k^{3/2}}{L}$$

Using these assumptions and the eddy viscosity/diffusivity expressions for $\overline{u_i u_j}$ and $\overline{u_i \phi}$, the equation can be written as

$$\frac{\partial k}{\partial t} + U_i \frac{\partial k}{\partial x_i} = \frac{\partial}{\partial x_i} \left(\frac{E_v}{\sigma_k} \frac{\partial k}{\partial x_i}\right) + E_v \left(\frac{\partial U_i}{\partial x_j} + \frac{\partial U_j}{\partial x_i}\right) \cdot \frac{\partial U_i}{\partial x_j} + \beta g_i \frac{E_v}{\sigma_t} \frac{\partial \phi}{\partial x_i} - C_D \frac{k^{3/2}}{L} \tag{3.17}$$

where $\sigma_k$ and $C_D$ are empirical constants, and $\sigma_t$ is the turbulent Prandtl or Schmidt number.

Rodi (1984) uses the equation

$$E_v = C_E \sqrt{k}\, L \tag{3.18}$$

to define the eddy viscosity, where $C_E$ is an empirical constant, and L is a length scale. It has been found that $C_E$ and $C_D \approx 0.08$, and $\sigma_k \approx 1$. Once the eddy viscosity has been determined, the eddy diffusivity can be calculated using the Prandtl or Schmidt number, and the mean flow equations can be solved.

A one-equation model includes transport of turbulence and is therefore preferred over a zero-equation model in areas where transport is important. The difficulty with this method lies in the fact that a turbulence length scale must still be determined. In regions where a length scale can be clearly defined, the one-equation model can work quite well. A boundary

layer is an example. In areas where no length scale can be clearly defined, the method tends to break down, and two-equation models would be a better choice.

Several methods have been developed to determine the length scale. An empirical formula that uses one length scale when turbulence production dominates and a second scale when convection is dominant is described by Rodi (1984). Bernard's method seems to work well, but in some situations different constants are required to accurately describe the flow field. A common method to determine the length scale, as originally proposed by von Karman, uses local derivatives of the velocity. Gawain and Pritchett (1970) developed different methods for the length scale, but there are no data currently available to validate the models over a wide range of flows. A different one-equation model was developed by Bradshaw (1978). In this model a transport equation for the shear stress, $\overline{uv}$, was solved instead of using the eddy viscosity concept.

All these methods are fairly complicated, and some require considerable computer time because they are iterative methods. Also, all these methods were developed for wall-boundary layer flows and would require modification if they were used in a free-flow situation. The simplest methods are those based on the ideas of von Karman, which should be considered before attempting the more complicated methods of Bernard or Bradshaw (1978), in which no length scale is clearly defined.

## 3.3 TWO-EQUATION MODELS

These models require the solution of two partial different equations to obtain a closed solution of the mean velocity field equations. In the previous section, the TKE equation was presented as a velocity scale; here, an equation will be defined for the length scale. This allows the use of transport and history effects in the length scale as previously used in the velocity scale.

One of the most common ways to define the length scale is to use the rate of TKE dissipation ($\epsilon$), resulting in the k-$\epsilon$ model. Others disagree

with the term $\epsilon$ and have developed a method using the term kL where k is the TKE, and L is the length scale. These two methods are discussed below.

The transport equation for the rate of TKE dissipation is

$$\frac{\partial \epsilon}{\partial t} + U_i \frac{\partial \epsilon}{\partial x_i} = \frac{\partial}{\partial x_i} \left(\frac{E_v}{\sigma_\epsilon} \frac{\partial \epsilon}{\partial x_i}\right) + C_{1\epsilon} \frac{\epsilon}{k} (P + C_{3\epsilon} G) - C_{2\epsilon} \frac{\epsilon^2}{k} \tag{3.19}$$

where $\sigma_\epsilon$, $C_{1\epsilon}$, $C_{2\epsilon}$, and $C_{3\epsilon}$ are empirical constants, and P and G are turbulence production due to stress and buoyancy, respectively. The constants $C_{1\epsilon}$, $C_{2\epsilon}$, and $\sigma_\epsilon$ have been found to be 1.44, 1.92, and 1.3, respectively. The value for $C_{3\epsilon}$ varies depending on the flow field; when G is a source term, $C_{3\epsilon} \simeq 1.0$, and when G is a sink term, $C_{3\epsilon} \simeq 0$. There are some questions as to the validity of the constants, but they have proved accurate in many test situations and are a good starting point.

After the determination of k and $\epsilon$, the eddy viscosity and diffusivity can be found from

$$E_v = C_u \frac{k^2}{\epsilon} \tag{3.20}$$

$$K_v = \frac{E_v}{\sigma_t} \tag{3.21}$$

where $C_u$ is an empirical parameter assumed constant ($\simeq$0.09), and $\sigma_t$ is the Prandtl or Schmidt number.

There are several problems with the $\epsilon$ equation, which is based on the idea of isotropic dissipation. While this may be true sometimes, it does not allow for variation of the eddy viscosity and diffusivity in different directions, and it is known that the horizontal values of the eddy viscosity/diffusivity are several orders of magnitude greater than the vertical components. The isotropic restriction has been eased by some researchers who have varied the eddy viscosity/diffusivity in the vertical and horizontal

directions. Although this does seem to work, it does not accord with the strict definition of the equations.

Mellor and Yamada (1982) disagreed with the use of the energy dissipation rate as the length scale and have developed an equation using kL:

$$\frac{\partial kL}{\partial t} + U_i \frac{\partial kL}{\partial x_i} = \frac{\partial}{\partial x_i} \left(\sqrt{2}\, S_\ell \sqrt{k}\, L \frac{\partial kL}{\partial x_i}\right) \tag{3.22}$$

$$+ \frac{E_1}{2} L\,(P + G) - \frac{\sqrt{2}\, k^{3/2}}{B_1} \left[1 + E_2 \left(\frac{L}{\kappa L z}\right)^2\right]$$

where $S_\ell$, $E_1$, $E_2$, and $B_1$ = 0.2, 1.8, 1.33, and 16.6, respectively, and $\kappa$ is von Karman's constant ($\approx$0.4). Rodi (1987) states that the argument on the relative merits of either equation is rather academic, because both equations are fairly empirical, and with the correct constants these methods should perform satisfactorily. Mellor and Yamada (1982) believe that using $\epsilon$ is wrong because it describes small-scale turbulence, and the length scale should be based on large-scale turbulence. Either method should work satisfactorily if the correct constants are used.

A problem arises when the effects of stratification must be taken into account. It has been found in some cases that the value of $C_u$ in Equation (3.20) is not really constant but varies with the buoyancy effects. A model known as the extended k-$\epsilon$ model (algebraic stress/flux model) is given in Rodi (1987) as a method to solve the stratification problem

$$\overline{u_i u_j} = 2/3\ \delta_{ij} k + \frac{k}{C_1 \epsilon} (1 - C_2)\ [P_{ij} + G_{ij}] - 2/3\ \delta_{ij}\ (P + G) \tag{3.23}$$

$$\overline{u_i \phi} = \frac{1}{C_{1\phi}} \frac{k}{\epsilon} \left[\overline{u_i u_\ell} \frac{\partial \phi}{\partial x_\ell} + (1 - C_{2\phi})\ \left(\overline{u_\ell \phi} \frac{\partial U_i}{\partial x_\ell} + \beta g_i\, \phi^2\right)\right] \tag{3.24}$$

$$\phi^2 = -\ 2R \frac{k}{\epsilon} \overline{u_\ell \phi} \frac{\partial \phi}{\partial x_\ell}$$

where the empirical constants, $C_1$, $C_2$, $C_{1\phi}$, $C_{2\phi}$, and R are 1.8, 0.6, 3.0, 0.33, and 0.8, respectively. This method also requires the solution of the k and $\epsilon$ equations. In shear layers, the equations reduce to the original eddy viscosity/diffusivity formula of the k-$\epsilon$ model with $C_\mu$ and $\sigma_t$ depending on stratification. This method requires additional computational time, but it should more accurately define the effects of stratification.

# 4.0 MODEL DESCRIPTION

## 4.1 TEMPEST©/FLESCOT© MODEL

The TEMPEST© model is an unsteady, three-dimensional finite difference model (Trent et al. 1989; Onishi et al. 1985a,b) cast in cylindrical or Cartesian coordinates. It simulates flow, turbulent kinetic energy (TKE), heat transfer, and general dissolved mass transfer (e.g., salt). The model has been continuously updated and modified to expand its applicability to a wide range of hydrodynamic problems. For example, it is currently being modified to use an orthogonal curvilinear coordinate system. It can compute local (heterogeneous) isotropic eddy viscosity and dispersion coefficients by using the k-$\epsilon$ TKE and dissipation model if this option is chosen. Otherwise, it uses eddy viscosity as input data.

The model can calculate these variables with either the dynamic pressure approach or the hydrostatic pressure assumption based on

- conservation of mass for fluid (the continuity equation)
- conservation of momentum (the Navier-Stokes equations)
- conservation of TKE (k-$\epsilon$ model)
- conservation of heat (the first law of thermodynamics)
- conservation of mass for constituents including salt.

The FLESCOT© model is a sediment-contaminant transport version of the TEMPEST© model. Thus, it is also an unsteady, three-dimensional finite difference model (Onishi and Trent 1982). FLESCOT© simulates time-varying movements of flow, TKE, salt, heat, sediment, and dissolved and sediment-sorbed contaminants (e.g., radionuclides, heavy metals, pesticides, PCBs, etc.) in surface waters. In addition to the equations described for the TEMPEST© model, FLESCOT© has equations describing sediment-contaminant transport and accumulation on the bottom. Sediment movement and particulate contaminant transport in FLESCOT© are modeled separately for three sediment size fractions or sediment types. The sediment transport submodel includes the mechanisms of 1) advection and dispersion of sediments, 2) fall velocity and cohesiveness, 3) deposition on the seabed or ocean bottom, 4) erosion from

the bed (bed erosion and armoring), and 5) sediment contributions from point/nonpoint sources and subsequent mixing. This submodel also calculates changes in bed conditions, including bed elevation changes caused by scouring and/or disposition, and gives a three-dimensional distribution of sediment sizes within the bed. FLESCOT© also includes wave mechanisms to enhance bottom shear stress and increase suspended sediments in shallow water based on the Grant's model (Grant and Madsen 1979).

Dissolved contaminants interact both with sediments in motion (suspended and bed-load sediments) and with stationary sediments on the seabed or ocean bottom. To account for the interactions, the transport of sediment-attached contaminants in FLESCOT© is solved separately for each sediment size fraction. The model includes the mechanisms of 1) advection and dispersion of particulate contaminants; 2) adsorption/desorption of dissolved contaminants with sediment; 3) chemical and biological degradation, or radionuclide decay (if applicable) of contaminants; 4) deposition of particulate contaminants on the bed or erosion from the bed; and 5) contaminant contributions from point/nonpoint sources and subsequent mixing. The three-dimensional distributions of the particulate contaminants within the bed are also computed.

For simplicity, we use Cartesian coordinates to express governing equations of the model.

## 4.2 HYDRODYNAMIC EQUATIONS

Continuity equation

$$\frac{\partial u}{\partial x} + \frac{\partial v}{\partial y} + \frac{\partial w}{\partial z} = 0 \tag{4.1}$$

where u, v, and w = velocity components in the x-, y-, and z-directions, respectively

x, y, and z = longitudinal, lateral, and vertical (upward) directions, respectively.

Momentum equations

For the x-component,

$$\frac{\partial u}{\partial t} + \frac{\partial uu}{\partial x} + \frac{\partial uv}{\partial y} + \frac{\partial uw}{\partial z} + f_x = -\frac{1}{\rho}\frac{\partial P}{\partial x} + \frac{\partial}{\partial x}\left(\epsilon_x \frac{\partial u}{\partial x}\right) + \frac{\partial}{\partial y}\left(\epsilon_y \frac{\partial u}{\partial y}\right) + \frac{\partial}{\partial z}\left(\epsilon_z \frac{\partial u}{\partial z}\right) - \frac{1}{\rho}\left(F_x^{\,b} + F_x^{\,s}\right) \tag{4.2}$$

For the y-component,

$$\frac{\partial v}{\partial t} + \frac{\partial uv}{\partial x} + \frac{\partial vv}{\partial y} + \frac{\partial vw}{\partial z} + f_y = -\frac{1}{\rho}\frac{\partial P}{\partial y} + \frac{\partial}{\partial x}\left(\epsilon_x \frac{\partial v}{\partial x}\right) + \frac{\partial}{\partial y}\left(\epsilon_y \frac{\partial v}{\partial y}\right) - \frac{\partial}{\partial z}\left(\epsilon_z \frac{\partial v}{\partial z}\right) - \frac{1}{\rho}\left(F_y^{\,b} + F_y^{\,s}\right) \tag{4.3}$$

For the z-component,

$$\frac{\partial w}{\partial t} + \frac{\partial uw}{\partial x} + \frac{\partial vw}{\partial y} + \frac{\partial ww}{\partial z} + f_z = -\frac{1}{\rho}\frac{\partial P}{\partial z} - g + \frac{\partial}{\partial x}\left(\epsilon_x \frac{\partial w}{\partial x}\right) - \frac{\partial}{\partial y}\left(\epsilon_y \frac{\partial w}{\partial y}\right) + \frac{\partial}{\partial z}\left(\epsilon_z \frac{\partial w}{\partial z}\right) - \frac{1}{\rho} F_z^{\,b} \tag{4.4}$$

where $f_x = 2\Omega\,(w \cos\phi - v \sin\phi)$ (Coriolis force in x-direction)

$f_y = 2\Omega\, u \sin\phi$ (Coriolis force in y-direction)

$f_z = 2\Omega\, u \cos\phi$ (Coriolis force in z-direction)

$F_x^{\,b}$, $F_x^{\,s}$ = bottom shear stress and surface (wind) shear stress, respectively, in x-direction

$F_y^{\,b}$, $F_y^{\,s}$ = bottom shear stress and surface (wind) shear stress, respectively, in y-direction

$F_z^{\,b}$ = shear stress along the vertical solid boundaries

$g$ = acceleration due to gravity

$P$ = pressure

$\rho$ = water density

$\phi$ = geographical latitude

$\Omega$ = rate of earth's rotation (= $7.29 \times 10^{-5}\ s^{-1}$)

$\epsilon_x$, $\epsilon_y$, $\epsilon_z$ = eddy viscosity components in the x-, y-, and z- directions, respectively.

Note that the hydrostatic pressure assumption is not made and that the vertical momentum equation retains all terms of the flow acceleration, Coriolis, eddy viscosity, and friction, in addition to pressure and gravitational terms.

For wind shear stresses,

$$F_x^s = c^* \rho_a W_a^2 \sin \Psi \tag{4.5}$$

$$F_y^s = c^* \rho_a W_a^2 \cos \Psi \tag{4.6}$$

where $c^*$ = wind stress drag coefficient

$W_a$ = wind speed measured at some specified height (such as 10 m)

$\rho_a$ = air density

$\Psi$ = angle between the wind and current directions.

Similarly, bottom friction is commonly expressed by

$$F_x^b = a\rho u \sqrt{u^2 + v^2} \tag{4.7}$$

$$F_y^b = a\rho v \sqrt{u^2 + v^2} \tag{4.8}$$

$$F_z^b = a\rho w \sqrt{u^2 + w^2} \quad \text{or} \quad a\rho w \sqrt{v^2 + w^2} \tag{4.9}$$

where coefficient "a" is a dimensionless drag coefficient that can be correlated to Manning and Chezy coefficients. If the Chezy coefficient, C, is used, the above expressions become

$$F_x^b = \rho g \frac{u \sqrt{u^2 + v^2}}{C^2} \tag{4.10}$$

$$F_y^b = \rho g \frac{v \sqrt{u^2 + v^2}}{C^2} \tag{4.11}$$

Eddy viscosity in the Navier-Stokes equations must be either assigned as input data or internally computed based on the k-$\epsilon$ model.

In addition, the following equation of state relates fluid density to constituent concentrations (e.g., water temperature, salinity, and possibly sediment concentrations):

$$\rho = R\ (T,\ S) \tag{4.12}$$

where R = functional relationship
T = water temperature
S = salinity

Note that the water density is not a function of pressure when the incompressibility assumption is made.

The following kinematic boundary condition on the water surface is used to express a water surface

$$\frac{\partial \zeta}{\partial t} = -\ u \frac{\partial \zeta}{\partial x} - v \frac{\partial \zeta}{\partial y} + w \tag{4.13}$$

where $\zeta$ = water surface elevation.

TEMPEST©/FLESCOT© has built in two options of the pressure calculations; one is to assume the commonly-used hydrostatic pressure assumption, and the other not to assume the hydrostatic pressure assumption, thus solving Equation (4.4) with all the terms included. Solving the continuity and momentum equations is difficult, especially the iterative pressure calculation in Equations (4.2), (4.3), and (4.4). This process (dynamic pressure

calculation approach) of not assuming the hydrostatic pressure assumption is used by a few hydrodynamic models, such as TEMPEST©/FLESCOT© (Trent et al. 1989; Onishi and Trent 1982), FLOWER (Eraslan et al. 1983), and REMIXCS (Freitas et al. 1985).

Fortunately, most flows occurring in the natural environment have very small vertical velocities and essentially negligible vertical acceleration, as compared to the gravitational term. Thus, the hydrostatic pressure assumption can be made in most cases. The adaptation of the hydrostatic pressure assumption reduces the vertical equation of motion, Equation (4.4), to the following simple form:

$$\frac{\partial P}{\partial z} = - \rho g \tag{4.14}$$

where the assumption is made that the temporal and spatial vertical velocity accelerations and shear stress changes (eddy viscosity terms) are much smaller than the gravitational acceleration. Thus, under the hydrostatic pressure assumption, TEMPEST©/FLESCOT© uses Equation (4.14) instead of Equation (4.4). The vertical velocity in the Coriolis force may also be dropped in this case. Under the hydrostatic pressure assumption, the kinematic boundary condition Equation (4.13) is further simplified by dropping the water surface gradient terms in the x- and y-directions, resulting in the following equation:

$$\frac{\partial \zeta}{\partial t} \approx w \tag{4.15}$$

## 4.3 HEAT TRANSFER

### Heat transfer equation

$$\rho_o C_p \left[\frac{\partial T}{\partial t} + u \frac{\partial T}{\partial x} + v \frac{\partial T}{\partial y} + w \frac{\partial T}{\partial z}\right] = \frac{\partial}{\partial x} \left(\sigma_x \frac{\partial T}{\partial x}\right) + \frac{\partial}{\partial y} \left(\sigma_y \frac{\partial T}{\partial y}\right) + \frac{\partial}{\partial z} \left(\sigma_z \frac{\partial T}{\partial z}\right) + q_T \tag{4.16}$$

where $C_p$ = specific heat

$q_T$ = rate of heat generation or dissipation including heat loss or gain through water surface and/or ocean bottom

$\rho_0$ = fluid density

$\sigma_x$, $\sigma_y$, $\sigma_z$ = thermal conductivity in the x, y, and z directions, respectively.

## 4.4 MASS TRANSPORT

Dissolved mass transfer equation

$$\frac{\partial C}{\partial t} + u \frac{\partial C}{\partial x} + v \frac{\partial C}{\partial y} + w \frac{\partial C}{\partial z} = \frac{\partial}{\partial x} (k_x \frac{\partial C}{\partial x}) + \frac{\partial}{\partial y} (k_y \frac{\partial C}{\partial y}) + \frac{\partial}{\partial y} (k_z \frac{\partial C}{\partial z}) + q_c \tag{4.17}$$

where $C$ = concentration of mass (e.g., salt)

$k_x$, $k_y$, $k_z$ = dispersion coefficients in the x, y, and z directions, respectively

$q_c$ = rate of mass generation or dissipation.

These equations or corresponding equations in other coordinate systems are solved by many three-dimensional computer codes to obtain distributions of velocity, water temperature, salinity, and other constituents.

## 4.5 TURBULENCE EQUATIONS

Modeled transport equations for TKE, k, and dissipation of TKE, $\epsilon$, are solved to obtain the turbulent effective viscosity, $\mu_T$. As discussed in Chapter 3.0, the modeled forms of the equations are

Turbulent kinetic energy

$$\rho_0[\frac{\partial k}{\partial t} + \frac{\partial}{\partial x} (uk) + \frac{\partial}{\partial y} (uk) + \frac{\partial}{\partial Z} (wk)] = \frac{\partial}{\partial R} (\xi_k \frac{\partial k}{\partial x}) + \frac{\partial}{\partial y} (\xi_k \frac{\partial k}{\partial y}) + \frac{\partial}{\partial z} (\xi_k \frac{\partial k}{\partial z}) - \rho\epsilon + S_k \tag{4.18}$$

where $\xi_k = \mu + \frac{\mu_T}{\sigma_k}$.

$$S_k = P_k + G_k$$

Shear production

$$P_k = \mu_T \{2[(\frac{\partial u}{\partial x})^2 + (\frac{\partial v}{\partial y})^2 + (\frac{\partial w}{\partial z})^2]$$

$$+ (\frac{\partial u}{\partial y} + \frac{\partial v}{\partial x})^2 + (\frac{\partial u}{\partial z} + \frac{\partial w}{\partial x})^2 + (\frac{\partial u}{\partial z} + \frac{\partial w}{\partial y})^2\} \tag{4.19}$$

Buoyant production

$$G_k = \frac{\mu_T}{\rho\sigma_T} (\frac{\partial \rho}{\partial x} g_x + \frac{\partial \rho}{\partial y} g_y + \frac{\partial \rho}{\partial z} g_z) \tag{4.20}$$

Dissipation of turbulent kinetic energy

$$\rho_0 [\frac{\partial \epsilon}{\partial t} + \frac{\partial}{\partial x} (u\epsilon) + \frac{\partial}{\partial y} (v\epsilon) + \frac{\partial}{\partial z} (w\epsilon)]$$

$$= \frac{\partial}{\partial x} (\xi_\epsilon \frac{\partial \epsilon}{\partial x}) + \frac{\partial}{\partial y} (\xi_\epsilon \frac{\partial \epsilon}{\partial y}) + \frac{\partial}{\partial z} (\xi_\epsilon \frac{\partial \epsilon}{\partial z})$$

$$+ \frac{1}{k} (S_\epsilon - \rho C_{\epsilon 2} \epsilon) \epsilon \tag{4.21}$$

where

$$\xi_\epsilon = \mu + \frac{\mu_T}{\sigma_\epsilon}$$

$$S_\epsilon = C_{\epsilon 1} P_k + C_{\epsilon 3} G_k$$

where $\mu$ = dynamic viscosity

The turbulent viscosity, $\mu_T$, is computed using the Prandtl-Kolmolgorov hypothesis:

$$\mu_T = C_\mu \rho k^2/\epsilon \tag{4.22}$$

Recommended turbulent model constants (Jones and Launder 1973) are

| | | |
|---|---|---|
| $\sigma_T = 0.9$ | $C_{\epsilon 1} = 1.44$ | $C_\mu = 0.09$ |
| $\sigma_k = 1.0$ | $C_{\epsilon 2} = 1.92$ | |
| $\sigma_\epsilon = 1.3$ | $C_{\epsilon 3} = 1.44$ | |

## 4.6 SEDIMENT TRANSPORT EQUATION

The governing equation for the transport of the j-th sediment in the FLESCOT model is

$$\frac{\partial C_j}{\partial t} + \frac{\partial}{\partial x}(uC_j) + \frac{\partial}{\partial y}(vC_j) + \frac{\partial}{\partial z}\{(w - w_{sj})C_j\}$$

$$= \frac{\partial}{\partial x}\left(k_x \frac{\partial C_j}{\partial x}\right) + \frac{\partial}{\partial y}\left(k_y \frac{\partial C_j}{\partial y}\right) + \frac{\partial}{\partial z}\left(k_z \frac{\partial C_j}{\partial z}\right) + \left(\frac{S_{Rj}}{h} - \frac{S_{Dj}}{h}\right) + q_{cj} \tag{4.23}$$

where $C_j$ = concentration of j-th sediment
$h$ = water depth
$q_{cj}$ = rate of sediment generation
$S_{Dj}$ = j-th sediment deposition rate per unit bottom surface area
$S_{Rj}$ = j-th sediment erosion rate per unit bottom surface area
$W_{sj}$ = fall velocity of the j-th sediment.

To obtain the sediment concentration, sediment erosion and deposition rates, $S_{Rj}$ and $S_{Dj}$, are calculated for each sediment size fraction separately. For noncohesive sediment (e.g., sand), if the amount actually being transported is less than the flow can carry for given hydrodynamic conditions, the flow

will scour noncohesive sediment from the seabed and ocean bottom. This process will increase the sediment transport rate with the rate based on the difference between the sediment transport capacity of the flow and the actual sediment transport rate. The process occurs until the actual sediment transport rate becomes equal to the carrying capacity of the flow or until all the available bottom noncohesive sediment is scoured, whichever occurs first. Conversely, noncohesive sediment is deposited with the deposition rate again based on the difference between the actual sediment transport rate and sediment transport capacity of the flow. Because of the simplicity of the formulation, FLESCOT© currently uses DuBoy's formula (Vanoni 1975) to estimate the noncohesive sediment transport capacity of flow. Partheniades' (1962) and Krone's (1962) formulas are used to calculate cohesive sediment erosion and deposition rates.

FLESCOT© divides the seabed and ocean bottom into a number of bottom layers. Contaminant distributions associated with each sediment size fraction within each bottom layer are also obtained by keeping track of the amount of contaminants removed from or added to each bottom layer during the simulation period. The mechanisms of erosion and deposition of contaminated or clean sediment, and direct absorption/desorption occurring between dissolved contaminant and bottom sediment are used in determining contaminant distributions in the bottom.

## 4.7 DISSOLVED CONTAMINANT TRANSPORT EQUATION

A governing equation for a dissolved contaminant is

$$\begin{aligned}
&\frac{\partial G_w}{\partial t} + \frac{\partial}{\partial x}(uG_w) + \frac{\partial}{\partial y}(vG_w) + \frac{\partial}{\partial z}(wG_w) \\
&\quad = \frac{\partial}{\partial x}\left(k_x \frac{\partial G_w}{\partial x}\right) + \frac{\partial}{\partial y}\left(k_y \frac{\partial G_w}{\partial y}\right) + \frac{\partial}{\partial z}\left(k_z \frac{\partial G_w}{\partial z}\right) \\
&\qquad - \lambda G_w + \sum_j K_j (C_j K_{dj} G_w - G_j) + \sum_j K_j' (C_j K_{dj}' G_w - G_j) + Q_w \\
&\qquad - \frac{1}{h} \sum_j \gamma_j (1\text{-POR}) D_j K_{Bj} (K_{dj} G_w - G_{Bj}) \\
&\qquad - \frac{1}{h} \sum_j \gamma_j (1\text{-POR}) D_j K_{Bj}' (K_{dj}' G_w - G_{Bj})
\end{aligned} \tag{4.24}$$

where $D_j$ = diameter of j-th sediment size fraction

$K_{Bj}$, $K_{Bj}'$ = transfer rate of contaminants for adsorption and desorption, respectively, with j-th nonmoving sediment in bottom

$K_{dj}$, $K_{dj}'$ = distribution (or partition) coefficient between dissolved contaminant and particulate contaminant associated with j-th sediment for adsorption and desorption, respectively

$G_{Bj}$ = particulate-contaminant concentration per unit weight of sediment in j-th sediment size fraction in the bottom

$G_j$ = particulate-contaminant concentration associated with j-th sediment (radionuclide activity or weight of contaminant) per unit volume of water

$G_w$ = dissolved-contaminant concentration (radionuclide activity or weight of contaminant) per unit volume of water

$G_{wo}$ = constant concentration of dissolved contaminant

POR = porosity of bottom sediment

$Q_w$ = lateral influx or other source strength of dissolved contaminant

$\gamma_j$ = specific weight of j-th sediment

$\gamma$ = radionuclide decay, or chemical and biological degradation rates of contaminant, where applicable.

The particulate-contaminant concentration associated with sediment in the water column, $G_j$, in Equation (4.24) is expressed in terms of the contaminant weight or radionuclide activity per unit volume of water, instead of per unit weight of sediment. The printout of particulate radionuclide concentration, however, is converted to contaminant weight or radionuclide activity per unit weight of sediment.

## 4.8 SEDIMENT-SORBED CONTAMINANT TRANSPORT EQUATION

A governing equation of a sediment-sorbed contaminant associated with j-th sediment is

$$\frac{\partial G_j}{\partial t} + \frac{\partial}{\partial x}(uG_j) + \frac{\partial}{\partial y}(vG_j) + \frac{\partial}{\partial z}\{(w - w_{sj})G_j\}$$

$$= \frac{\partial}{\partial x}\left(k_x \frac{\partial G_j}{\partial x}\right) + \frac{\partial}{\partial y}\left(k_y \frac{\partial G_j}{\partial y}\right) + \frac{\partial}{\partial z}\left(k_z \frac{\partial G_j}{\partial z}\right) - \lambda G_j - \frac{S_{Dj}}{h} G_j \qquad (4.25)$$

$$+ K_j (K_{dj} C_j G_w - G_j) + K_j' (K_{dj}' C_j G_w - G_j) + \frac{G_{Bj} S_{Rj}}{h} + Q_j$$

where $Q_j$ = rate of generation of sediment-sorbed contaminant associated with j-th sediment.

Using the dynamic pressure condition, TEMPEST©/FLESCOT© solves seven unknowns (u, v, w, P, $\rho$, T, and C) with seven equations [(4.1), (4.2), (4.3), (4.4), (4.12), (4.16), and (4.17)] using the kinematic boundary condition [Equation (4.13)]. To do so, Equation (4.12) is first used to update the water density, $\rho$, with known values of T and C. Then Equations (4.2) through (4.4) are used to calculate velocity components, u, v, and w. Equation (4.1), together with some residual terms in Equations (4.2) through (4.4), are then used iteratively to update u, v, w, and P to satisfy the fluid mass balance. This iteration is needed because the values of u, v, and w calculated by Equations (4.2) through (4.4) use values of P and $\rho$ at the previous time step. These velocities do not necessarily satisfy fluid mass continuity at the present time step with a current pressure value. Corrected velocity values, through the fluid mass balance iteration

procedure, are then used to calculate T and C with Equations (4.16) through (4.25). This procedure is repeated at every time step.

Using the hydrostatic pressure assumption, the TEMPEST©/FLESCOT© model solves the unknowns faster and more easily. As before, $\rho$ is first updated using the known values of T and C. Then by using the horizontal momentum equations [Equations (4.2) and (4.3)], the horizontal velocity components, u and v, are calculated with known values of P and $\rho$. By using calculated u and v, the vertical velocity, w, is then computed using the continuity Equation (4.1) alone. The new water surface is then computed by Equation (4.15). A new pressure distribution is calculated from Equation (4.14) with the new water surface elevation. The calculated u, v, and w are then used to calculate T and C with Equations (4.16) through (4.25).

This much simpler hydrostatic pressure approach to calculate velocity and pressure is much faster (one to two orders) than using the dynamic pressure approach. The vertical velocity calculation is decoupled from the horizontal velocity calculations, and there is no need to iterate to obtain the pressure value.

However, the hydrostatic pressure assumption is less applicable to an area where vertical velocity and acceleration are important. Potential computational errors with the hydrostatic pressure assumption are potentially greater than those associated with the dynamic pressure assumption because any computational mass balance errors in u and v calculations with Equations (4.2) and (4.3) will be absorbed by the vertical velocity, water surface, and pressure calculations without corrective (iterative) actions taken by the dynamic pressure approach.

# 5.0 MODEL APPLICATIONS

The TEMPEST©/FLESCOT© code was applied to a two-dimensional, 3000-m-deep, rectangular basin to conduct a preliminary examination of the code applicability to a deep-ocean environment. First, the code was applied to calculate the vertical eddy viscosity. With this calculated eddy viscosity, the code then calculated the flow, water temperature, sediments, and radionuclide distributions.

## 5.1 EDDY VISCOSITY DISTRIBUTIONS

The code was applied to a 12,000-m-long, 3000-m-deep rectangular basin under three stratified and nonstratified conditions. For three sets of eddy viscosity calculations, we used the dynamic pressure approach, even though the hydrostatic pressure approach can also be used for these cases. Note that we used computational cells near the bottom with very small vertical increments (0.1 m) to obtain the detailed distributions of flow, turbulence, and eddy viscosity near the bottom. Because the longitudinal grid spacing is fixed at 500 m, there is a large aspect ratio of computational cells near the bottoms, and their impact on the k-$\epsilon$ model is not clarified in this study. In all simulation cases in this study, initial and boundary velocity distributions were assigned a constant value of 0.1 m/s.

### 5.1.1 Nonstratified Case (Case 1)

The first case was the nonstratified condition with water temperature of 10°C and salinity of 32‰ over the entire flow region. After 2 days of simulations, distributions of calculated turbulent kinetic energy (TKE), turbulent energy dissipation, and eddy viscosity are shown in Figures 5.1 through 5.3 over the entire flow region. Contour levels for TKE (Figure 5.1) are $1 \times 10^{-10}$, $1 \times 10^{-8}$, $1 \times 10^{-6}$, $5 \times 10^{-6}$, $1 \times 10^{-5}$, $1.5 \times 10^{-5}$, $2 \times 10^{-5}$, and $3 \times 10^{-5}$ $m^2/s^2$. Contour levels for turbulent energy dissipation (Figure 5.2) are $1 \times 10^{-15}$, $1 \times 10^{-12}$, $1 \times 10^{-10}$, $1 \times 10^{-9}$, $5 \times 10^{-9}$, $1 \times 10^{-8}$, $5 \times 10^{-8}$, $1 \times 10^{-7}$, $5 \times 10^{-7}$, and $1 \times 10^{-6}$ $m^2/s^3$. For the eddy viscosity, the contour levels used in Figure 5.3 are $1 \times 10^{-4}$, $5 \times 10^{-4}$, $1 \times 10^{-3}$, $5 \times 10^{-3}$, $1 \times 10^{-2}$, $5 \times 10^{-2}$, $1 \times 10^{-1}$, $5 \times 10^{-1}$, 1, 5, 10, 15, and 20 Pascal-seconds. Note that these values are highest near the bottom and

rapidly become smaller as the distance from the bottom increases. Vertical contour lines shown in Figures 5.1 and 5.3 are due to extremely small values assigned at the upstream boundary. Figures 5.4 through 5.6 show these values within approximately 70 m of the bottom. Contour levels for TKE (Figure 5.4) and turbulent energy dissipation (Figure 5.5) are the same as those used for Figures 5.1 and 5.2, respectively. Contour levels for the eddy viscosity (Figure 5.7) are the same as those used for Figure 5.3, except the levels of $1 \times 10^{-4}$ and $5 \times 10^{-4}$ Pascal-seconds were eliminated in Figure 5.7. Figures 5.7 through 5.9 show the vertical distribution of TKE, turbulent energy dissipation, and eddy viscosity at 10,000 m downstream. Figures 5.4 and 5.5 as well as Figures 5.7 and 5.8 reveal that the TKE is generated most at the bottom and also that the turbulent energy is dissipated most at the bottom. Figures 5.6 and 5.9 indicate that the eddy viscosity calculated by the k-$\epsilon$ model increases originally with the vertical distance from the bottom almost linearly until it peaks out around 30 m from the bottom. The values of eddy viscosity sharply dropped down to the level near the molecular viscosity level around 65 m from the bottom. The TKE and eddy viscosity reduce their calculated values sharply with the vertical distance beyond approximately 45 m from the bottom. This is due to the fact that the vertical gradient of the calculated longitudinal velocity above 45 m is almost zero (i.e., the longitudinal velocity above 45 m reaches its uniform value of 0.1 m/s), thus no shear production of TKE due to the velocity gradient (see Equation 4.19) above 45 m. This results in sharp reduction of the TKE and eddy viscosity values above that height. The maximum calculated eddy viscosity after 2 days of simulation is approximately 20 pascal-seconds (or 200 $cm^2/s$) occurring around 30 to 45 m above the bottom. This value is higher than those shown in Table 3.1. This high value of calculated eddy viscosity for this case may be due to the lack of stratification which suppresses the TKE, thus the eddy viscosity. As we discussed under Case 3 with stratification near the bottom, the calculated eddy viscosity values near the bottom are very close to 1 $cm^2/s$ report in Table 3.1. However, there are no values available to specifically compare to this case. Resulting calculated velocity distribution is shown in Figure 5.10., displaying well-developed flattened velocity profiles.

### 5.1.2 Stratified Cases (Cases 2 and 3)

There were two stratified cases examined in this study. Note that the stratification was imposed by water temperature distribution, not by the salinity distribution, both of which are shown in Tables 5.1 and 5.2.

TABLE 5.1. Initial Water Temperature and Salinity Distribution for Case 2

| Distance from the Bottom, m | Water Temperature, °C | Salinity, ‰ |
|---|---|---|
| 2960 - 3000 | 16 | 32 |
| 2930 - 2960 | 13 | 32 |
| 150 - 2930 | 10 | 32 |
| 120 - 150 | 6 | 32 |
| 0 - 120 | 2 | 32 |

TABLE 5.2. Initial Water Temperature and Salinity Distribution for Case 3

| Distance from the Bottom, m | Water Temperature, °C | Salinity, ‰ |
|---|---|---|
| 2960 - 3000 | 16 | 32 |
| 2950 - 2960 | 13 | 32 |
| 7.5 - 2950 | 10 | 32 |
| 6.0 - 7.5 | 6 | 32 |
| 0 - 6 | 2 | 32 |

Calculated TKE, turbulent energy dissipation, and corresponding eddy viscosity over the entire flow field for Case 2 are shown in Figures 5.11 through 5.13. Those within 70 m from the bottom are shown in Figures 5.14 through 5.16. Contour level, for Figure 5.11 through 5.16 are the same as those used in corresponding figure for case 1 Figures 5.1 through 5.6. Vertical distributions of TKE, turbulent energy dissipation and eddy viscosity at 10,000 m downstream are shown in Figures 5.17 through 5.19. These figures show the small reduction of these values from those obtained under the nonstratified case (Case 1) discussed above because of the

stratification. For Case 2, the maximum calculated eddy viscosity is approximately 17 Pascal-seconds (170 $cm^2/s$) occurring at 45 m above the bottom. This is due to the fact that the existance of the density gradient reduces both the TKE and the dissipation of turbulent kinetic energy through the negative buoyant production (see Equations 4.18, 4.20, and 4.21). The net result is also the reduction of the eddy viscosity. However, since the TKE is generated near the bottom and the initial water temperature was constant (2°C) at bottom 200 m, effects of stratification on TKE, the turbulent energy dissipation, and eddy viscosity were very small, as compared to those of Case 1. Note that because of the density gradient occurring around 120 to 150 m from the bottom, calculated longitudinal velocity did not become uniform until approximately 250 m above the bottom. This results in more gradual variations of the TKE and eddy viscosity values in the bottom 78 m area (Figures 5.17 and 5.19), as compared to those of Case 1 (Figures 5.7 and 5.9). The calculated velocity distribution is shown in Figure 5.20.

To further test stratification effects on TKE dissipation, thus on eddy viscosity, the code was applied under Case 3 conditions having water temperature gradients including that at 6 to 7.5 m above the bottom (see Table 5.2). Corresponding calculated distributions are shown in Figures 5.21 through 5.30. Contour levels of TKE used in Figures 5.21 and 5.24 are $1 \times 10^{-10}$, $1 \times 10^{-9}$, $1 \times 10^{-8}$, $5 \times 10^{-8}$, $1 \times 10^{-7}$, $5 \times 10^{-7}$, $1 \times 10^{-6}$, and $5 \times 10^{-6}$ $m^2/s^2$. Contour levels of turbulent energy dissipation used in Figures 5.22 and 5.25 are $1 \times 10^{-13}$, $1 \times 10^{-12}$, $1 \times 10^{-11}$, $1 \times 10^{-9}$, $5 \times 10^{-9}$, $1 \times 10^{-8}$, $5 \times 10^{-8}$, and $1 \times 10^{-7}$ $m^2/s^3$. Contour levels of the eddy viscosity, (Figures 5.23 and 5.26) are $1 \times 10^{-4}$, $5 \times 10^{-4}$, $1 \times 10^{-3}$, $5 \times 10^{-3}$, $1 \times 10^{-2}$, $5 \times 10^{-2}$, $1 \times 10^{-1}$, and $2 \times 10^{-1}$ Pascal-seconds. Since Case 3 has a density gradient near the bottom (6 to 7.5 m above the bottom), where the activities of the TKE and turbulent energy dissipation are the greatest, this case clearly demonstrates the suppression effect of stratification (buoyant production term, Equation 4.20) on the TKE, turbulent energy dissipation, and eddy viscosity, especially the TKE and eddy viscosity. The reduction of the TKE and eddy viscosity are significant. Note the significant reduction of

computed eddy viscosity in this case, having the maximum eddy viscosity values of approximately 0.2 Pascal-second (2 $cm^2/s$) at 1 m above the bottom, as compared with the maximum value of 20 Pascal-seconds (200 $cm^2/s$) for the non-stratified Case 1. The calculated eddy viscosity of 2 $cm^2/s$ for this case agrees well with the vertical eddy diffusivity of 1.0 $cm^2/s$ estimated by U.S. AEC (1975) at 2000 m deep (see Table 3.1). The density gradient near the bottom also changed the computed velocity distribution near the bottom, as follows: the longitudinal velocity in this case reaches its uniform values of approximately 0.2 m/s closer to the bottom, around 20 m above the bottom. However, within the bottom 20 m, a velocity variation, especially those at the bottom 0.5 m, is much more gradual with the vertical distance, displaying a more parabolic character than the flattened turbulent velocity distribution displayed under Cases 1 and 2.

The model results demonstrate that the density gradient must be considered for the eddy viscosity calculation, and that the k-$\epsilon$ model reproduces at least qualitatively the vertical eddy viscosity variation occurring in a deep ocean environment. Although we have not applied the k-$\epsilon$ model to a three-dimensional deep water case yet, the TEMPEST© code was previously successfully applied to three-dimensional thermal plume cases to calculate the turbulence with the k-$\epsilon$ model.

## 5.2 RADIONUCLIDE DISTRIBUTIONS

### 5.2.1 Simulation Conditions

With the eddy viscosity calculated by Cases 1 and 2, three additional cases (Cases 4 through 6) were simulated to obtain the following distributions:

- velocity
- water temperature
- suspended sand concentration
- suspended silt concentration
- suspended clay concentration
- dissolved radionuclides

- radionuclide sorbed by sand
- radionuclide sorbed by silt
- radionuclide sorbed by clay.

Note that the code also calculated the change on bottom conditions; that is, the radionuclide distribution sorbed by the three fractions (sand, silt, and clay) of bottom sediment.

In all three cases (Cases 4 through 6), it was assumed that there were no radionuclides in the water column initially, and the radionuclides originally existed only in the bottom sediment of the 500-m reach between 2000 and 2500 m from the upstream end of the study area. Conditions imposed in Cases 4 through 6 are shown in Table 5.3. Note that to save computation time, the hydrostatic pressure approach was selected for Cases 4 through 6.

Eddy viscosity at each computational cell for all three cases was assigned as follows to allow non-isotropic field of eddy viscosity:

Vertical eddy viscosity

= molecular viscosity + eddy viscosity calculated by corresponding Case 1 or 2

Longitudinal eddy viscosity

= molecular viscosity + eddy viscosity calculated by corresponding Case 1 or 2

\+ oceanic longitudinal/lateral eddy viscosity assumed to be 1000 Pascal-seconds in this study

Non-isotropic dispersion coefficients were estimated by the corresponding eddy viscosity and Schmidt/Prandtl numbers (which are assumed to be 0.71) by using Equation 3.4.

TABLE 5.3. Simulation Conditions and Model Parameters for Cases 4 through 6

| | Case 4 | Case 5 | Case 6 |
|---|---|---|---|
| Stratified Condition | Same as Case 2 | Same as Case 2 | Same as Case 1 |
| Sediment Diameter (mm) | | | |
| Sand | 0.25 | 0.25 | 0.25 |
| Silt | 0.016 | 0.016 | 0.016 |
| Clay | 0.002 | 0.002 | 0.002 |
| Sediment Specific Weight ($g/cm^3$) | | | |
| Sand | 2.65 | 2.65 | 2.65 |
| Silt | 2.65 | 2.65 | 2.65 |
| Clay | 2.65 | 2.65 | 2.65 |
| Sediment Settling Velocity (m/s) | | | |
| Sand | $5 \times 10^{-3}$ | $5 \times 10^{-3}$ | $5 \times 10^{-3}$ |
| Silt | $5 \times 10^{-6}$ | $5 \times 10^{-6}$ | $5 \times 10^{-6}$ |
| Clay | $1 \times 10^{-6}$ | $1 \times 10^{-6}$ | $1 \times 10^{-6}$ |
| Initial Sediment Concentration in Water Column (mg/L) | | | |
| Sand | 0 | 0 | 0 |
| Silt | 0.1 | 100 | 100 |
| Clay | 0.1 | 100 | 100 |
| Initial Sediment Fraction in Bottom | | | |
| Sand | 0.2 | 0.2 | 0.2 |
| Silt | 0.6 | 0.6 | 0.6 |
| Clay | 0.2 | 0.2 | 0.2 |
| Radionuclide Concentration at the Bed Source (mCi/g) | | | |
| Sorbed by bed sand | 0.001 | 0.001 | 0.001 |
| silt | 1 | 1 | 1 |
| clay | 5 | 5 | 5 |
| Distribution Coefficient $K_d$ ($cm^3/g$) with | | | |
| Sand | 0.02 | 0.02 | 0.02 |
| Silt | 20 | 20 | 20 |
| Clay | 100 | 100 | 100 |
| Adsorption/Desorption Rate, $K_j$ (1/s) | | | |
| Sand | $1 \times 10^{-6}$ | $1 \times 10^{-6}$ | $1 \times 10^{-6}$ |
| Silt | $1 \times 10^{-6}$ | $1 \times 10^{-6}$ | $1 \times 10^{-6}$ |
| Clay | $1 \times 10^{-6}$ | $1 \times 10^{-6}$ | $1 \times 10^{-6}$ |

### 5.2.2 Simulation Results of Stratified Case 4

As stated above, by using the eddy viscosity calculated above, the code then simulated radionuclide transport phenomena. Because of the very small vertical grid spacing near the bottom with a total water depth of 3000 m, we used a 0.1-s time step for Cases 4 through 6 to ensure the computational stability. The calculated results are those obtained after 6 h of simulation. Radionuclide concentrations have not reached in a final steady state yet.

The model predicted that a small portion of radionuclide sorbed by bottom sediment leached out to the overlying water volume. Once in the water column, some leached, dissolved radionuclides were then transported downstream by the current. Moreover, some of them were then adsorbed by suspended silt and clay. The model predicted that the ratio of the radionuclide sorbed by suspended silt and clay is equal to the ratio of the distribution coefficients associated with silt and clay. According to the model prediction, the originally clear bottom sediment downstream of the contaminated bottom portion, then adsorbs a fraction of the radionuclide in the water column back into the bed.

Figures 5.31 through 5.33 show the predicted distribution for dissolved, suspended-silt-sorbed and suspended-clay-sorbed radionuclides in the water column up to 40 m above the bottom. Note that the unit of dissolved concentration is pCi/L, while the sediment-sorbed radionuclide concentrations are in pCi/g. Table 5.4 shows the predicted radionuclide distribution in the top 3-cm bed layer in pCi/g. Note that the bottom sediment between 2000 to 2500 m is the original radionuclide source.

### 5.2.3 Simulation Results of Stratified Case 5

The only difference between Cases 4 and 5 is that the suspended sediment concentration for Case 5 has 1000 times higher values than those of Case 4. Although the sediment concentration of 200 mg/L is not reasonable, this case was performed to examine the effect of sediment concentration on the

TABLE 5.4. Calculated Radionuclide Concentration Sorbed by Bed Sediment in the Top 3-cm Bed Layer After 6 h Simulation

| Downstream Distance, m | Radionuclide Concentration, pCi/g | | | |
|---|---|---|---|---|
| | Sand | Silt | Clay | Composite Sediment |
| 2000 - 2500 (source) | $9.993 \times 10^{-4}$ | $9.9998 \times 10^{-1}$ | 4.99996 | 1.60018 |
| 2500 - 3000 | $5.99 \times 10^{-13}$ | $1.60 \times 10^{-11}$ | $3.00 \times 10^{-11}$ | $1.59 \times 10^{-11}$ |
| 3000 - 3500 | $2.25 \times 10^{-13}$ | $5.99 \times 10^{-12}$ | $1.12 \times 10^{-11}$ | $5.89 \times 10^{-12}$ |
| 3500 - 4000 | $9.98 \times 10^{-14}$ | $2.64 \times 10^{-12}$ | $4.94 \times 10^{-12}$ | $2.59 \times 10^{-12}$ |
| 4000 - 4500 | $4.47 \times 10^{-14}$ | $1.19 \times 10^{-12}$ | $2.23 \times 10^{-12}$ | $1.17 \times 10^{-12}$ |
| 4500 - 5000 | $1.96 \times 10^{-14}$ | $5.24 \times 10^{-13}$ | $4.82 \times 10^{-13}$ | $5.14 \times 10^{-13}$ |

radionuclide transport. Even though normal sediment concentrations in the deep ocean near the 3800-m site are 0.02 to 0.1 mg/L, there were also measurements indicating the suspended sediment concentration near the ocean bottom can be up to 100 mg/L.

Figures 5.34 through 5.36 show the computed radionuclide results. Sediment-sorbed radionuclide concentrations per unit weight of sediment are almost identical to those of Case 4. Thus, the sediment sorbed concentration per unit volume of water in this case is 1000 times higher than those of Case 4. Although dissolved concentrations calculated for Case 5 are smaller than those of Case 4, additional adsorption by the greater amount of suspended sediment for Case 5 is still too small to be discernable in these figures. These results indicate the predictable effect of suspended sediment concentrations on the radionuclide distribution.

### 5.2.4 Simulation Results of Nonstratified Case 6

This is the same as Case 5 except that there is not stratification caused by water temperature. Computed results are shown in Figures 5.37 through 5.39, displaying the almost identical distributions as those shown in Case 5. Close comparisons of computed radionuclide concentrations of Cases 5 and 6 revealed up to several percent differences in concentrations between

these two cases, due to slightly different eddy viscosity values calculated for the stratified and non-stratified cases. If we run a case with a much smaller eddy viscosity calculated by the stratified Case 3, we expect to see much more drastic difference in computed radionuclides. Although under this study we did not apply the FLESCOT© code to three-dimensional cases, the model has been applied to calculate these quantities in three-dimensional shallow estuarine/coastal waters (Onishi et al. 1985).

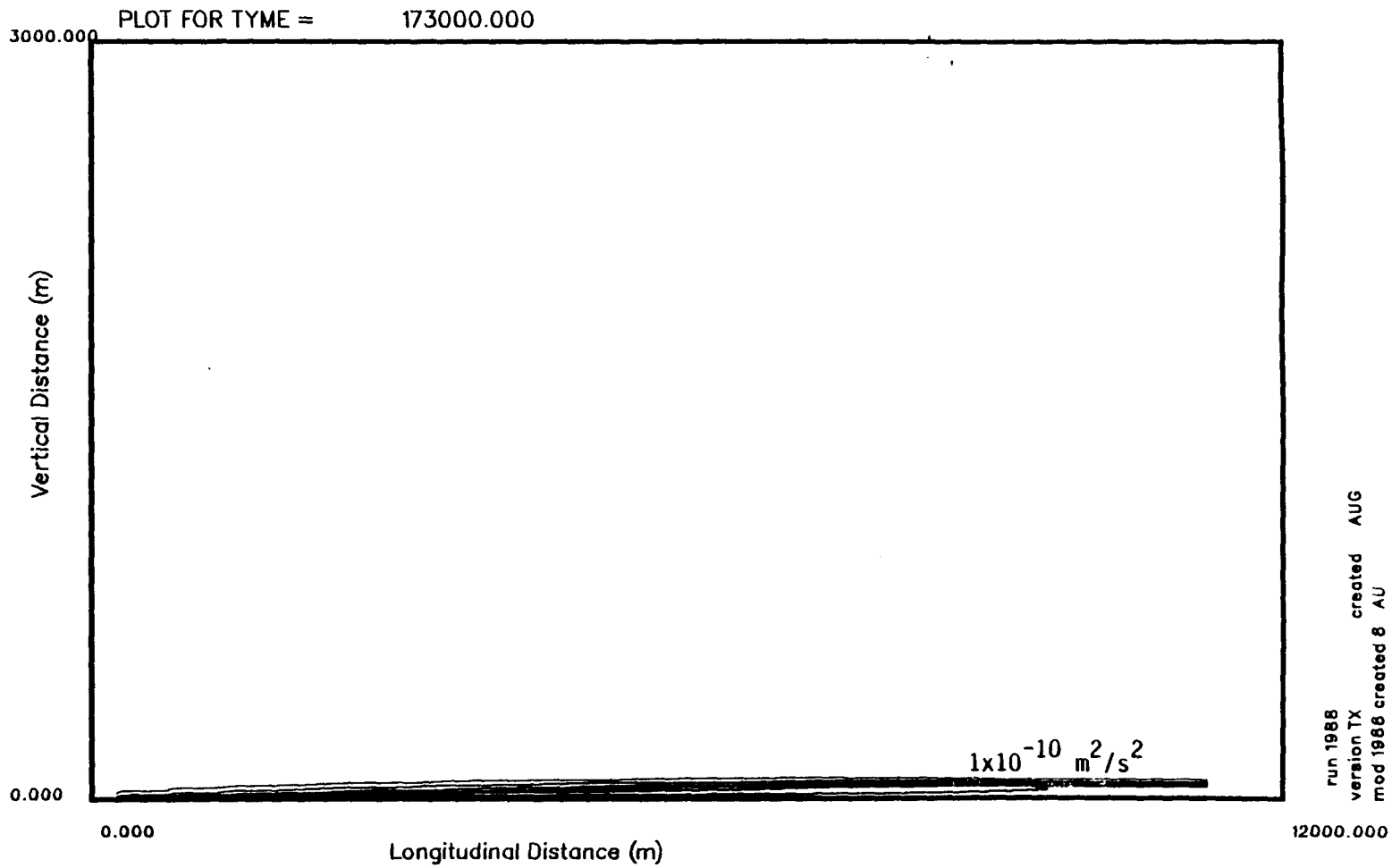


FIGURE 5.1. Calculated Turbulent Kinetic Energy Over the Whole Flow Region for Nonstratified Case 1

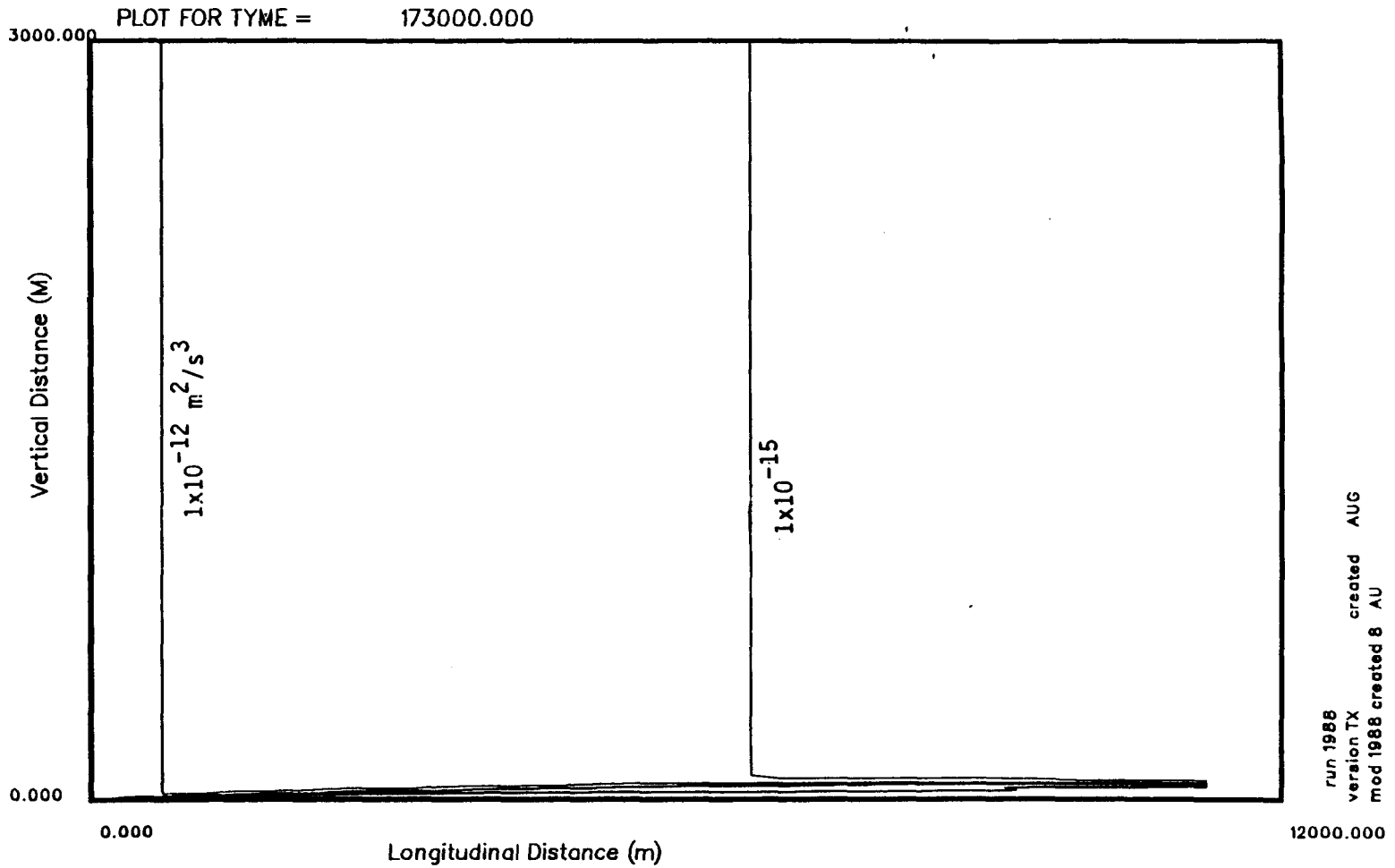


FIGURE 5.2. Calculated Turbulent Energy Dissipation Over the Whole Flow Region for the Nonstratified Case 1

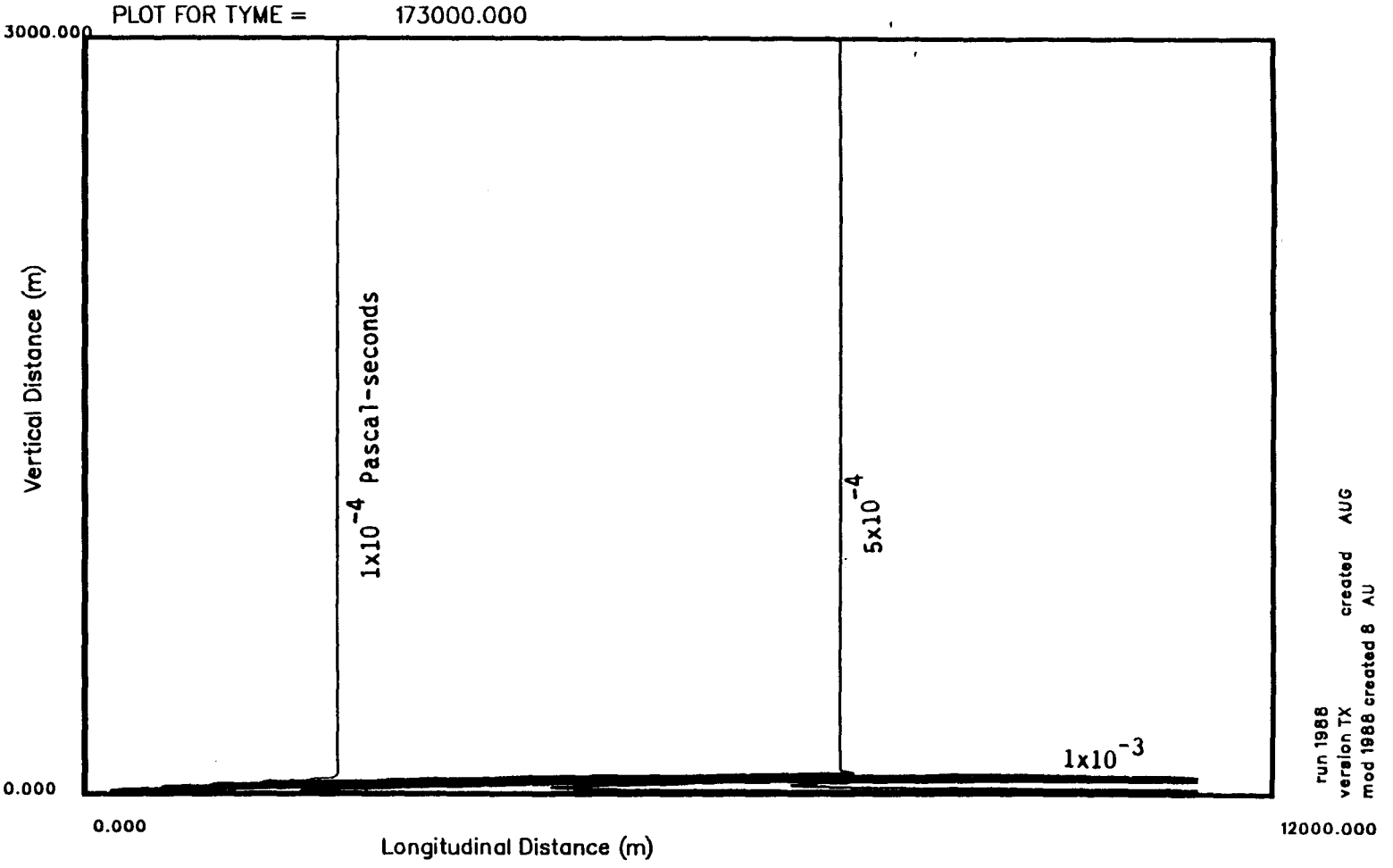


FIGURE 5.3. Calculated Eddy Viscosity Over the Whole Flow Region for the Nonstratified Case 1

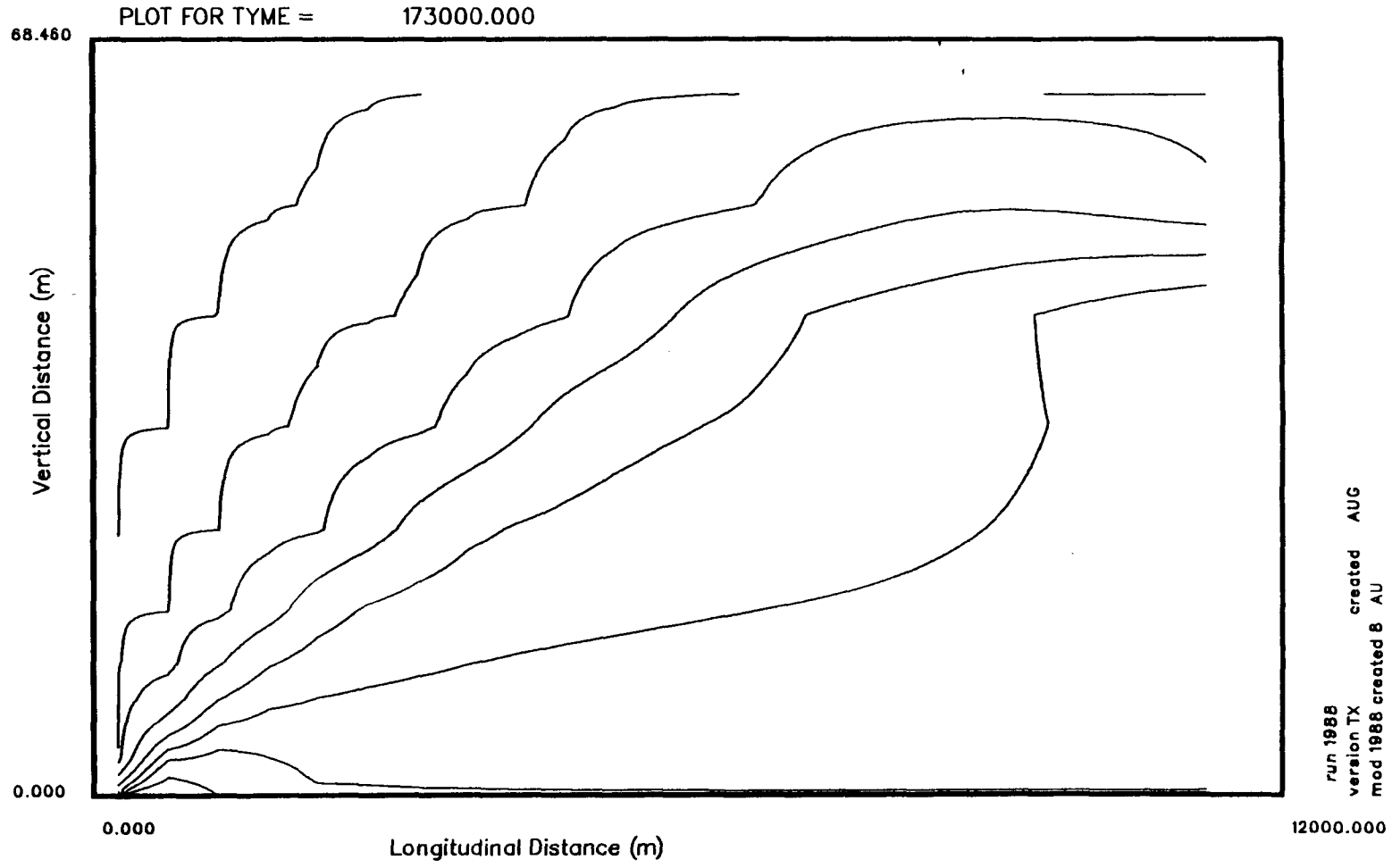


FIGURE 5.4. Calculated Turbulent Kinetic Energy Near the Bottom for the Nonstratified Case 1

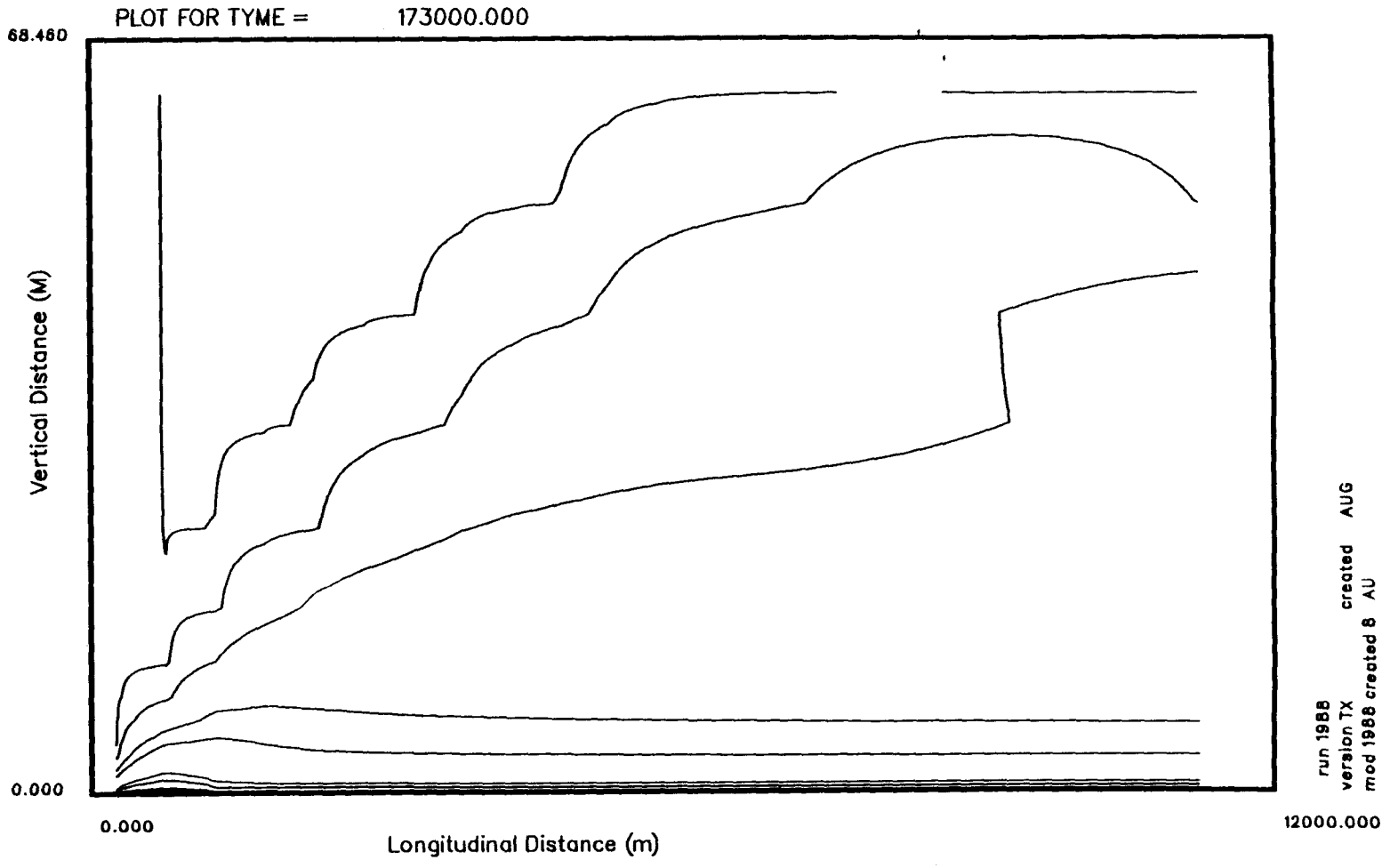


FIGURE 5.5. Calculated Turbulent Energy Dissipation Near the Bottom for the Nonstratified Case 1

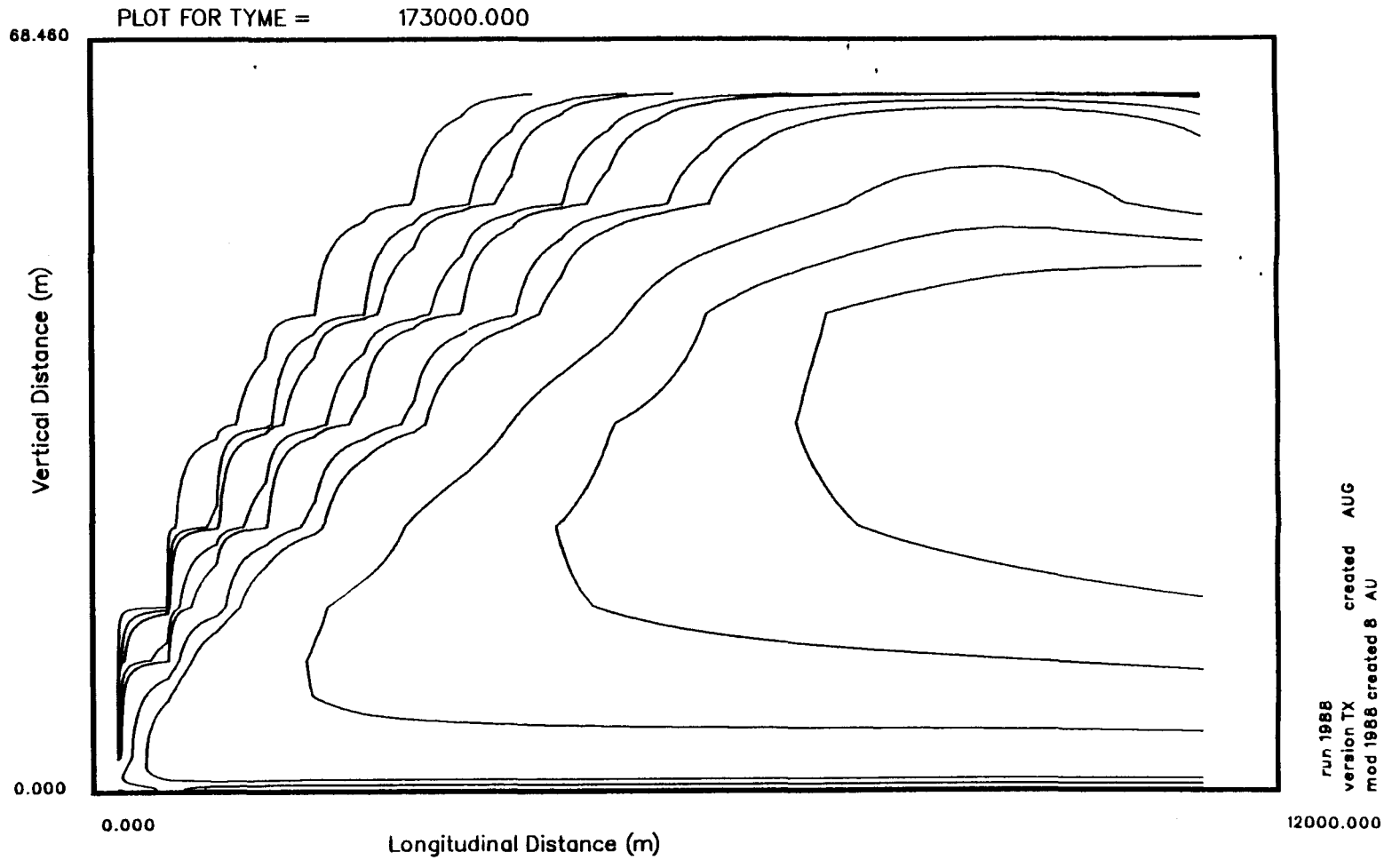


FIGURE 5.6. Calculated Eddy Viscosity Near the Bottom for the Nonstratified Case 1

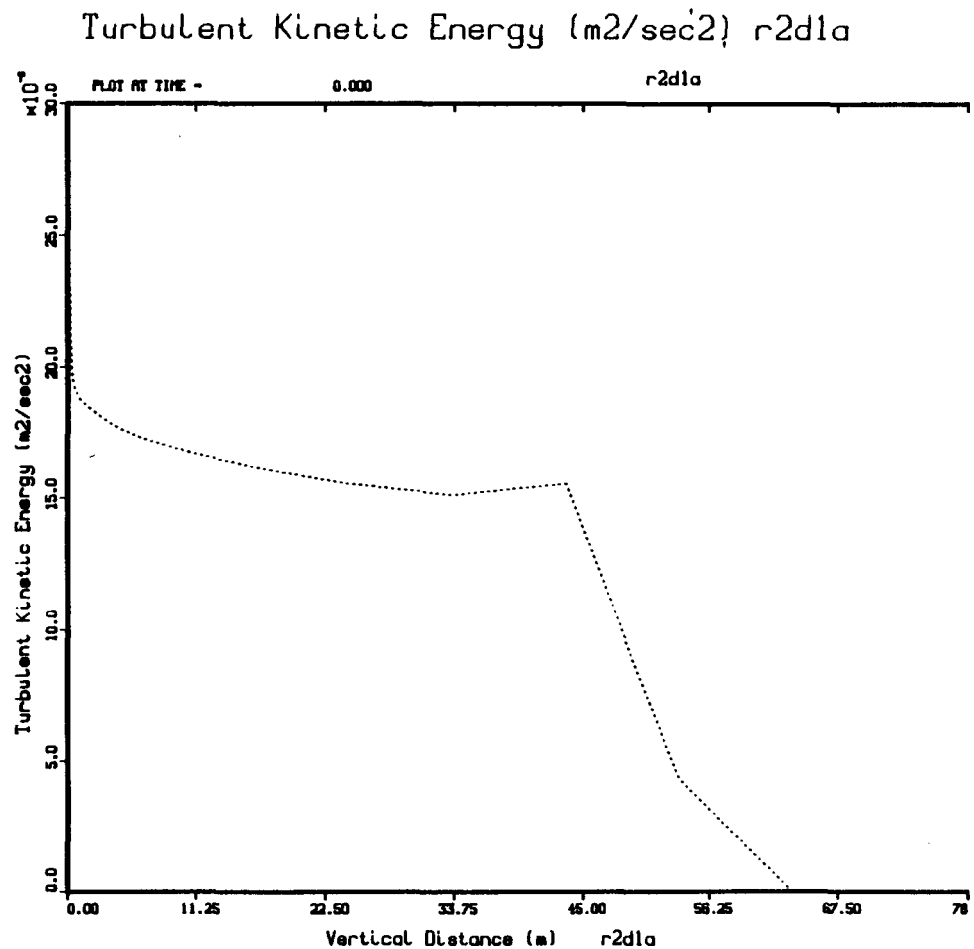


FIGURE 5.7. Vertical Distribution of Calculated Turbulent Kinetic Energy Near the Bottom for the Nonstratified Case 1

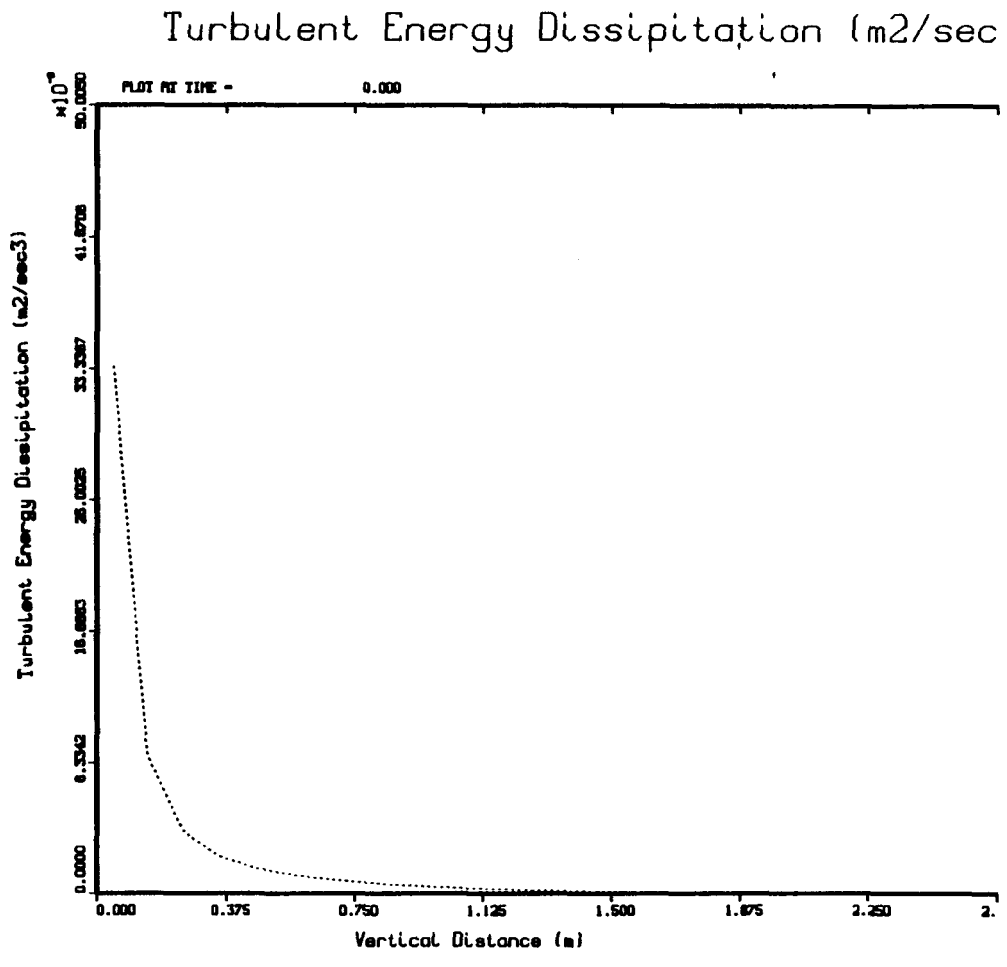


Figure 5.8. Vertical Distribution of Calculated Turbulent Energy Dissipation Near the Bottom for the Nonstratified Case 1

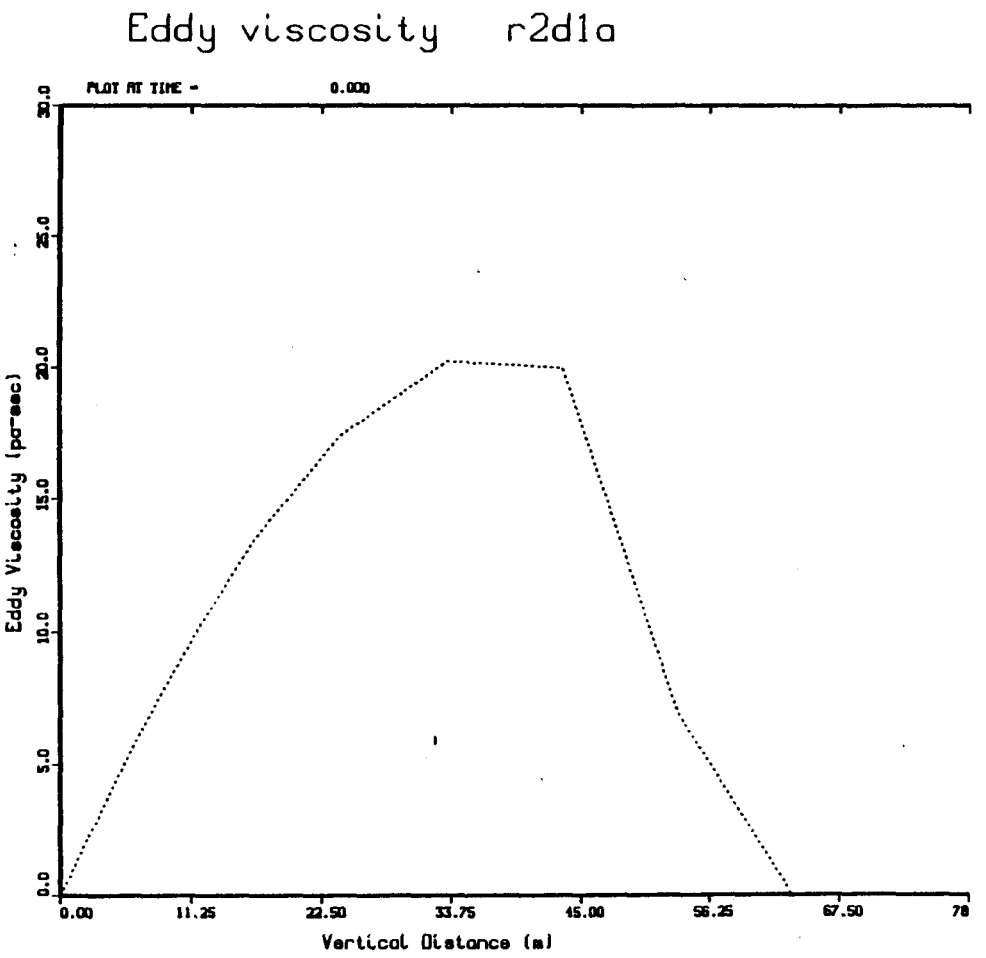


FIGURE 5.9. Vertical Eddy Viscosity Near the Bottom for the Nonstratified Case 1

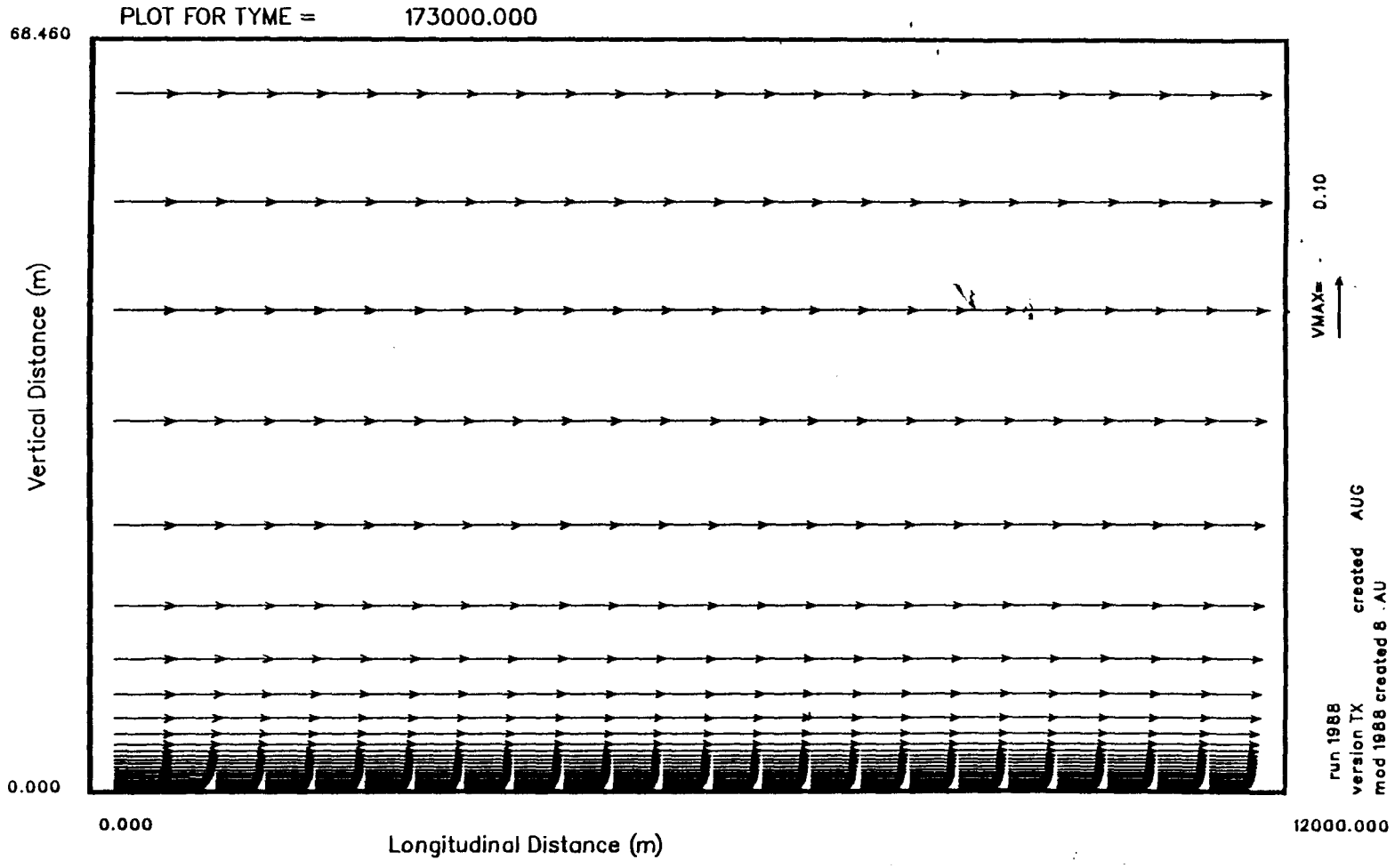


FIGURE 5.10. Calculated Velocity Distribution Near the Bottom for the Nonstratified Case 1

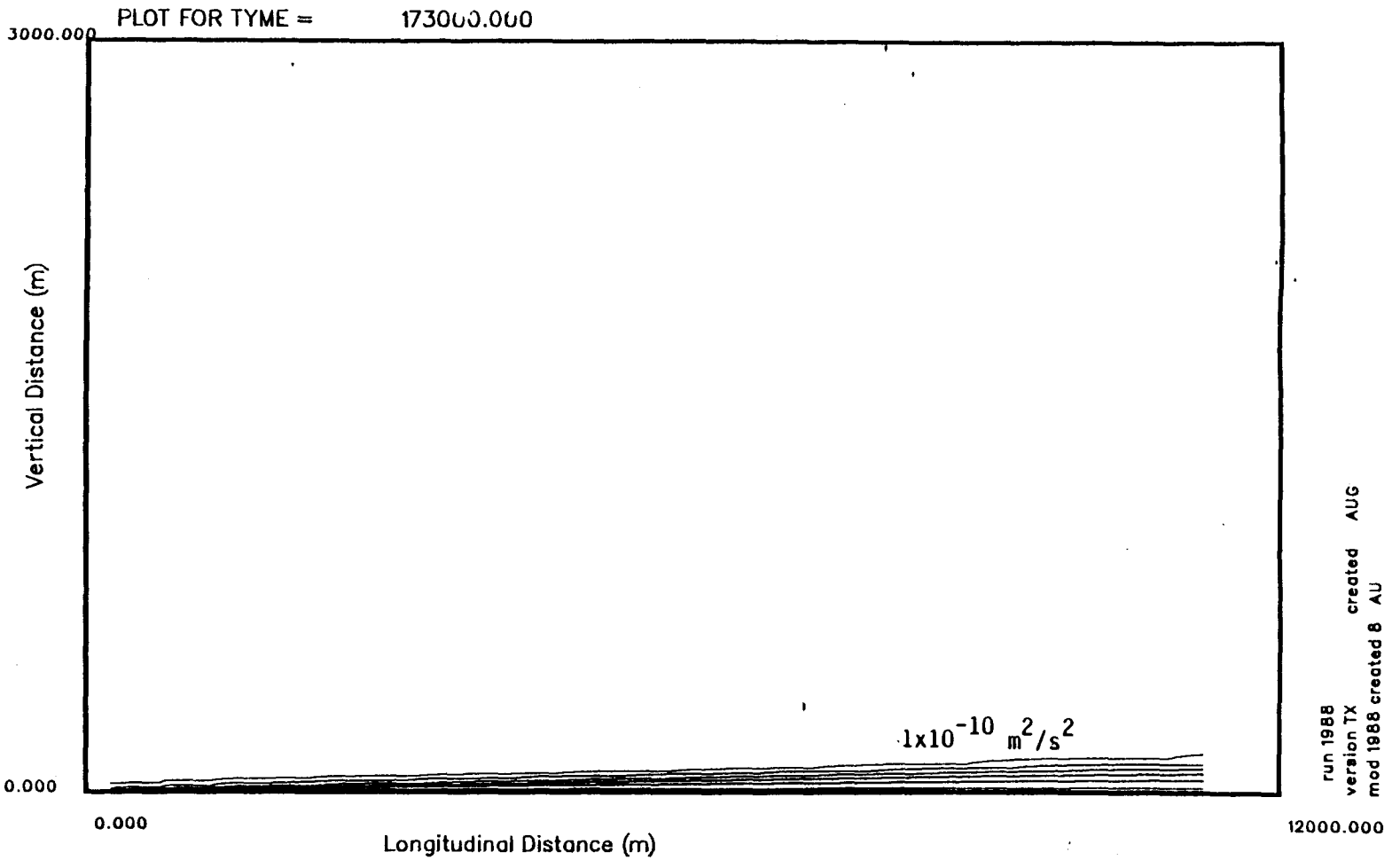


FIGURE 5.11. Calculated Turbulent Kinetic Energy Over the Whole Flow Region for Stratified Case 2

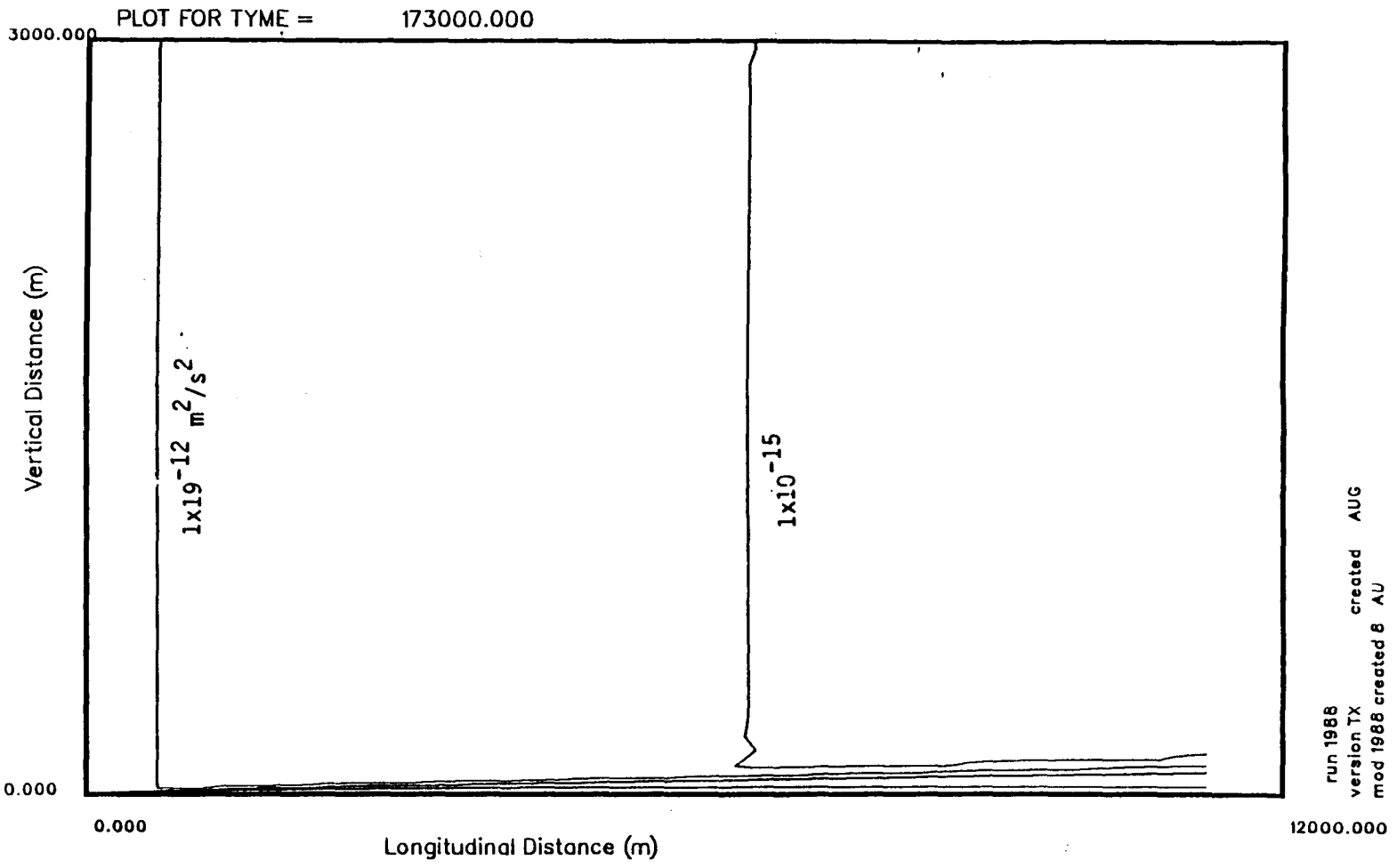


FIGURE 5.12. Calculated Turbulent Energy Dissipation Over the Whole Flow Region for the Stratified Case 2

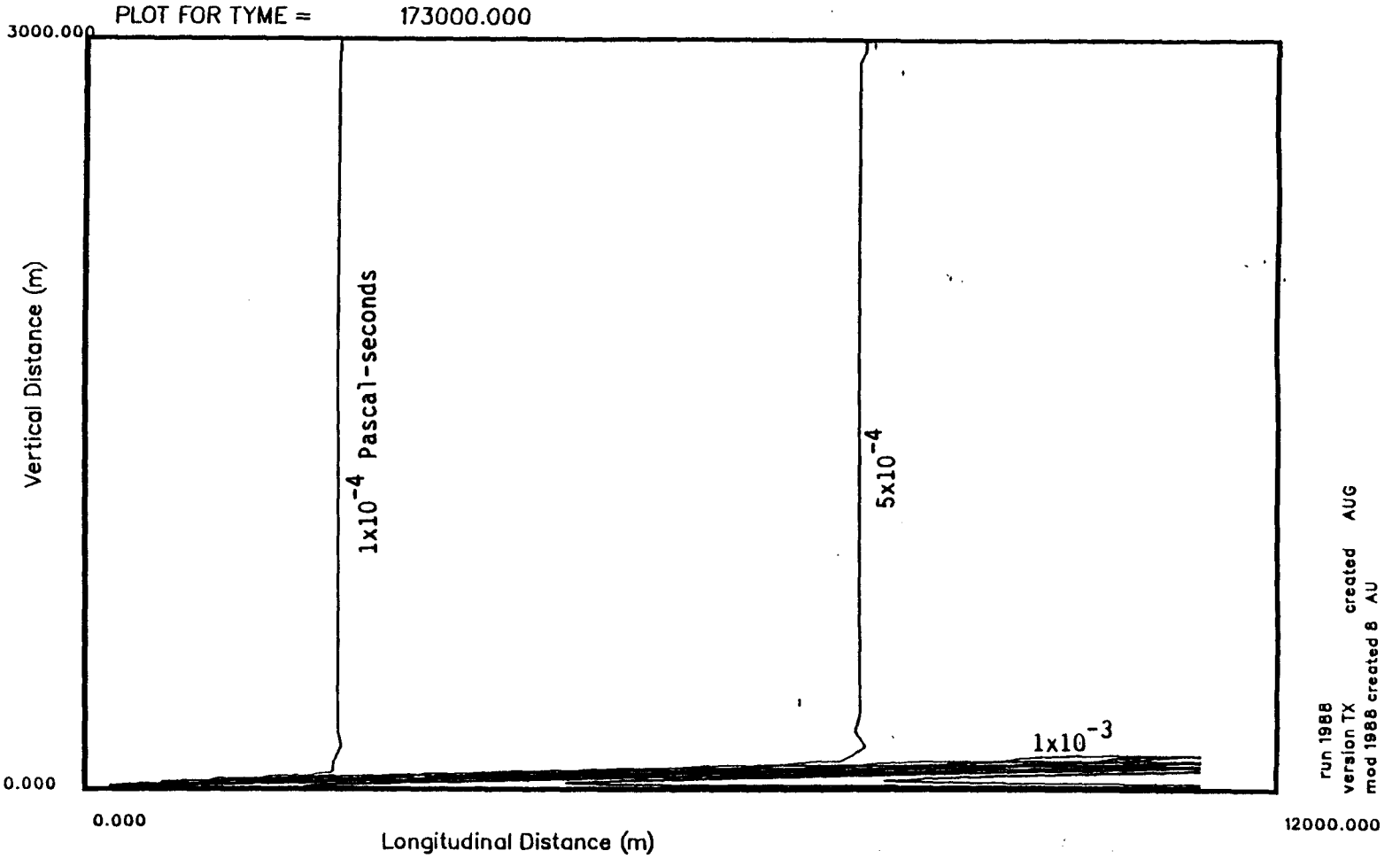


FIGURE 5.13. Calculated Eddy Viscosity Over the Whole Flow Region for the Stratified Case 2

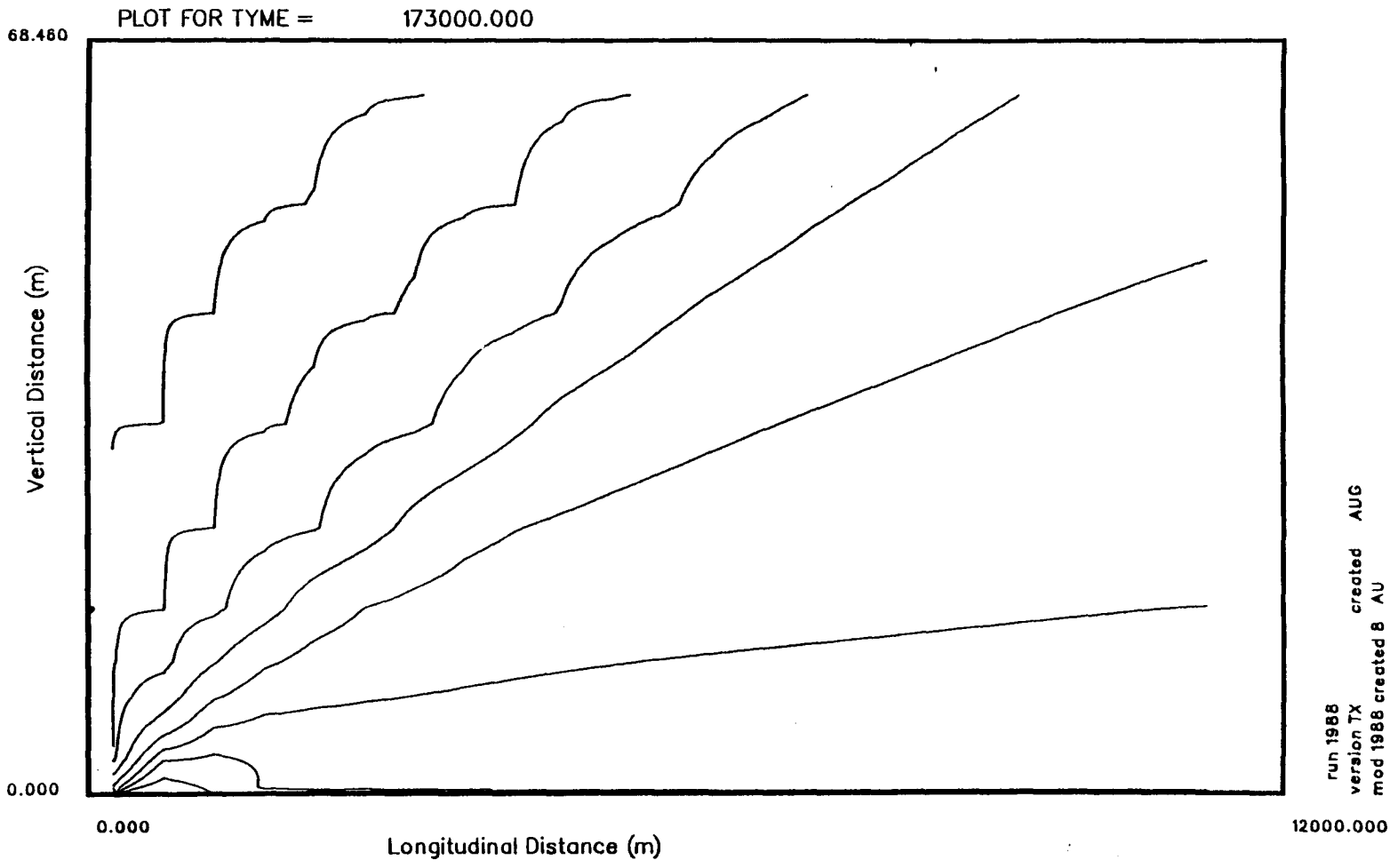


FIGURE 5.14. Calculated Turbulent Kinetic Energy Near the Bottom for the Stratified Case 2

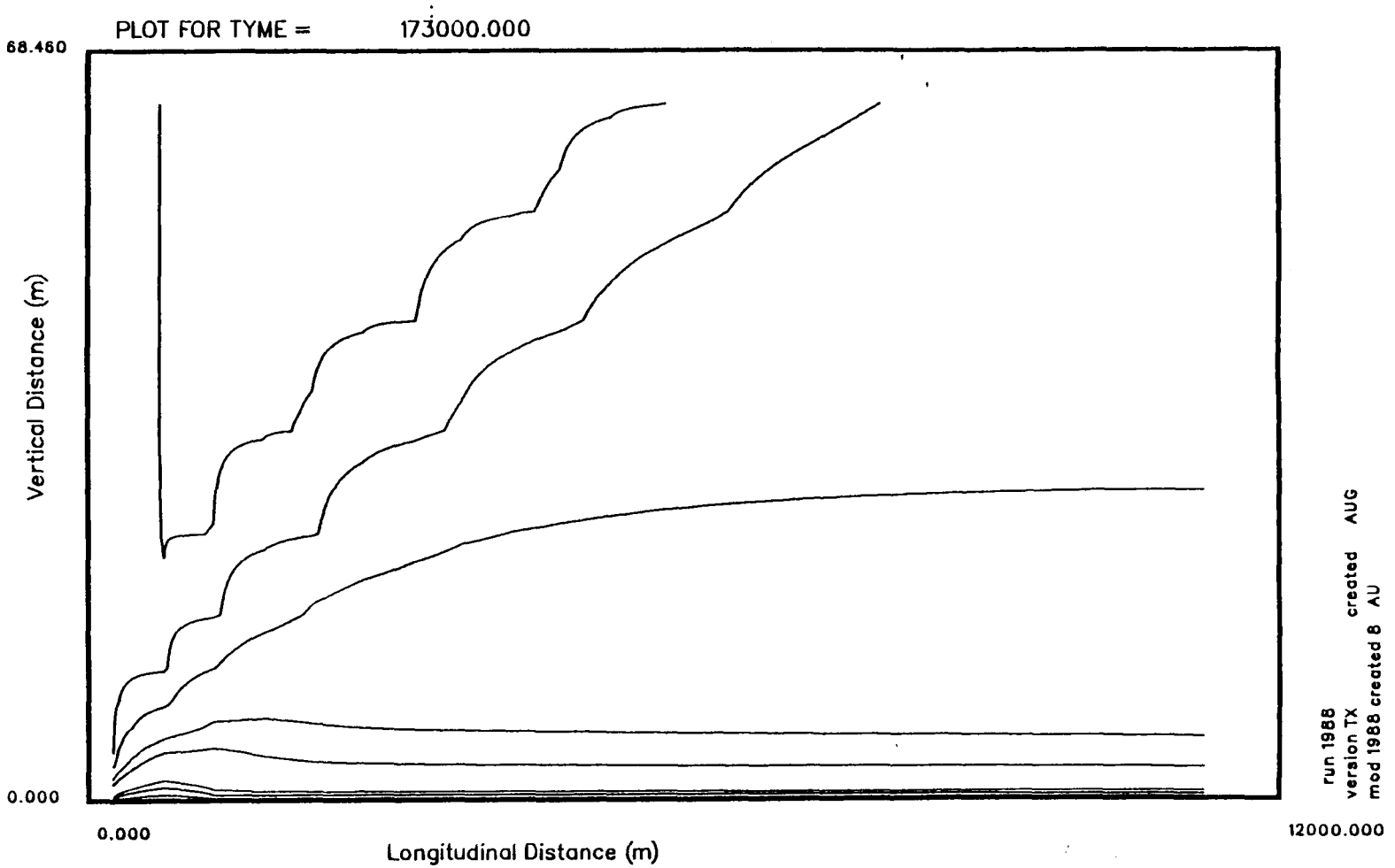


FIGURE 5.15. Calculated Turbulent Energy Dissipation Near the Bottom for the Stratified Case 2

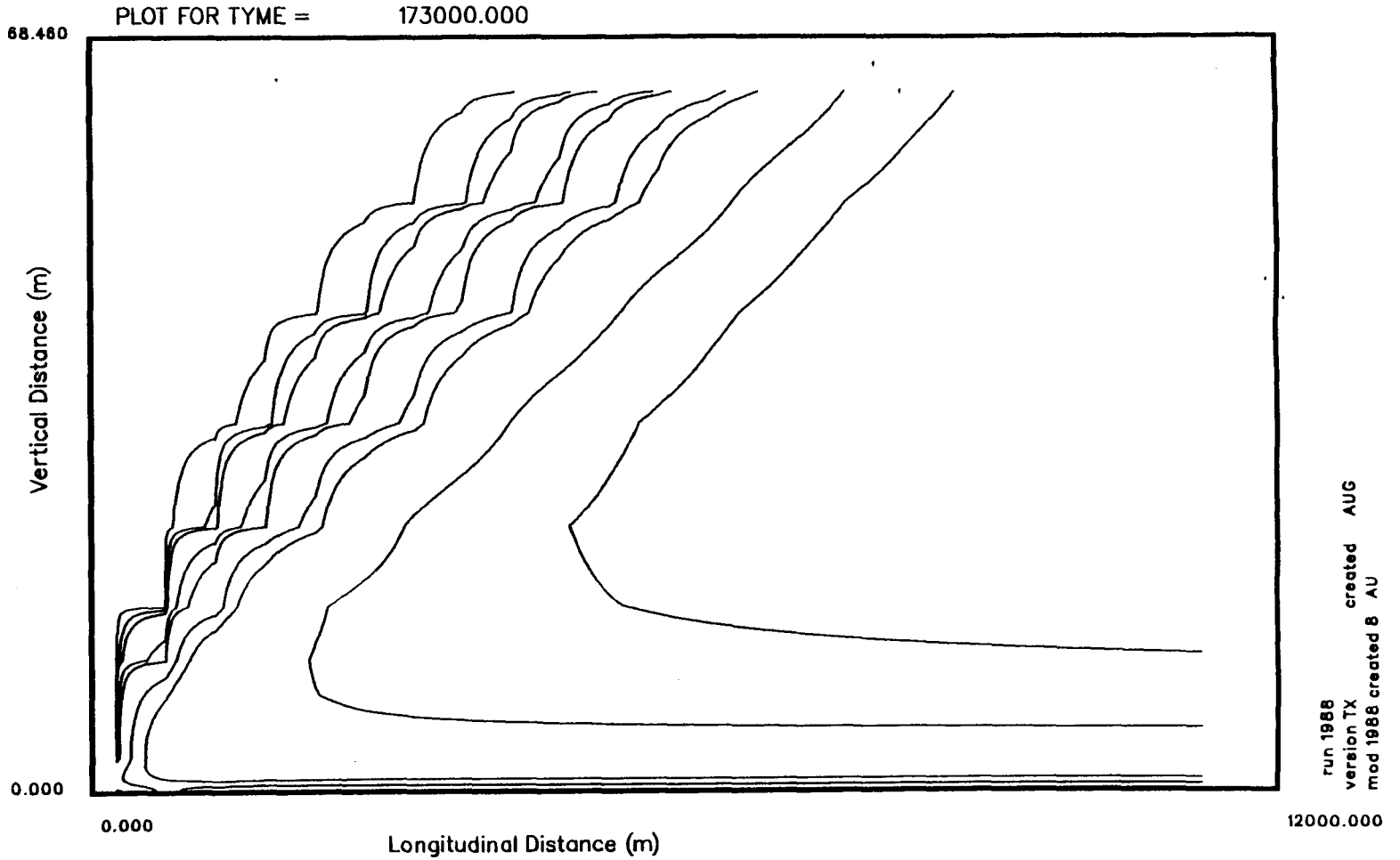


FIGURE 5.16. Calculated Eddy Viscosity Near the Bottom for the Stratified Case 2

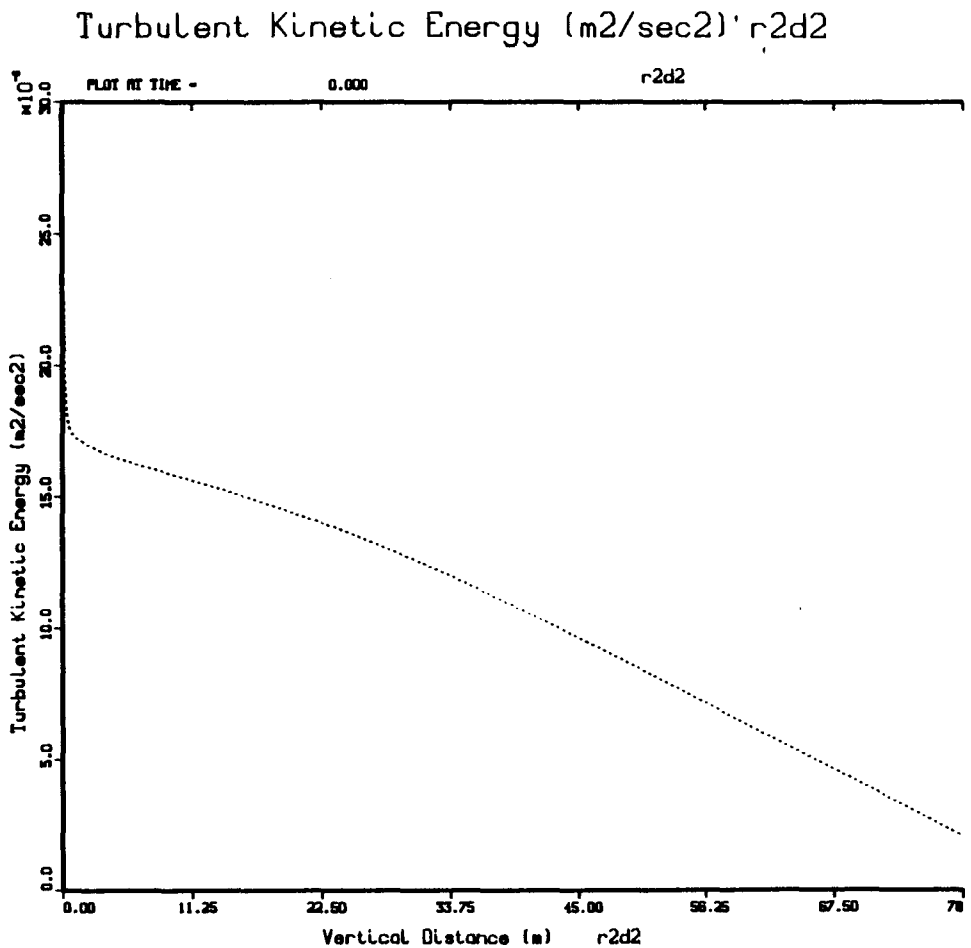


FIGURE 5.17. Vertical Distribution of Calculated Turbulent Kinetic Energy Near the Bottom for the Stratified Case 2

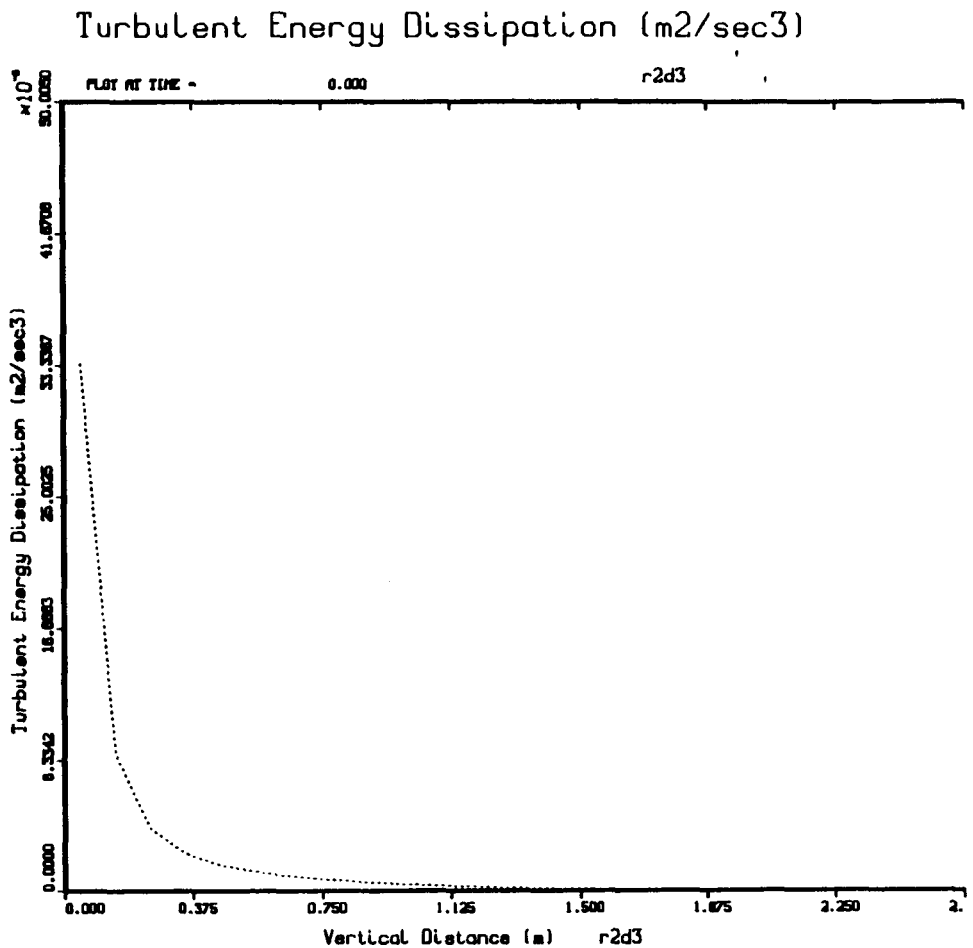


FIGURE 5.18. Vertical Distribution of Calculated Turbulent Energy Dissipation Near the Bottom for the Stratified Case 2

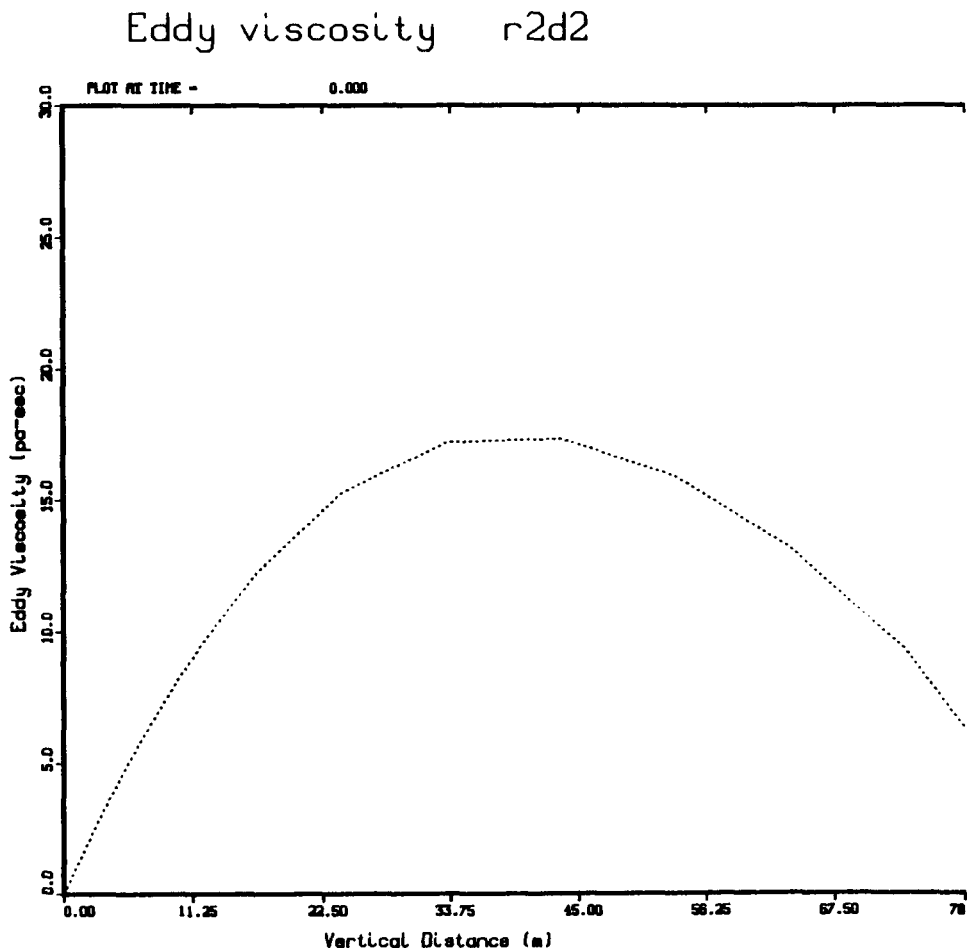


FIGURE 5.19. Vertical Eddy Viscosity Near the Bottom for the Stratified Case 2

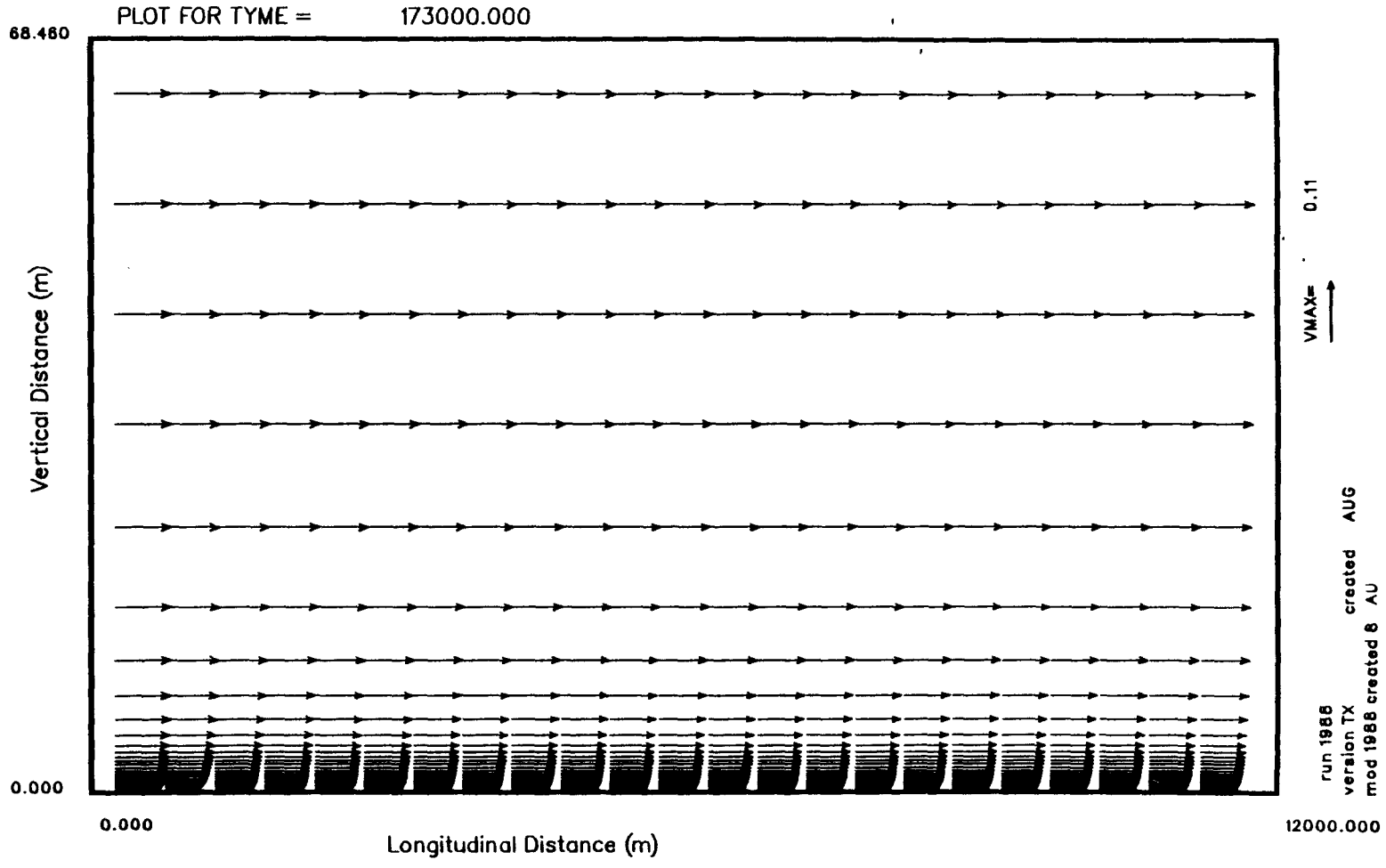


FIGURE 5.20. Calculated Velocity Distribution Near the Bottom for the Stratified Case 2

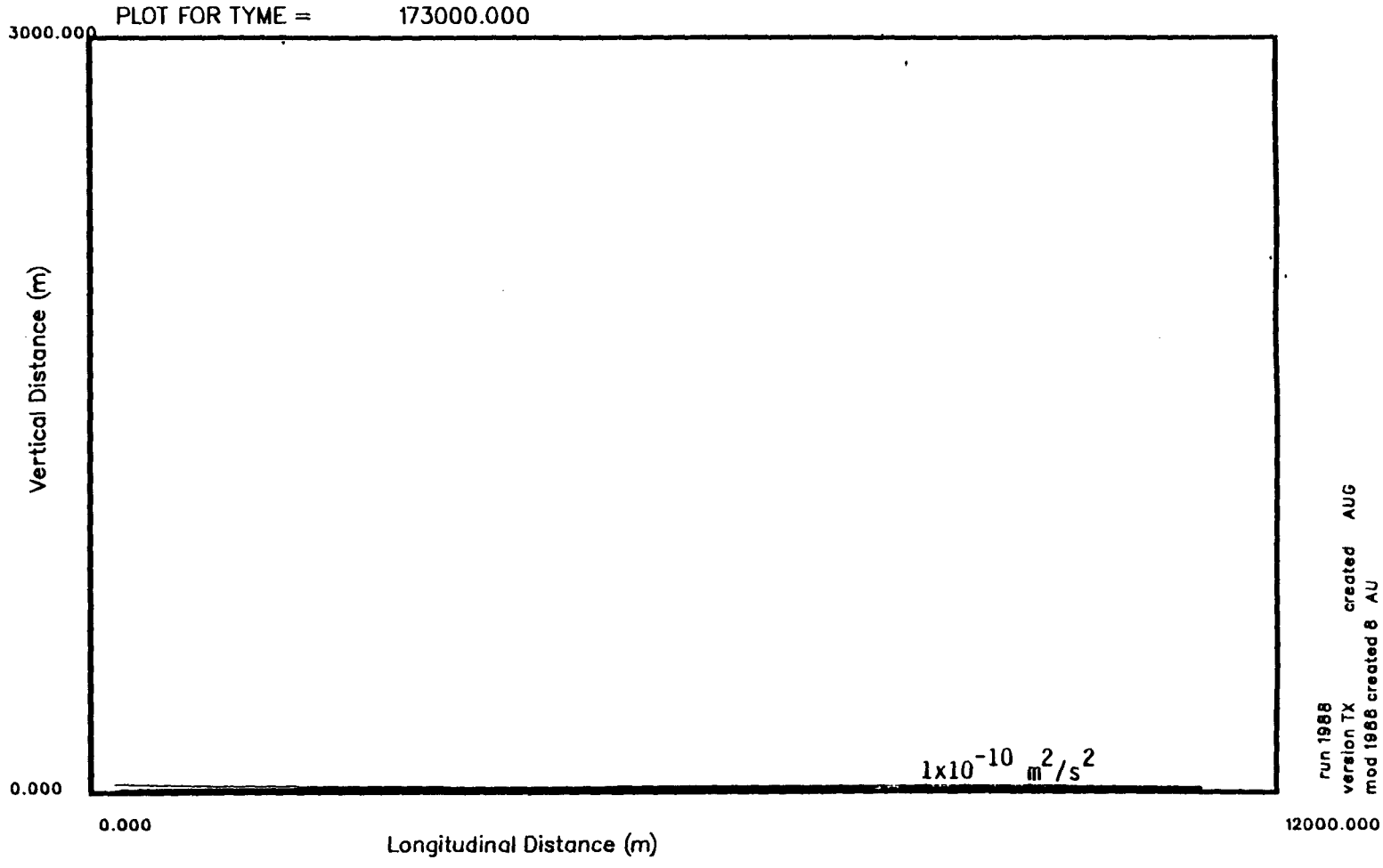


FIGURE 5.21. Calculated Turbulent Kinetic Energy Over the Whole Flow Region for Stratified Case 3

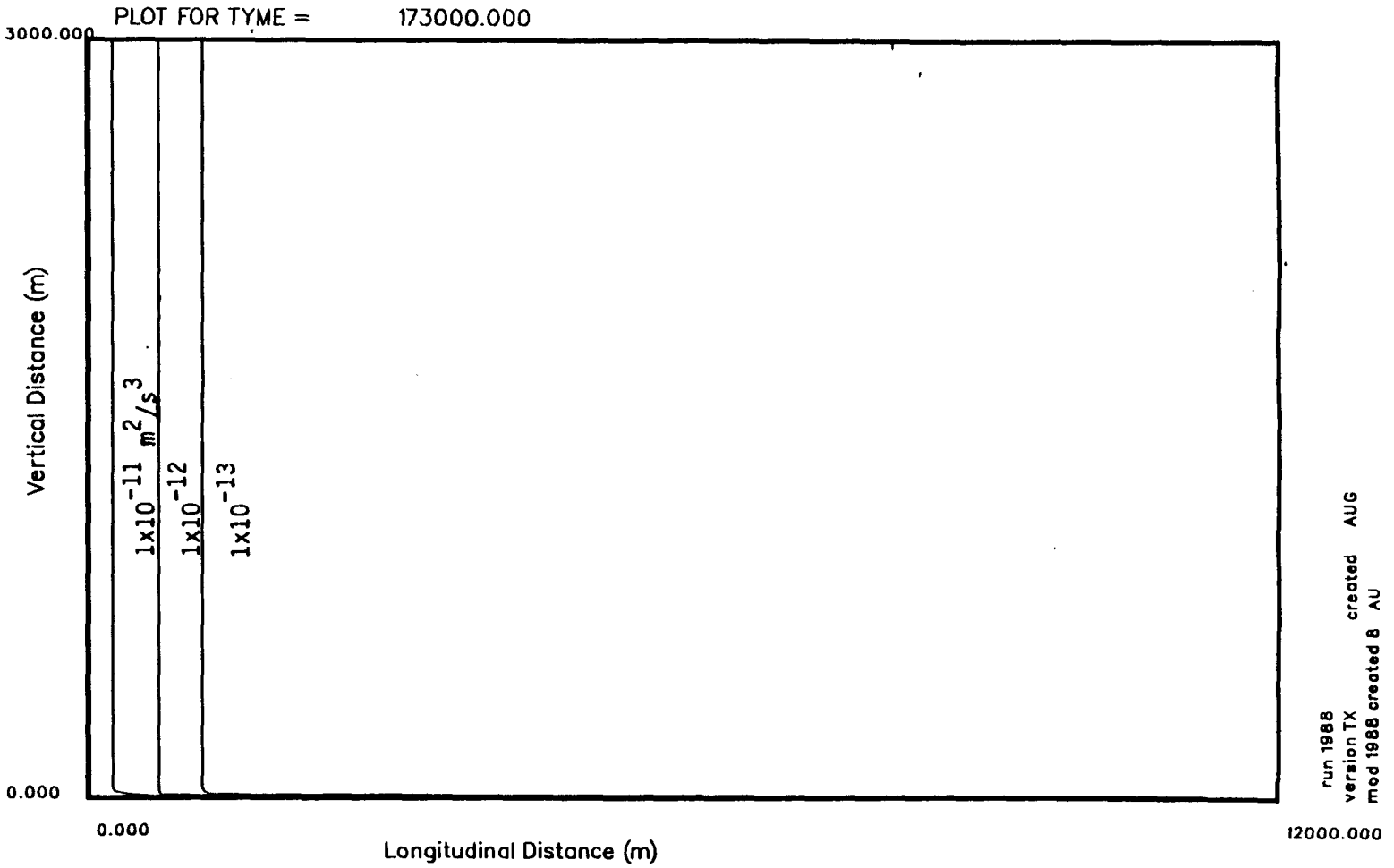


FIGURE 5.22. Calculated Turbulent Energy Dissipation Over the Whole Flow Region for the Stratified Case 3

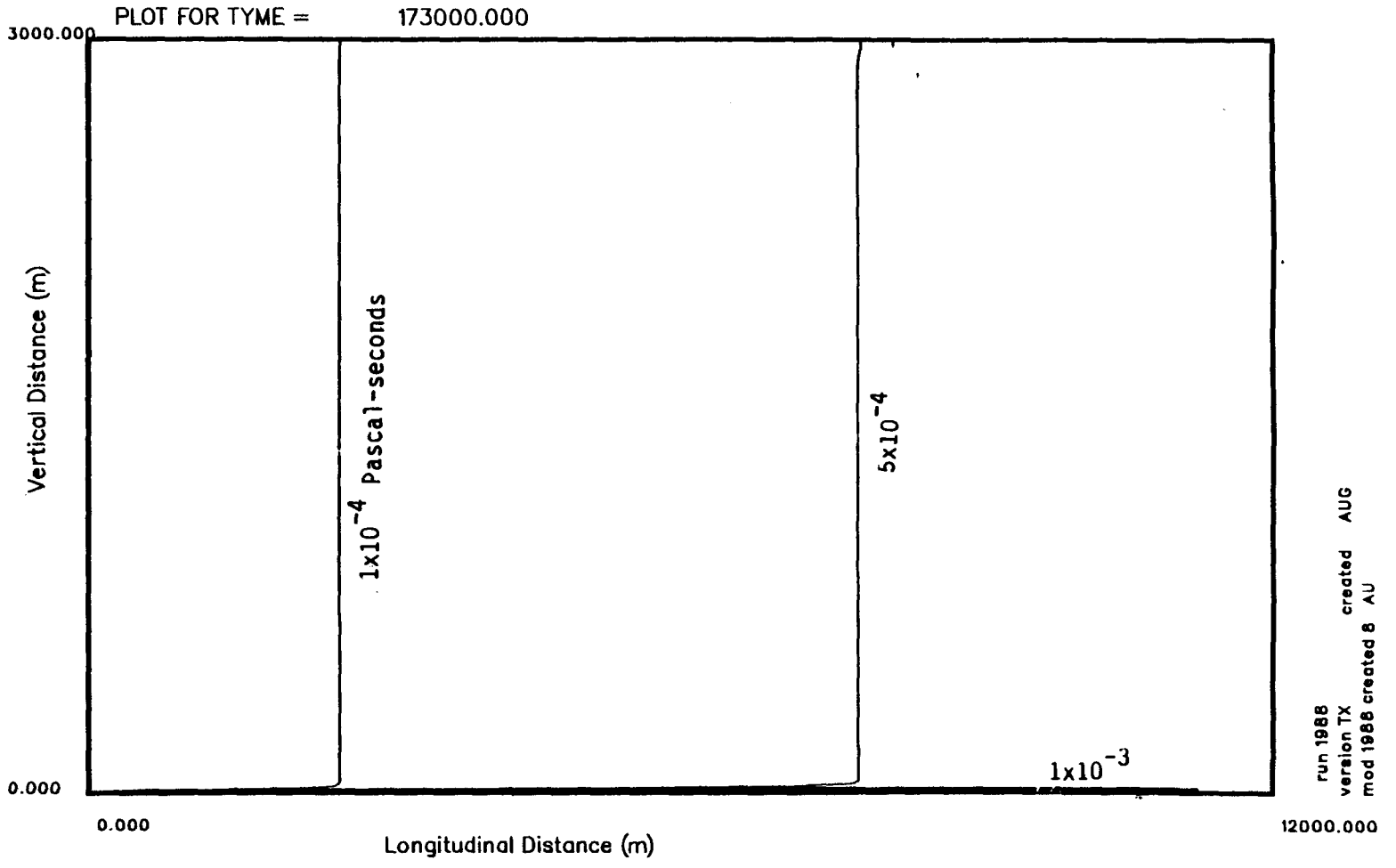


FIGURE 5.23. Calculated Eddy Viscosity Over the Whole Flow Region for the Stratified Case 3

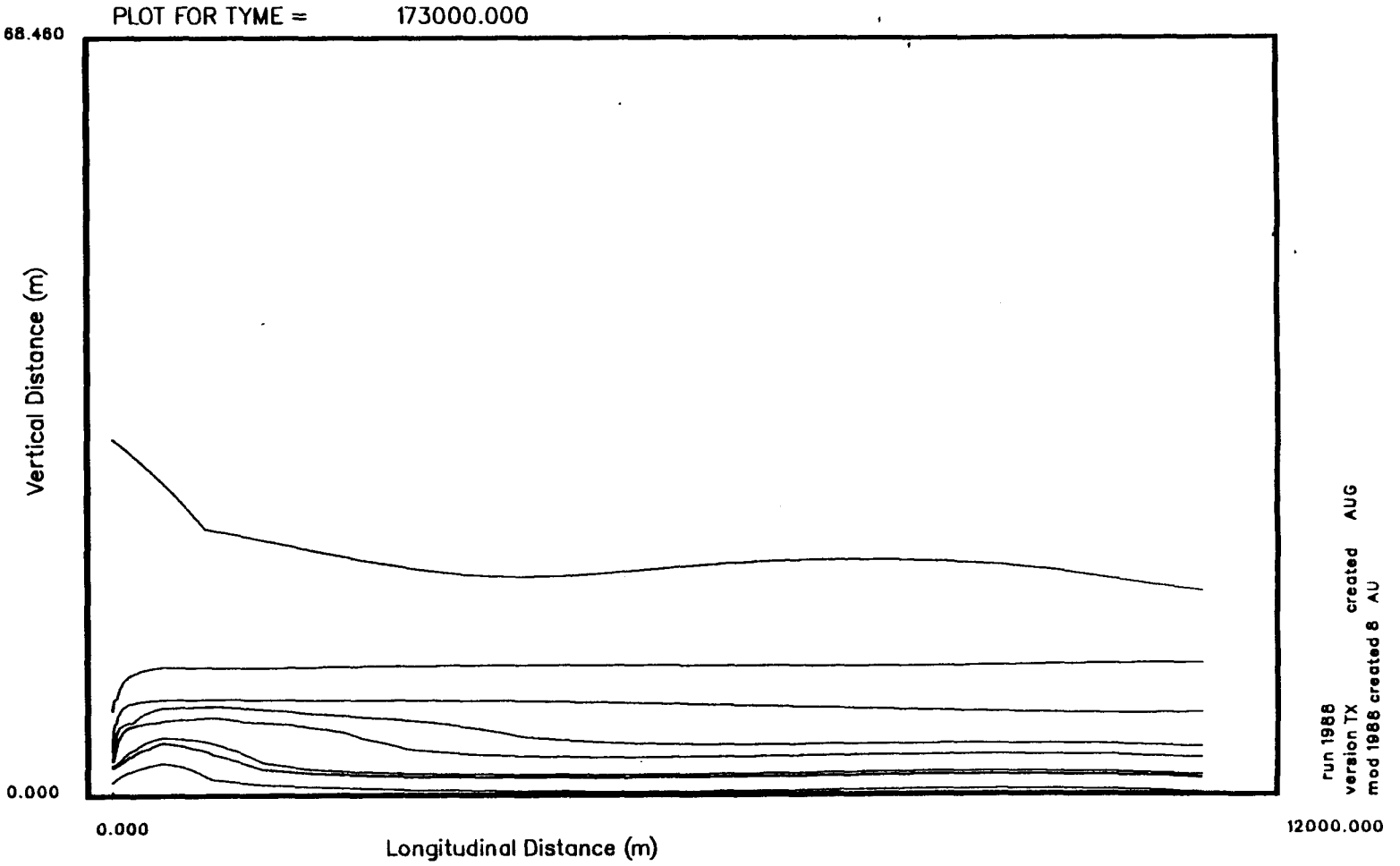


FIGURE 5.24. Calculated Turbulent Kinetic Energy Near the Bottom for the Stratified Case 3

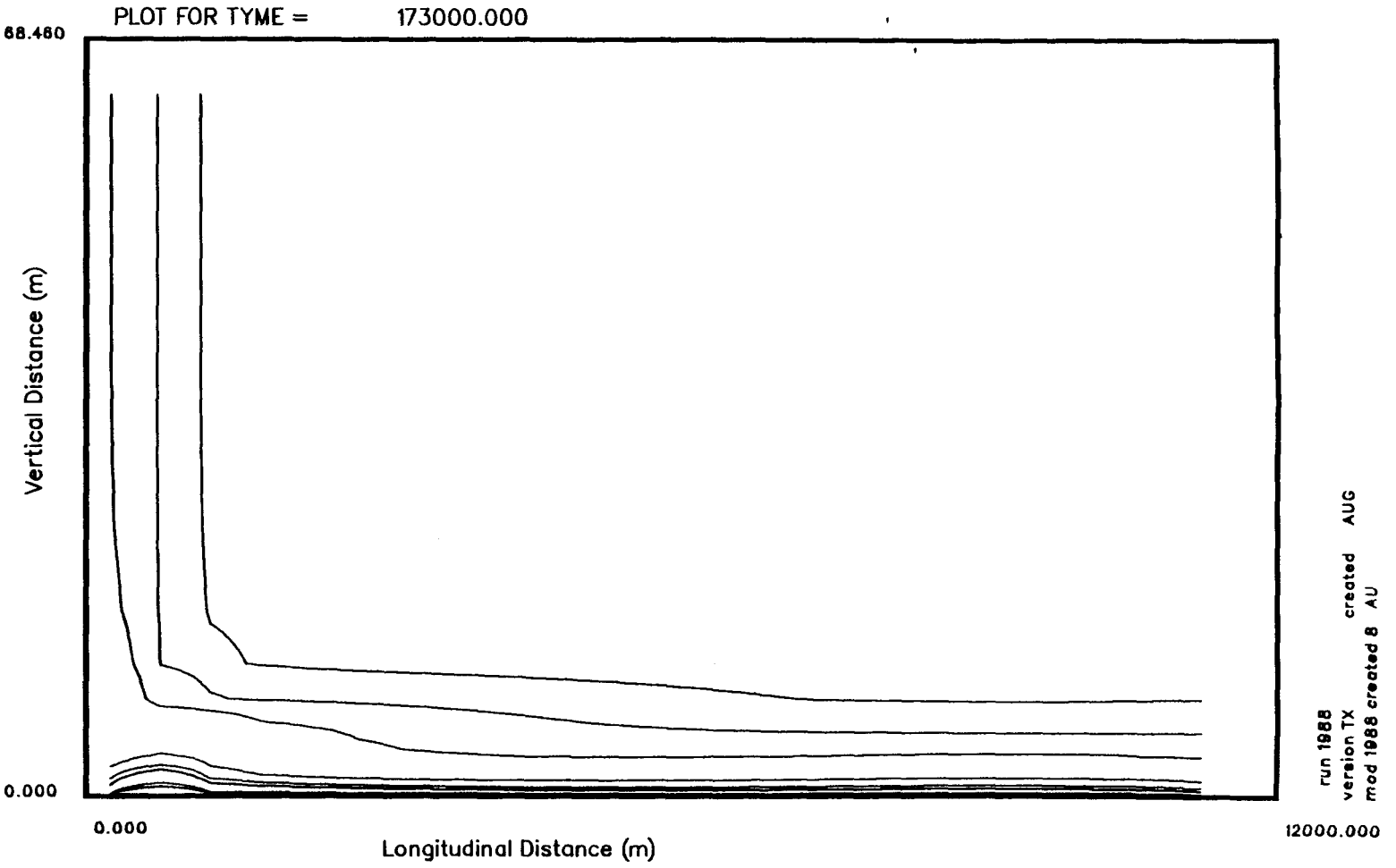


FIGURE 5.25. Calculated Turbulent Energy Dissipation Near the Bottom for the Stratified Case 3

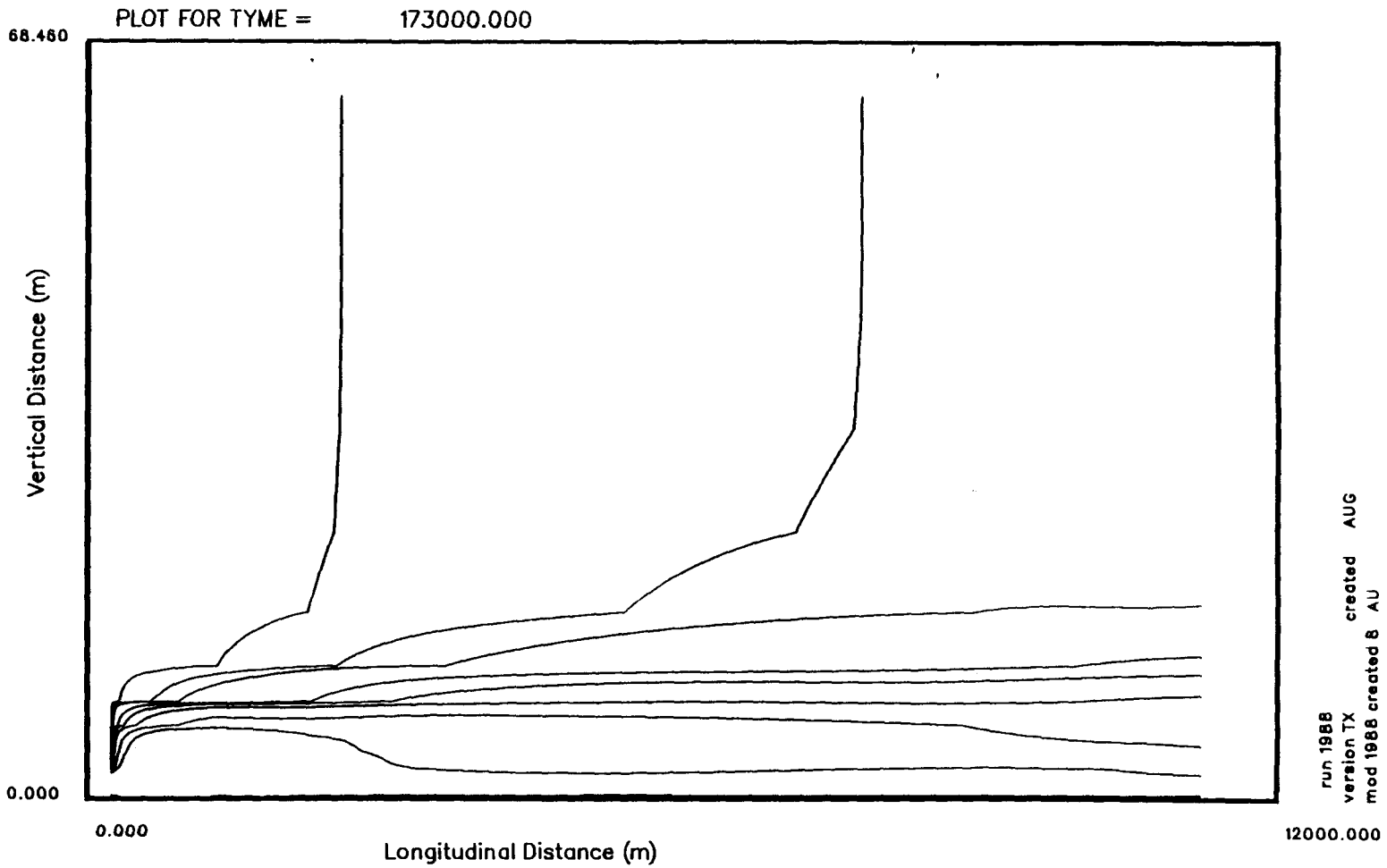


FIGURE 5.26. Calculated Eddy Viscosity Near the Bottom for the Stratified Case 3

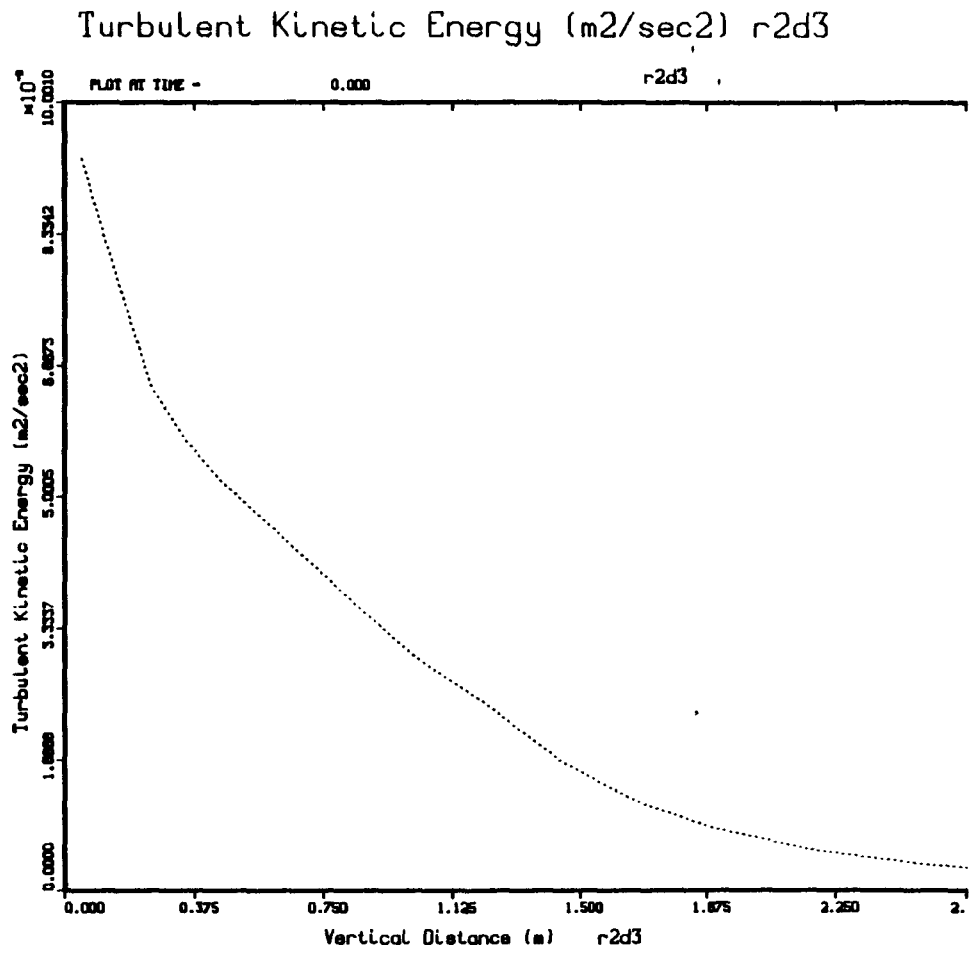


FIGURE 5.27. Vertical Distribution of Calculated Turbulent Kinetic Energy Near the Bottom for the Stratified Case 3

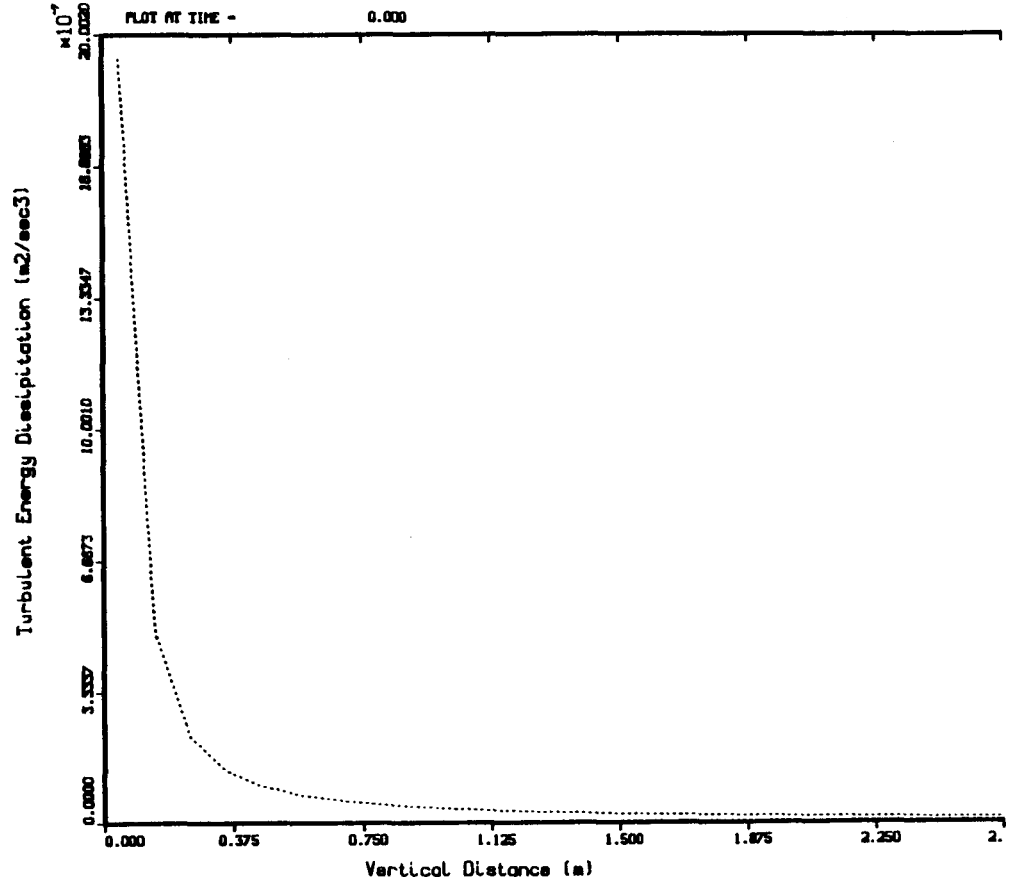


FIGURE 5.28. Vertical Distribution of Calculated Turbulent Energy Dissipation Near the Bottom for the Stratified Case 3

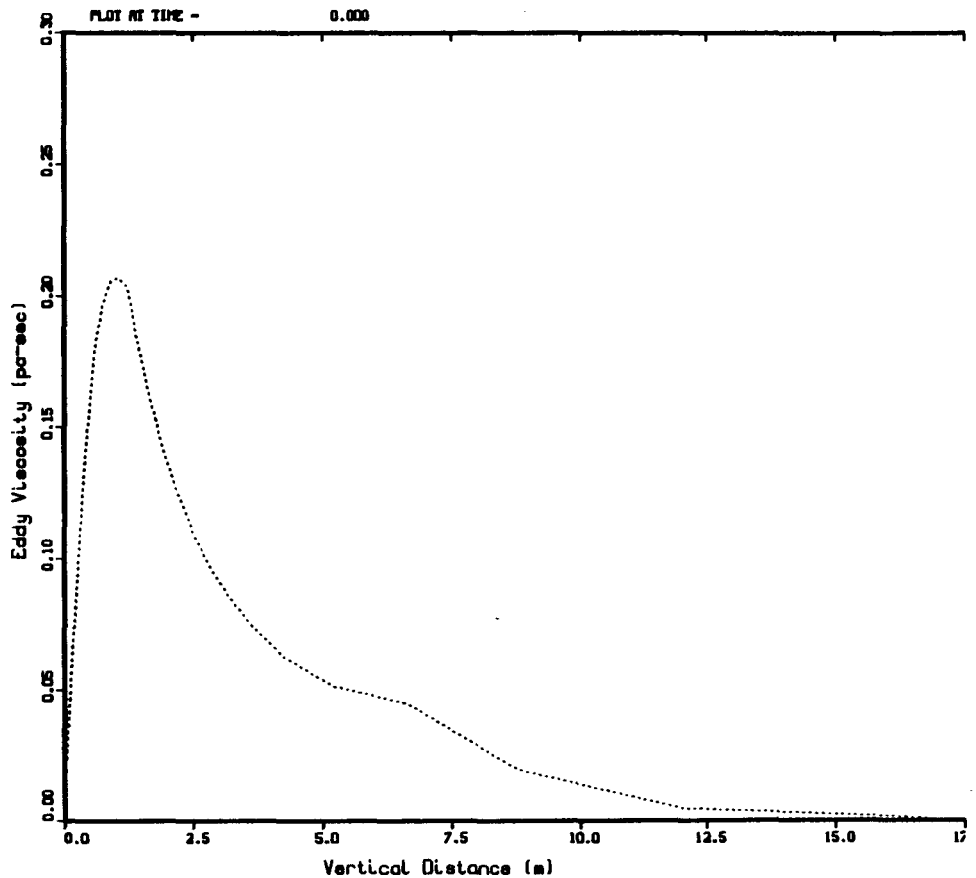


FIGURE 5.29. Vertical Eddy Viscosity Near the Bottom for the Stratified Case 3

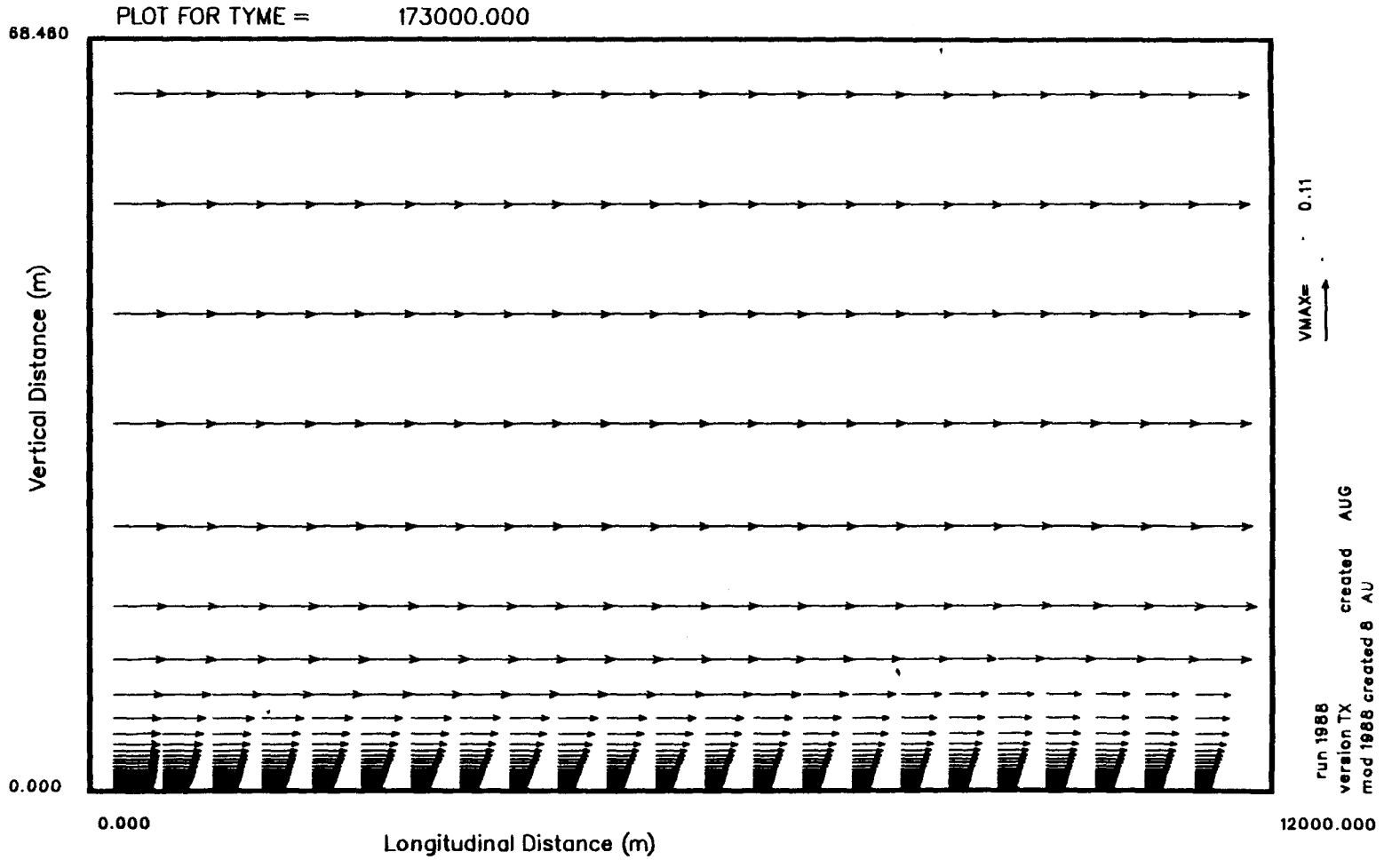


FIGURE 5.30. Calculated Velocity Distribution Near the Bottom for the Stratified Case 3

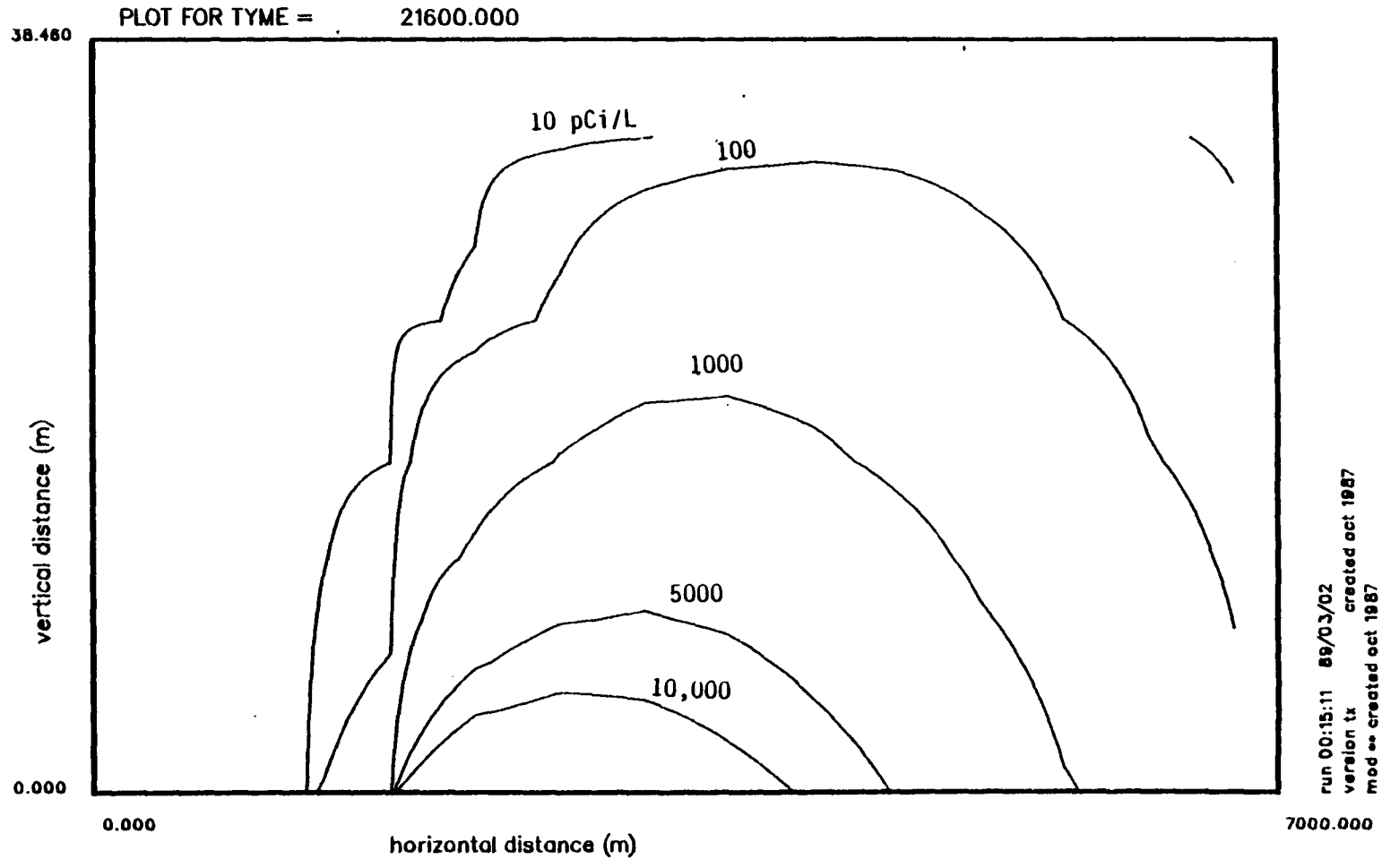


FIGURE 5.31. Calculated Dissolved Radionuclide Concentration (in pCi/L) Near the Bottom for the Stratified Case 4

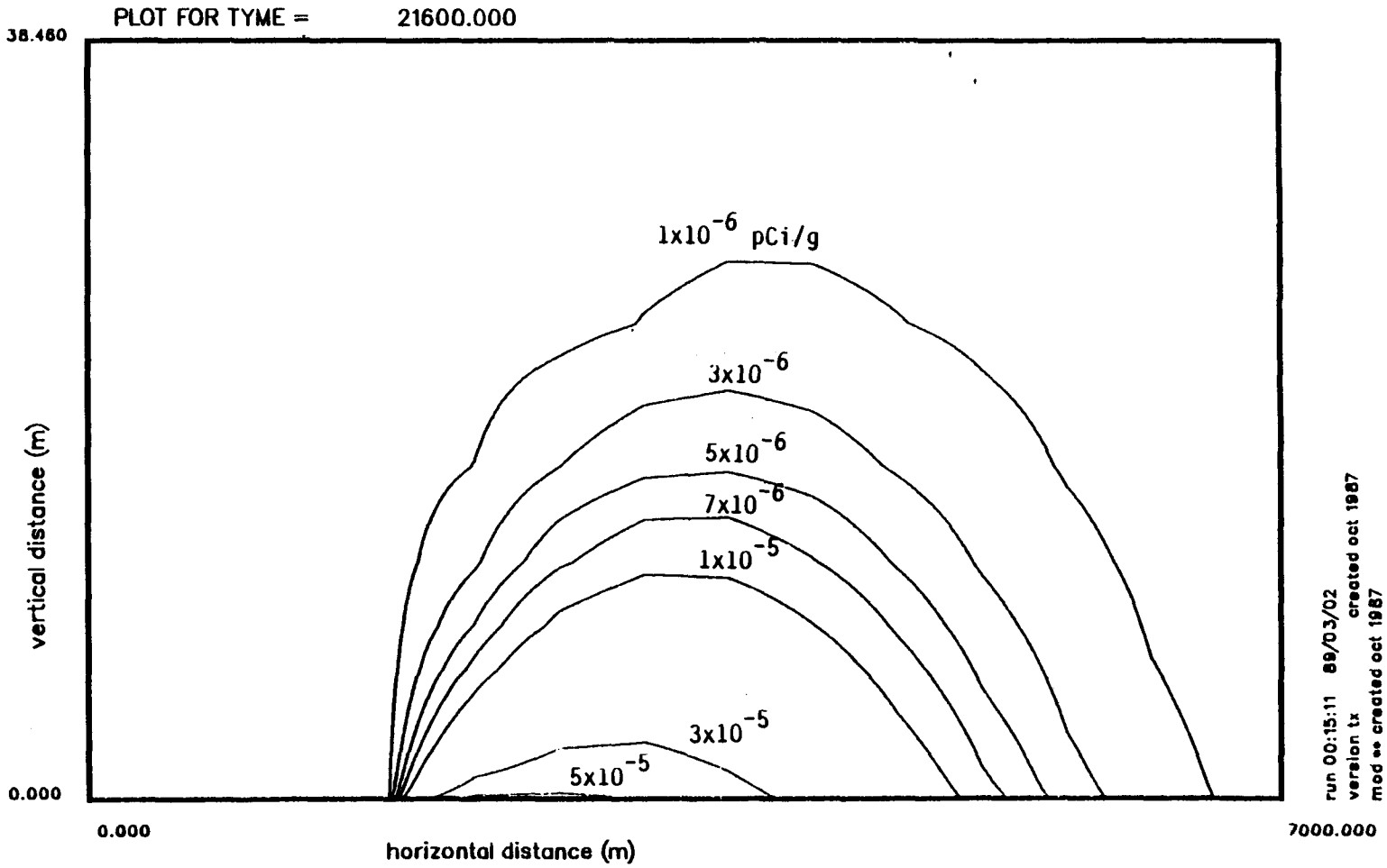


FIGURE 5.32. Calculated Suspended-Silt-Sorbed Radionuclide Concentration (in pCi/g) Near the Bottom for the Stratified Case 4

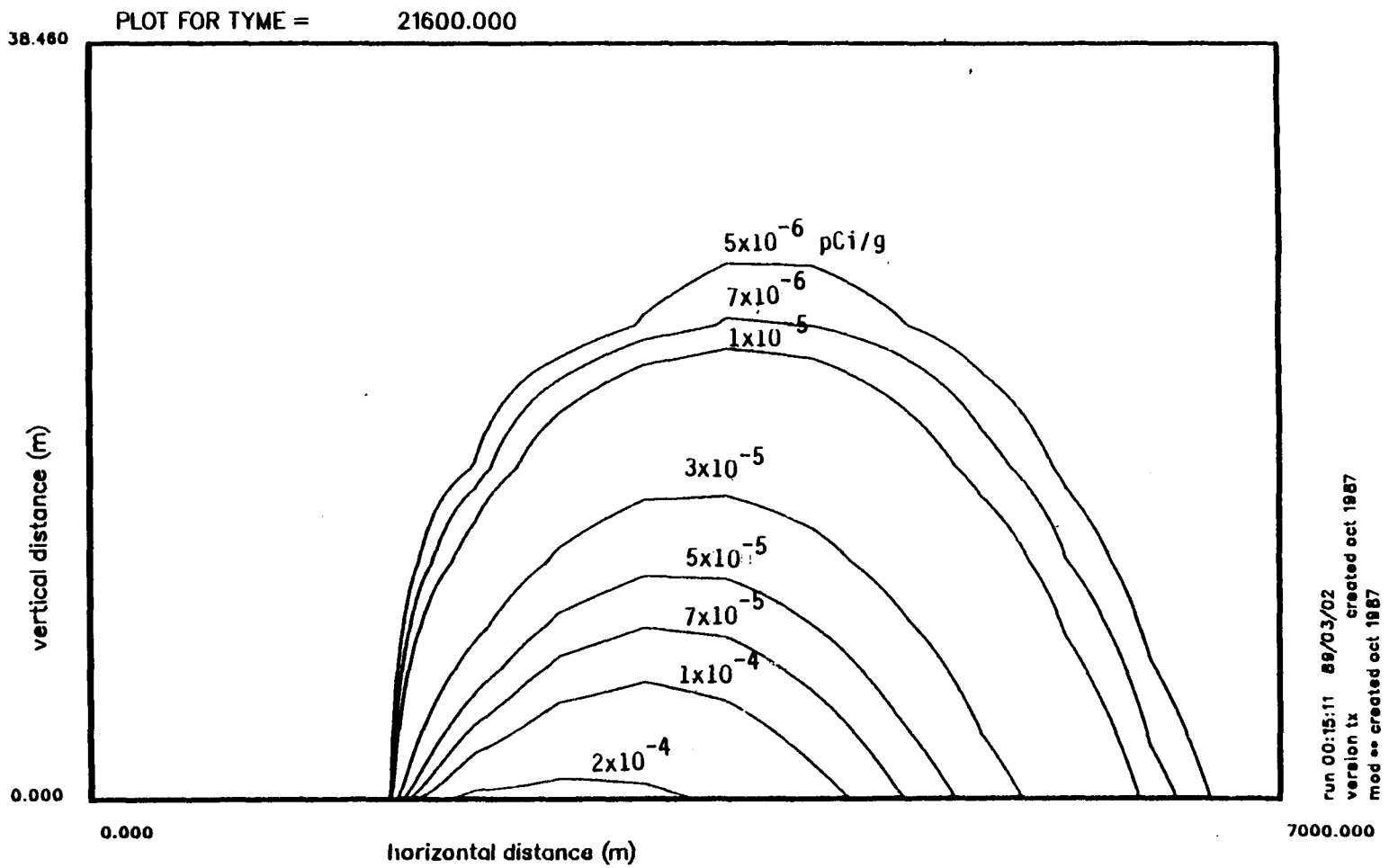


FIGURE 5.33. Calcualted Suspended-Clay-Sorbed Radionuclide Concentration (in pCi/g) Near the Bottom for the Stratified Case 4

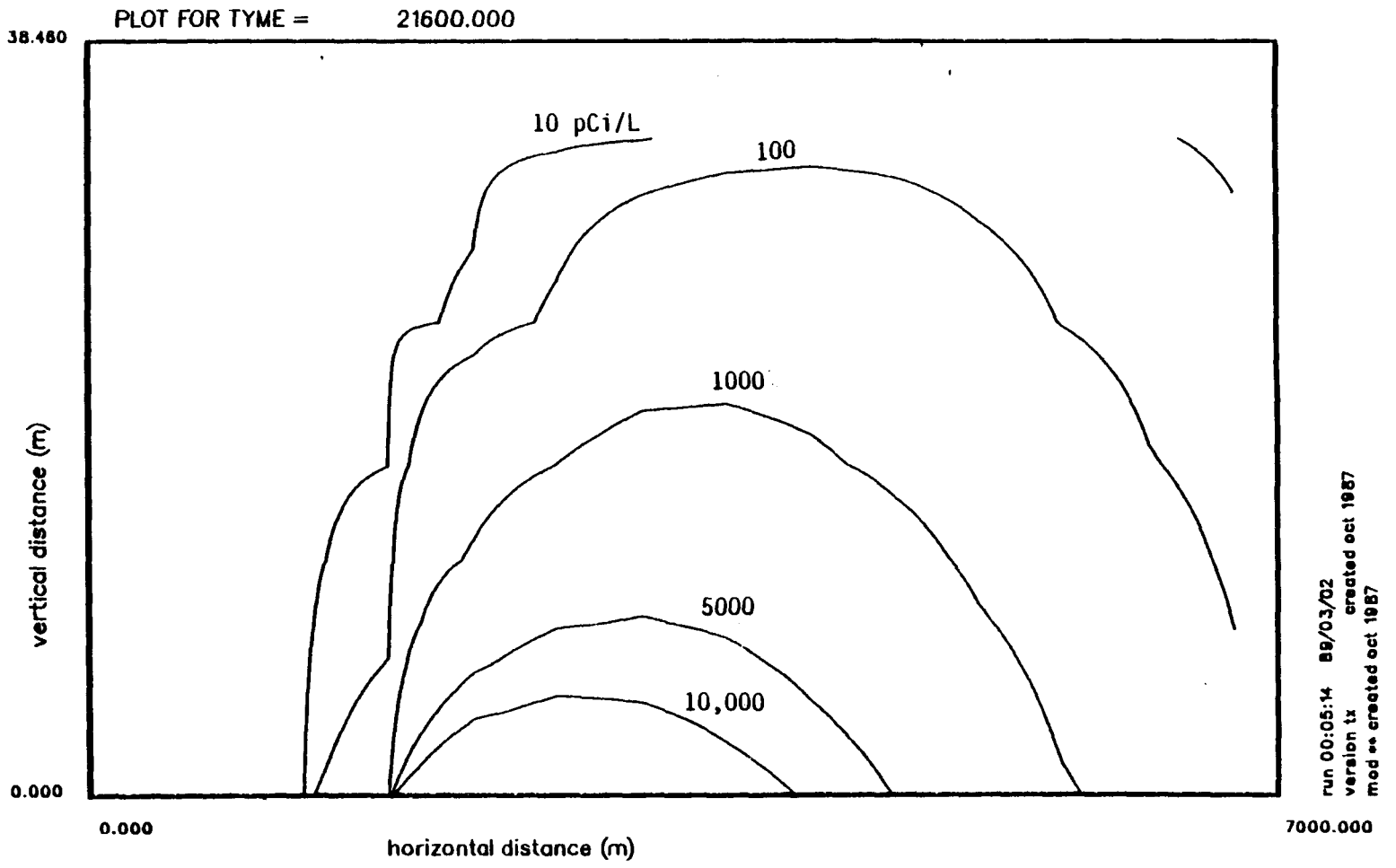


FIGURE 5.34. Calculated Dissolved Radionuclide Concentration (in pCi/L) Near the Bottom for the Stratified Case 5

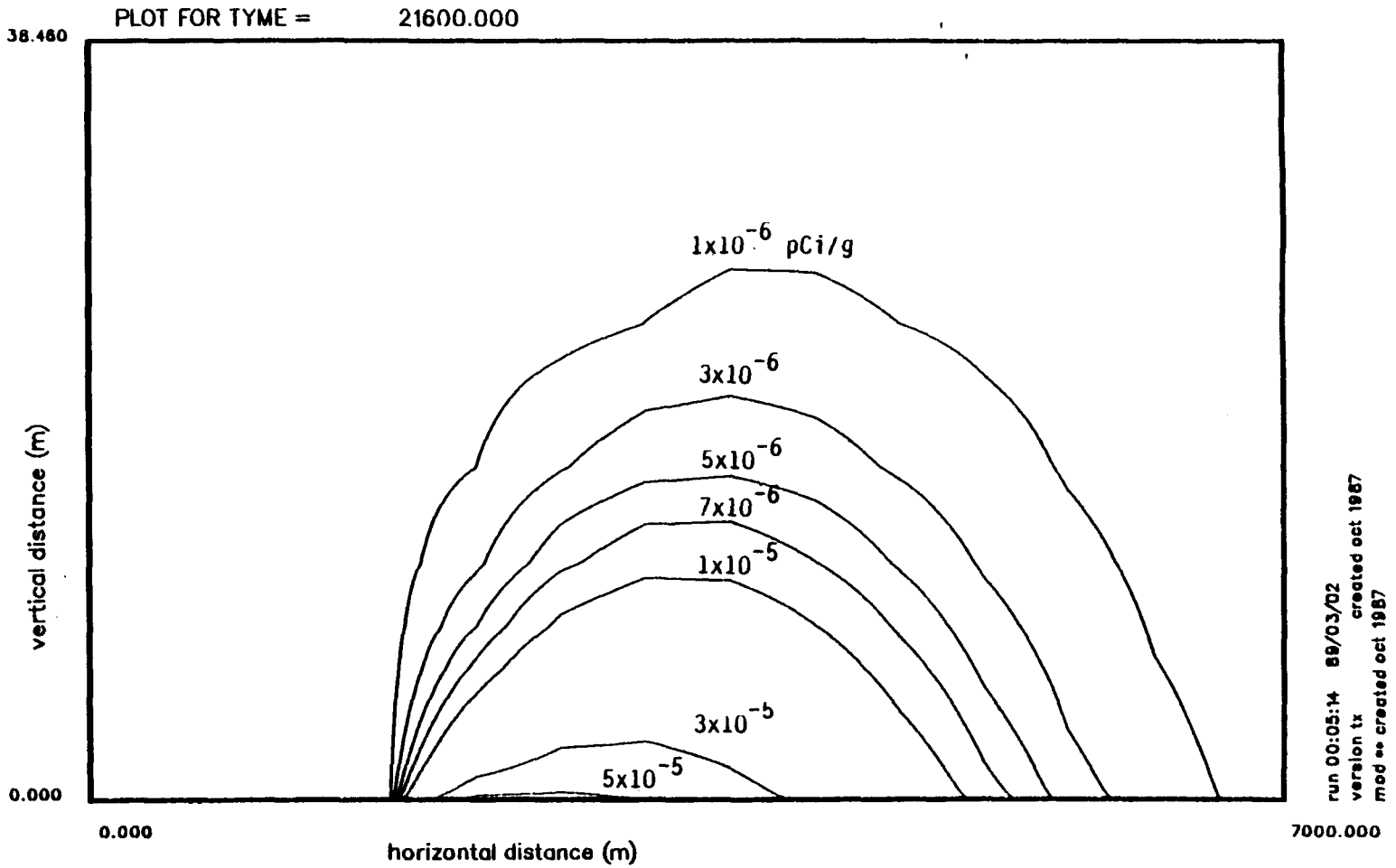


FIGURE 5.35. Calculated Suspended-Silt-Sorbed Radionuclide Concentration (in pCi/g) Near the Bottom for the Stratified Case 5

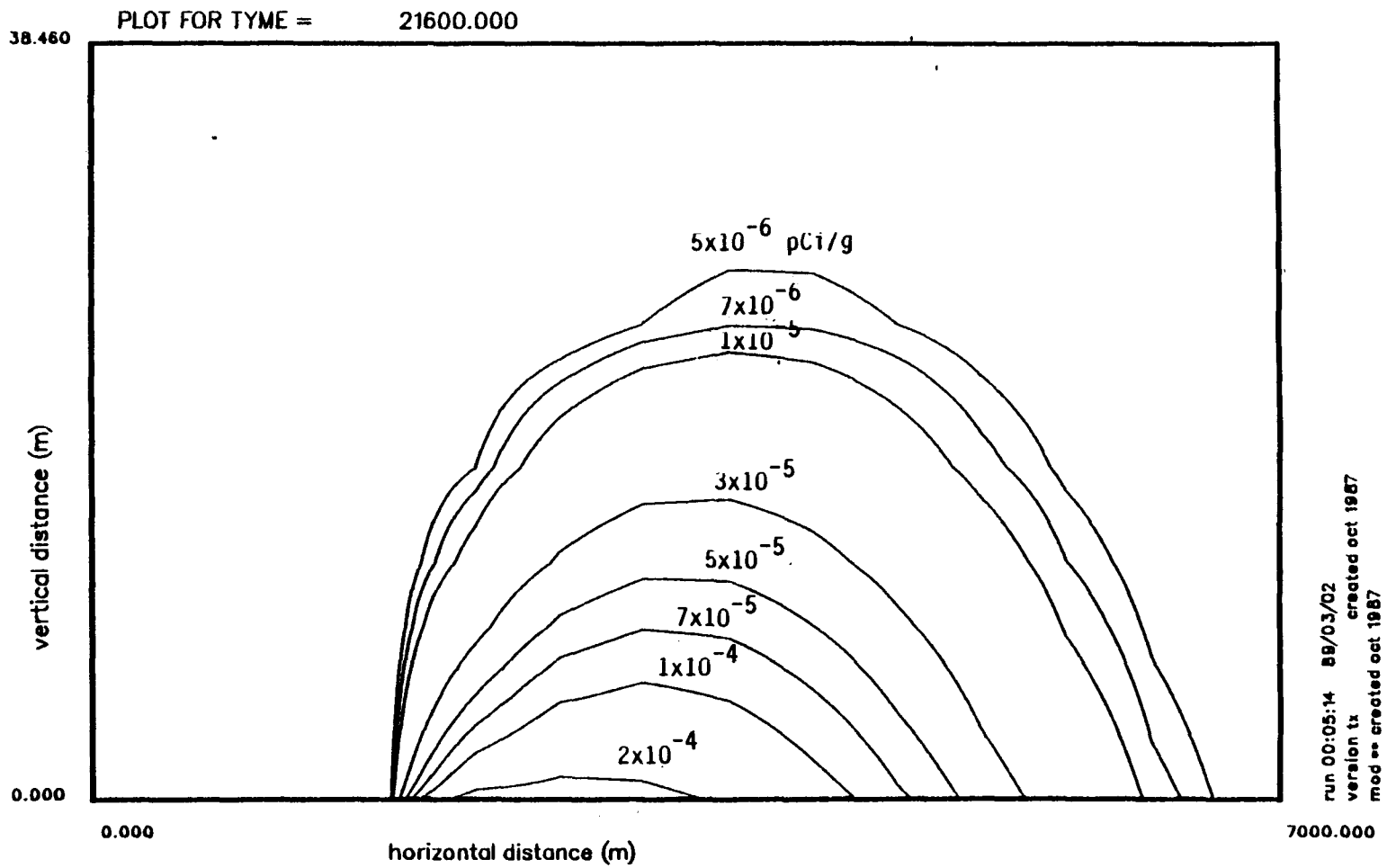


FIGURE 5.36. Calculated Suspended-Clay-Sorbed Radionuclide Concentration (in pCi/g) Near the Bottom for the Stratified Case 5

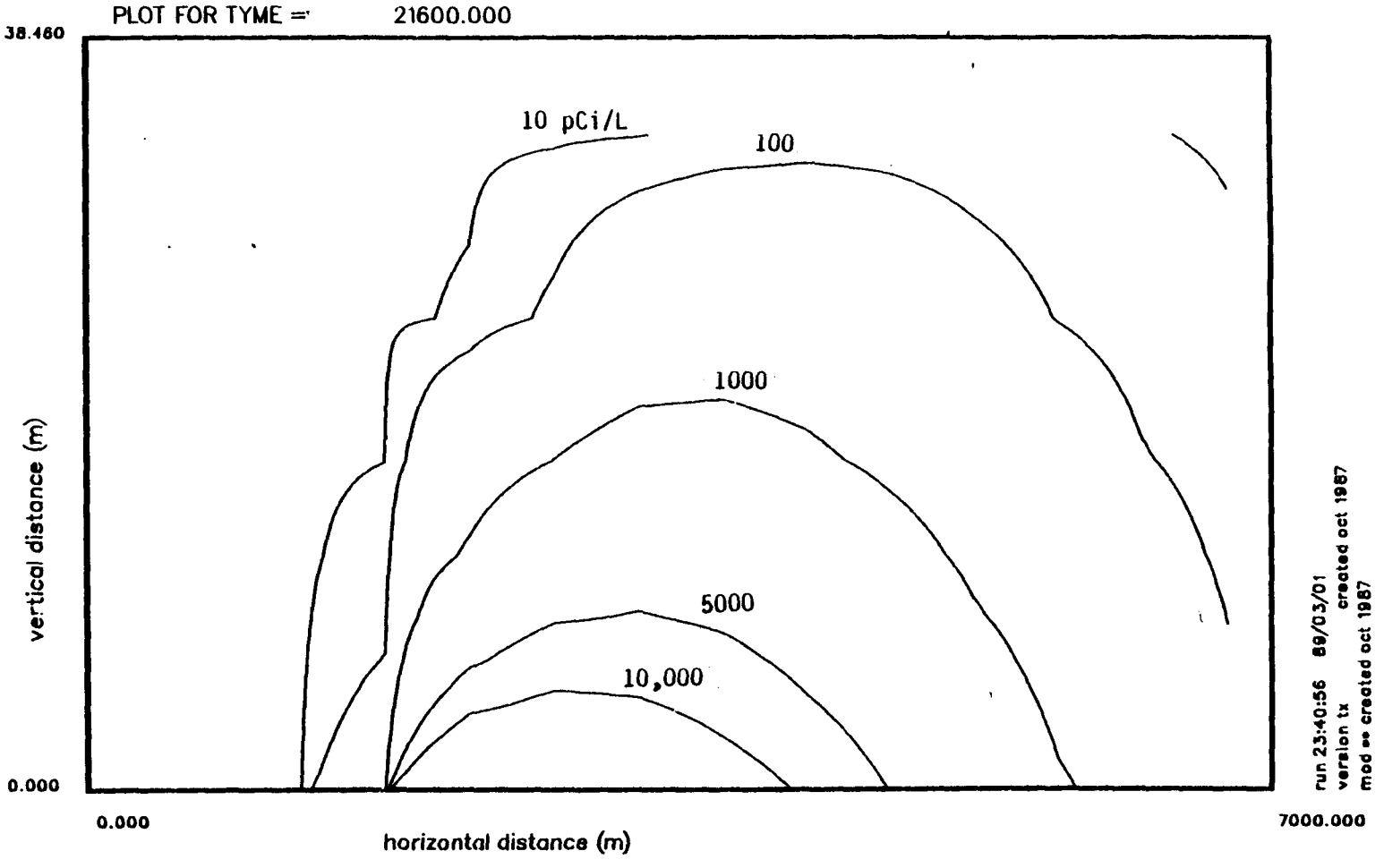


FIGURE 5.37. Calculated Dissolved Radionuclide Concentration (in pCi/L) Near the Bottom for the Stratified Case 6

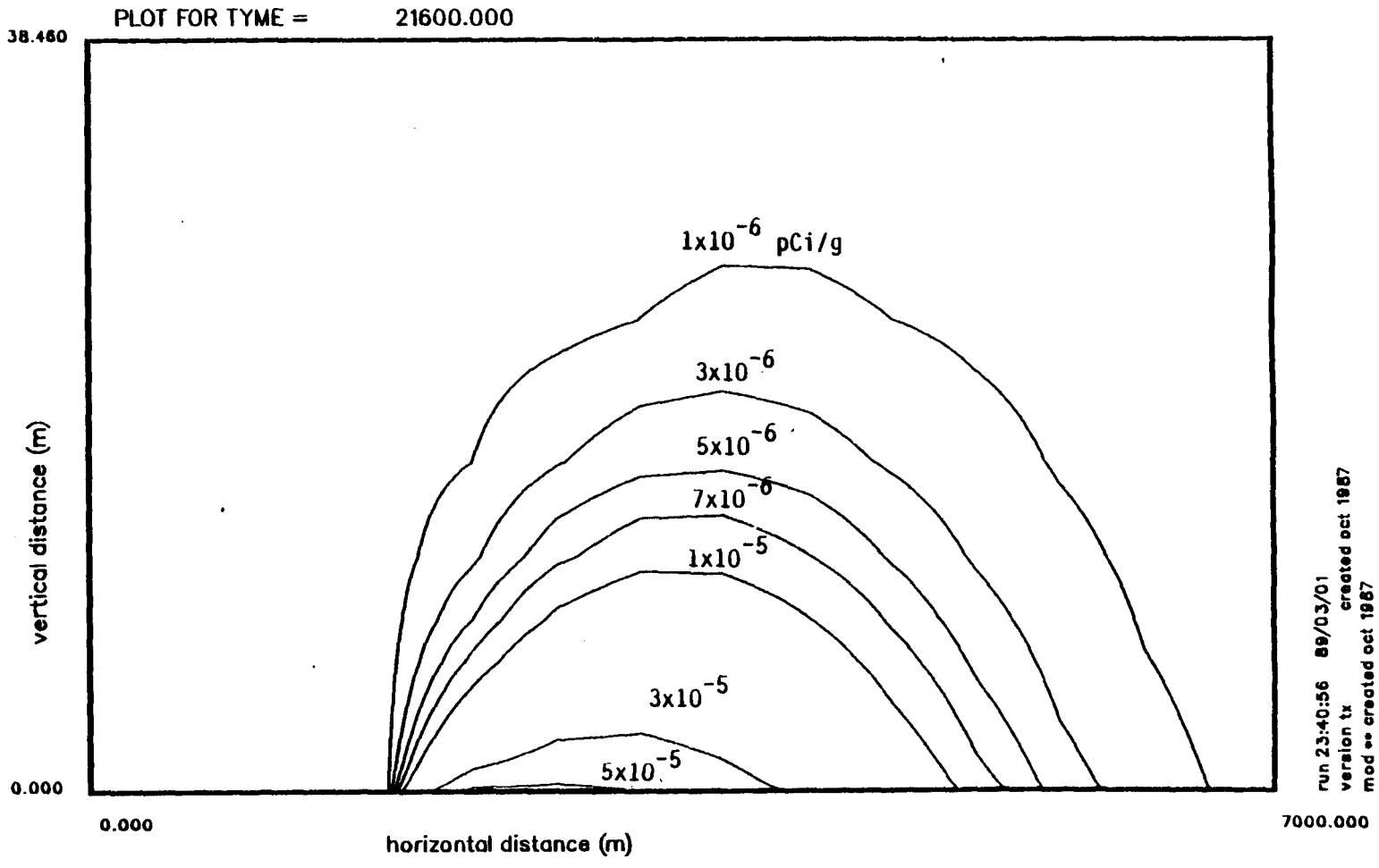


FIGURE 5.38. Calculated Suspended-Silt-Sorbed Radionuclide Concentration (in pCi/g) Near the Bottom for the Stratified Case 6

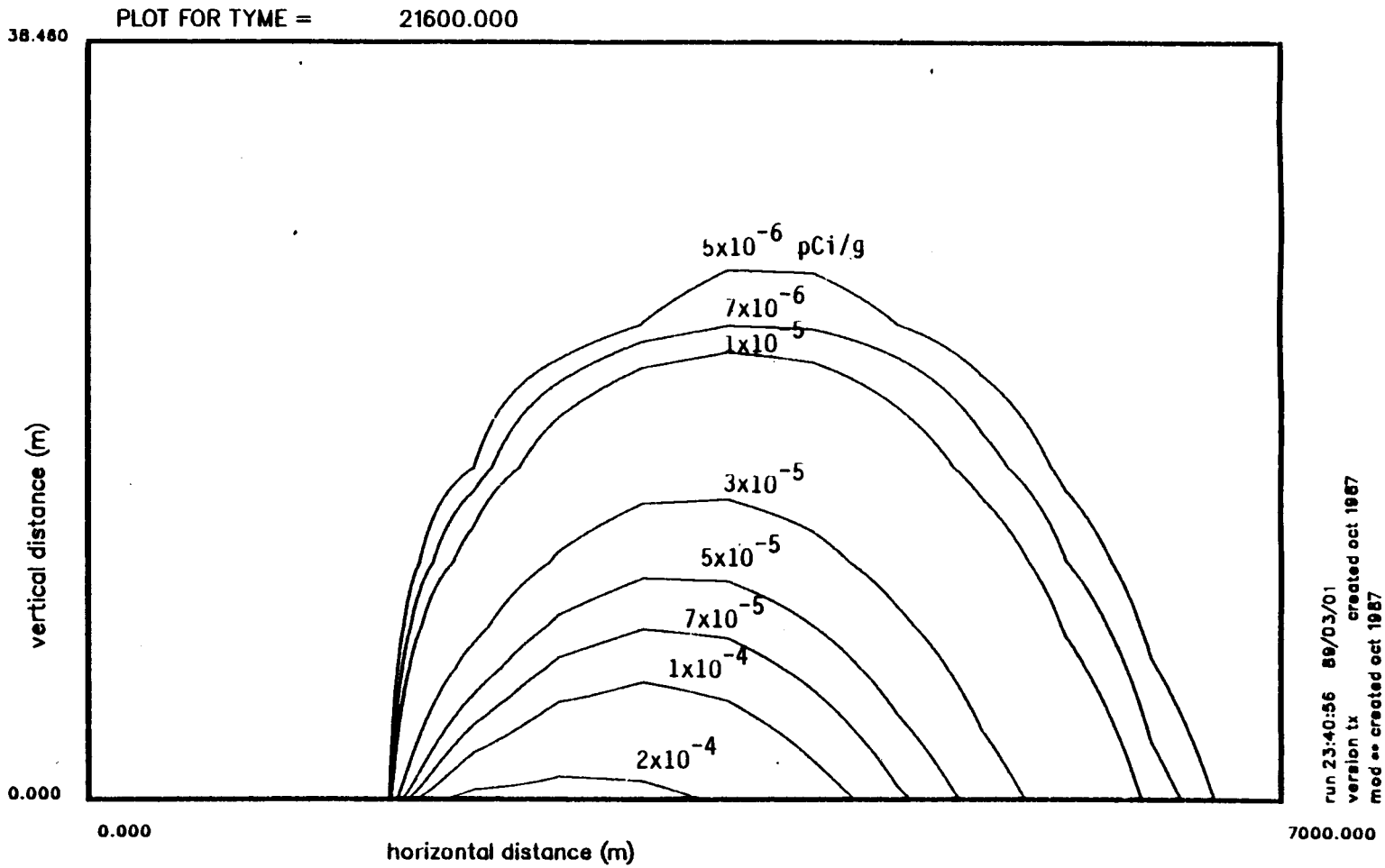


FIGURE 5.39. Calculated Suspended-Clay-Sorbed Radionuclide Concentration (in pCi/g) Near the Bottom for the Stratified Case 6

## 6.0 SUMMARY AND CONCLUSIONS

The TEMPEST©/FLESCOT©, FLOWER, Blumberg's, and RMA 10 models would be appropriate candidates for the regional modeling. Among these models, TEMPEST©/FLESCOT© is currently the only model that solves simultaneously distribution of flow, turbulence (with the k-$\epsilon$ model), salinity, water temperature, sediment, dissolved contaminants (e.g., radionuclides, pesticides, heavy metals, etc.), and sediment-sorbed contaminants.

Turbulence modeling has developed rapidly with the advent of high-speed computers, but there are still limits on the complexity of calculations that can be handled. Solving the Navier-Stokes equations using higher order correlations requires a large number of calculations and is not practical for modeling large areas where numerous grid points must be calculated. Therefore, assumptions must be made to solve the equations, which is where turbulence modeling comes into play.

In turbulence modeling, most of the work has gone into trying to define the turbulence correlations (Reynolds stresses) $\overline{u_i u_j}$ and $\overline{u_i \phi}$. Once these terms are obtained, it is possible to solve the equations for the flow field. The method used here for modeling the turbulence correlations is the eddy viscosity/diffusivity concept developed by Boussinesq in 1877. Zero, one, or two partial differential equations must be solved to define the eddy viscosity/diffusivity, depending on the assumptions made.

Zero-equation models do not require the solution of any additional partial differential equation. The eddy viscosity/diffusivity is defined by empirical means. One of the most common methods being used is that of constant eddy viscosity/diffusivity. This method is crude, especially in a deep ocean model, because it is known that the eddy viscosity/diffusivity will vary across the flow field. A simple method for solving this problem is to specify values of eddy viscosity/diffusivity for regions of the flow field, but this is still not very accurate. Defining the eddy viscosity/diffusivity as a function of shear stress and depth is probably the simplest method that will give a reasonably accurate representation of what is occurring in the flow field. This method has been used in boundary layers,

and there will have to be some modification before it will represent what is occurring throughout the ocean.

One-equation models are the first to take into account the history and transport effects in a flow field. This allows turbulence to travel downstream, which was not possible when the eddy viscosity/diffusivity was simply specified. The turbulent kinetic energy (TKE) equation is used to define the velocity scale in the eddy viscosity, and the eddy diffusivity is a function of the eddy viscosity and the Prandtl or Schmidt number. The main problem with this method is that the length scale must still be defined before a value for the eddy viscosity can be obtained. In regions where the length scale is clearly definable, as in the boundary layer, this method works rather well. In regions where there is no clearly defined length scale, empirical formulas have been developed, but because rather extensive computational time is required for the empirical formulas, it is sometimes easier to move up to the more complex two-equation models.

Two-equation models have partial differential equations for both the velocity scale and the length scale. The k-$\epsilon$ model, where k is the same TKE equation developed for the representation of the one equation model, and $\epsilon$ is the rate of dissipation used for the representation of the length scale, is probably one of the most common of this type. This method will include the history and transport effects of turbulence. Although the buoyancy term is built into the k-$\epsilon$ model, there may be potential problems in that it may not account fully for the effects of stratification on the production/dissipation of the TKE. This problem, if it exists, may be solved by using an extended k-$\epsilon$ model with an additional buoyane effect consideration that will more accurately define the effects of stratification at the expense of computer time.

Because the two-equation models have the highest potential to properly calculate the eddy viscosity/diffusion coefficients, we have selected the most common two-equation model, the k-$\epsilon$ model, to calculate the eddy viscosity in the deep ocean.

We have applied our model, TEMPEST©/FLESCOT©, with the k-$\epsilon$ model to a two-dimensional water body having a depth of 3000 m. The preliminary model results indicate, the adequacy of the k-$\epsilon$ model; that is, near the bed, the

vertical eddy viscosity increases at most linearly with the distance from the bed, and then decreases rapidly as the velocity distribution becomes almost uniform vertically. Except near the bed, the vertical eddy viscosity calculated by the model is uniform and is somewhat smaller than the molecular viscosity due to the upstream boundary conditions. Comparisons among stratified and nonstratified cases reveal the reducing effects of buoyancy term on the TKE and eddy viscosity, resulting in more reasonable level of calculated eddy viscosity under stratified conditions in a deep-ocean environment.

Also, the computer code successfully predicted at least qualitatively the leaching of radionuclide from an ocean bottom (a hypothetical original contamination source) to the overlying clean water column. Once in the water column, some of leached radionuclide was predicted to be adsorbed by suspended silt and clay based on the distribution coefficient and mass transfer rates while being transported downstream. Furthermore, the originally clean bottom sediment downstream of the location with the contaminated bottom sediment was predicted to adsorb a fraction of the leached radionuclide back into the bed, thus, spreading the potentially long-term source of contamination.

# 7.0 REFERENCES


Blumberg, A. F. 1977. "Numerical Model of Estuarine Circulation." J. Hydraul. Div. ASCE HY3:295-311.

Blumberg, A. F, and H. J. Herring. 1986. Circulation Modelling Using Curvilinear Coordinates. Report No. 81, Dyanalysis, Princeton, New Jersey.

Bradshaw, P., ed. 1978. Turbulence. 2nd edition.

Bryan, K. 1969. "A Numerical Method for the Study of the Circulation of the World Ocean." J. Comput. Phys. 4:347-376.

Davies, A. M. 1980. "Application of the Galerkin Method to the Formulation of a Three-Dimensional Nonlinear Hydrodynamic Sea Model." Appl. Math. Modeling 4:425-455.

Ditoro, D. M., J. J. Fitzpatrick, and R. B. Thomann. 1981. Documentation for Water Quality Analysis Simulation Program (WASP) and Model Verification Program (MVP). Prepared for the Environmental Research Laboratory, U.S. Environmental Protection Agency, Duluth, Minnesota, by Hydroscience, Inc., Westwood, New Jersey.

Eraslan, A. H., W. L. Lin, and R. D. Sharp. 1983. FLOWER: A Computer Code for Simulating Three-Dimensional Flow, Temperature, and Salinity Conditions in Rivers, Estuaries, and Oceans. NUREG/CR-3172, U.S. Nuclear Regulatory Commission, Washington, D.C.

Freitas, C. J., A. N. Findikakis, and R. L. Street. 1985. "Three-Dimensional Simulation of a Buoyancy-Driven Cavity Flow." In Proceedings of the 1985 ASCE Hydraulics Division Specialty Conference, Lake Buena Vista, Florida, August 12-17, 1985, pp. 1101-1106.

Gawain, T. H., and J. W. Pritchett. 1970. "A Unified Heuristic Model of Fluid Turbulence." J. Comput. Phys. 5:383-405.

Geyer, W. R. 1973. The Time-Dependent Dynamics of a Salt Wedge. Special Report 101, College of Oceanography and Fishery Sciences. University of Washington, Seattle, Washington.

Grant, W. D., and O. S. Madsen. 1979. "Combined Waves and Current Interaction with a Rough Bottom." J. of Geophys. Res. 84(4)1797-1808.

Holland, W. R., and L. B. Liu. 1975. "On the Generation of Mesoscale Eddies and Their Contribution to the Oceanic General Circulation." J. Phys. Oceanogr. 5(4):642-669.

Jones, W. P., and B. E. Launder. 1973. "The Calculation of Low-Reynolds-Number Phenomena with a Two-Equation Model of Turbulence." Int. J. Heat Mass Transfer 16:1119-1130.

King, I. P. 1982. "A Three Dimensional Finite Element Model for Stratified Flow." In Finite Element Flow Analysis, T. Kawai, ed., pp. 513-527. University of Tokyo Press, Japan.

Koplik, C. M., M. F. Kaplan, J. Y. Nalbandian, J. H. Simonson, and P. G. Clark. 1984. User's Guide to MARINRAD: Model for Assessing the Consequences of Release of Radioactive Material into the Oceans. SAND83-7104. Prepared for Sandia National Laboratories, Albuquerque, New Mexico, by Analytic Sciences Corp., Reading, Massachusetts.

Krone, R. B. 1962. Flume Studies of the Transport of Sediment in Estuarial Shoaling Processes. Hydraulic Engineering Laboratory and Sanitary Engineering Research Laboratory, University of California at Berkeley, Berkeley, California.

Leenderste, J. J., and S. K. Liu. 1975. "A Three-Dimensional Model for Estuaries and Coastal Seas." In Aspects of Computation, Vol. II. R-1784-OWRT, RAND Corp., Santa Monica, California.

Mellor, G. L., and T. Yamada. 1974. "A Hierarchy of Turbulence Closure Models for Planetary Boundary Layers." J. Atmos. Sci. 31:1791-1806.

Mellor, G. L., and T. Yamada. 1982. "Development of a Turbulence Closure Model for Geophysical Fluid Problems." Rev. Geophys. Space Phys. 20(4):851-875.

Munk, W. J., and E. R. Anderson. 1948. "Note on the Theory of the Thermocline." J. Mar. Res. 7(3):276-295.

Norton, W. R., and I. P. King. 1977. Operating Instructions for the Computer Program RMA2. RMA 6290, Resource Management Associates, Lafayette, California.

Onishi, Y. 1981. "Sediment and Contaminant Transport Model." J. Hydraul. Div. ASCE 107 (HY9):1089-1107.

Onishi, Y., and D. S. Trent. 1982. Mathematical Simulation of Sediment and Radionuclide Transport in Estuaries. NUREG/CR-2423. Prepared by Pacific Northwest Laboratory for U.S. Nuclear Regulatory Commission, Washington, D.C.

Onishi, Y., D. S. Trent, and A. S. Koontz. 1985a. "Three-Dimensional Simulation of Flow and Sewage Effluent Migration in the Strait of Juan De Fuca, Washington." In Proceedings of the 1985 ASCE Environmental Engineering Conference, Boston, Massachusetts, pp. 1006-1013.

Onishi, Y., R. M. Ecker, D. S. Trent, S. B. Yabusaki and L. W. Vail. 1985b. Oceanographic Modeling of the Beaufort Sea in Relation to the Proposed

Lisburne Development. Prepared for ARCO Alaska, Inc., by Battelle, Pacific Northwest Laboratories, Richland, Washington.

Onishi, Y., and D. S. Trent. 1985. Three-Dimensional Simulation of Flow, Salinity, Sediment, and Radionuclide Movements in the Hudson River Estuary. Proceedings of the ASCE Hydraulics Division Conference at Lake Buena Vista, Florida, August 1985, pp. 1095-1100.

Onishi, Y., L. F. Hibler, and C. R. Sherwood. 1987. Review of Hydrodynamic and Transport Models and Data Collected near the Mid-Atlantic Low-Level Radioactive Waste Disposal Sites. PNL-6331, Pacific Northwest Laboratory, Richland, Washington.

Partheniades, E. 1962. A Study of Erosion and Deposition of Cohesive Soils in Salt Water. Dissertation, University of California, Berkeley, California.

Robinson, A. R., and M. G. Marietta. 1985. Research, Progress and the Mark A Box Model for Physical, Biological and Chemical Transports. SAND84-0646, Sandia National Laboratories, Albuquerque, New Mexico. 202 p.

Rodi, W. 1984. Turbulence Models and Their Application in Hydraulics. University of Karlsruhe, Karlsruhe, Federated German Republic.

Rodi, W. 1987. "Examples of Calculation Methods for Flow and Mixing in Stratified Fluids." J. Geophys. Res. 92(C5):5305-5328.

Sheng, Y. P., W. Lick, R. T. Gedney, and F. B. Molls. 1978. "Numerical Computation of a Three-Dimensional Circulation in Lake Erie: A Comparison of a Free-Surface Model and a Rigid-Lid Model." J. Phys. Oceanogr. 8:713-727.

Shepard, J. G. 1978. "A Simple Model for the Dispersion of Radioactive Wastes Dumped on the Deep-Sea Bed." Marine Sci. Comm. 4(4):293-327.

Simons, T. J. 1973. "Development of Three-Dimensional Numerical Models of the Great Lakes." Scientific Series No. 12, Canada Center for Inland Waters, Burlington, Ontario, Canada.

Smith, J. H., W. R. Mabey, N. Bohonos, B. R. Holt, S. S. Lee, T. W. Chou, D. C. Bomberger, and T. Mill. 1977. Environmental Pathways of Selected Chemicals in Freshwater Systems. Part I: Background and Experimental Procedures. EPA-6000/7-77-113. Prepared by SRI International for the U.S. Environmental Protection Agency, Washington, D.C.

Spaulding, M. L., and D. Parish. 1984. "A Three-Dimensional Numerical Model of Particulate Transport for Coastal Water." Continental Shelf Res. 3(1):55-67.

Tee, K. T. 1981. "A Three-Dimensional Model for Tidal and Residual Currents in Bays." In Transport Models for Inland and Coastal Waters, H. B. Fischer, ed., pp. 284-309, Academic Press, New York.

Trent, D. S., L. L. Eyler, and M. J. Budden. 1989. TEMPEST - A Three-Dimensional Time-Dependent Computer Program for Hydrothermal Analysis. PNL-4348, Vol. 1, Rev. 2, Pacific Northwest Laboratory, Richland, Washington.

U.S. Atomic Energy Commission. 1975. Overall Safety Manual. Vol. 2. Space Nuclear Systems Division, Washington, D.C.

Vanoni, V. A. 1975. Sedimentation Engineering. Prepared by the ASCE Task Committee for the Preparation of the Manual on Sedimentation, Sedimentation Committee of the Hydraulics Division, ASCE, New York.

Walker, H. A., J. A. Nacito, J. F. Paul, V. J. Bierman, and J. H. Gentile. 1985. Methods for Waste Load Allocation of Municipal Sewage Sludge at the 106-Mile Ocean Disposal Site. Environmental Research Laboratory, U.S. Environmental Protection Agency, Narragansett, Rhode Island.

Wang, J. D., and J. J. Connor. 1975. Mathematical Modeling of Near Coastal Circulation. Report No. 200, Department of Civil Engineering, Massachusetts Institute of Technology, Cambridge, Massachusetts.

Wang, D. P. 1982. "Development of a Three-Dimensional, Limited-Area (Island) Shelf Circulation Model." J. Phys. Oceanogr. 12:605-617.

Weatherly, G. L., and P. J. Martin. 1978. "On the Structure and Dynamics of the Oceanic Bottom Boundary Layer." J. Phys. Oceanogr. 8:557-570.

Webb, G. A. M., and F. Morley. 1973. A Model for the Evaluation of Deep Ocean Disposal of Radioactive Waste. National Radiological Protection Board, p. 23.

# DISTRIBUTION

No. of Copies

## OFFSITE

10 DOE/Office of Scientific and Technical Information

6 U.S. Environmental Protection Agency
Office of Radiation Programs
401 M Street N.E., Room 206-A
Washington, DC 20460
ATTN: R. Dyer
K. W. Yeh (5)

M. H. Chaudhry
Civil Engineering Department
Washington State University
Pullman, WA 99163

2 P. Colombo
Brookhaven National Laboratory
Building 703
Upton, NY 11937

J. F. Kennedy
Institute of Hydraulic Research
University of Iowa
Iowa City, Iowa 52242

R. A. McGrath
Battelle New England Marine Research Laboratory
397 Washington Street
Duxbury, MA 02332

John Paul
Environmental Research Laboratory
Narragonsett, Delaware

W. Rudi
Institute of Hydrodynamics
University of Karlsruhe
Karlsruhe, FRG

5 D. S. Trent
Mechanical Engineering Department
Oregon State University
Corvalis, OR

No. of Copies

H. Wishen
Civil Engineering Department
University of California
Berkeley, CA

## ONSITE

2 DOE Richland Operations Office

J. J. Sutey/D. L. Sours

27 Pacific Northwest Laboratory

D. B. Cearlock
J. P. Downing
R. M. Ecker
L. L. Eyler
J. W. Falco
J. M. Hales
P. C. Hays
J. L. McElroy
Y. Onishi (15)
R. L. Skaggs
J. A. Stottlemyre
J. A. Strand
W. L. Templeton
S. B. Yabusaki
Publishing Coordination
Technical Report Files (5)